Hydrodynamic Interaction during Tug-Ship Operations

by

Sembukutti Vidanelage Buddhika Nirman Jayarathne
CEng, BSc, MRINA, MIEAust, MIMarEST, AFHEA

National Centre for Ports and Shipping
Australian Maritime College
University of Tasmania

Submitted in fulfilment of the requirements for the Doctor of Philosophy

University of Tasmania

April, 2018

This page intentionally left blank.

Declarations

Declaration of Originality and Authority of Access

This thesis contains no material which has been accepted for a degree or diploma by the University or any other institution, except by way of background information and duly acknowledged in the thesis, and to the best of my knowledge and belief no material previously published or written by another person except where due acknowledgement is made in the text of the thesis, nor does the thesis contain any material that infringes copyright.

This thesis may be made available for loan and limited copying and communication in accordance with the Copyright Act 1968.

Sembukutti Vidanelage Buddhika Nirman Jayarathne
April 30, 2018

Statement of Published Work Contained in Thesis

The publishers of the papers comprising Chapters 2, 3, 4 and 6 hold the copyright for that content, and access to the material should be sought from the respective journals and conference proceedings. The remaining non-published content of the thesis, which is Chapter 5, is submitted and under review, and may be made available for loan and limited copying and communication in accordance with the Copyright Act 1968.

Statement of Co-Authorship

The following people and institutions contributed to the publication of work undertaken as part of this thesis:

- Sembukutti Vidanelage Buddhika Nirman Jayarathne (Candidate)
- Prof Dev Ranmuthugala, University of Tasmania (Author 1)
- Dr Zhi Quan Leong, University of Tasmania (Author 2)
- Dr Jiangang Fei, University of Tasmania (Author 3)
- A/Prof Shuhong Chai, University of Tasmania (Author 4)

Publication list and proportion of work details

Chapter 2 (Paper 1) **Accuracy of Potential Flow Methods to Solve Real-time Ship-Tug Interaction Effects within Ship Handling Simulators** Candidate was the primary author and with Author 1 contributed to the design of the analysis, its formalisation and development. Author 3 and Author 4 assisted with presentation. [Candidate: 75%, Author 1: 15%, Author 3: 5%, Author 4: 5%]
Chapter 3 (Paper 2) **Numerical and Experimental Prediction of Hydrodynamic Interaction Effects Acting on Tugs during Ship Manoeuvres** Candidate was the primary author and with Author 1 and Author 2 contributed to the design of the analysis, its formalisation and development. Author 3 and Author 4 assisted with presentation. [Candidate: 70%, Author 1: 10%, Author 2: 10%, Author 3: 5%, Author 4: 5%]
Chapter 4 (Paper 3) **Non-Dimensionalisation of Lateral Distances Between Vessels of Dissimilar Sizes for Interaction Effect Studies** Candidate was the primary author and with Author 1 and Author 2 contributed to the design of the analysis, its formalisation and development. Author 4 assisted with presentation. [Candidate: 75%, Author 1: 10%, Author 2: 10%, Author 3: 5%]
Chapter 5 (Paper 4) **Safe Tug Operations During Ship-Assist Manoeuvres** Candidate was the primary author and with Author 1 and Author 2 contributed to its formalisation, development and presentation. [Candidate: 75%, Author 1: 15%, Author 2: 10%]
Chapter 6 – Part A (Paper 5) **Safe Operation of Tugs within Close Proximity to the Forward and Aft Regions of Larger Ships** Candidate was the primary author and with Author 1 and Author 2 contributed to its formalisation, development and presentation. [Candidate: 80%, Author 1: 10%, Author 2: 10%]
Chapter 6 – Part B (Paper 6) **Hydrodynamic Interaction Effects on Tugs Operating within the Midship Region alongside Large Ships** Candidate was the primary author and with Author 1 and Author 2 contributed to its formalisation, development and presentation. [Candidate: 80%, Author 1: 10%, Author 2: 10%]

We the undersigned agree with the above stated “proportion of work undertaken” for each of the above published (or submitted) peer-reviewed manuscripts contributing to this thesis.

Signed:

Prof Dev Ranmuthugala

Primary Supervisor

National Centre for Maritime Engineering and Hydrodynamics
Australian Maritime College
University of Tasmania

Date: 30/04/2018

A/Prof Shuhong Chai

Acting AMC Principal

Australian Maritime College
University of Tasmania

Date: 30/04/2018

Acknowledgements

Firstly, I would like to express my sincere gratitude to my primary supervisor, Professor Dev Ranmuthugala for the continuous support he has provided me in researching and writing this thesis. His guidance has contributed to all aspects of this work from beginning to end. I could not have imagined having a better supervisor and mentor for my thesis.

Besides my primary supervisor, I would like to thank my co-supervisor, Doctor Zhi Quan Leong for his insightful comments, which motivated me to widen the scope of my thesis. I would also like to thank the rest of my co-supervisors; Doctor Jiangang Fei and Associate Professor Shuhong Chai for also encouraging me throughout this thesis.

Very special gratitude goes out to all my friends down at the AMC Research Hub who have created a very memorable environment for researching, writing and celebrating life.

Special thanks must go to Associate Professor Jonathan Binns for his support during the potential flow analysis and to my graduate research coordinator, Doctor Hossein Enshaei for his great support throughout this thesis. I would also like to thank Doctor Zhi Quan Leong, Mister Luciano Mason and Mister Geli Kourakis for their dedication and continual work on the High Performance Cluster (HPC), which helped me to simulate a large number of CFD cases during this study. In addition, I would like to acknowledge the support given by Associate Professor Gregor Macfarlane, Doctor Jonathan Duffy, Mister Tim Lilienthal, Mister Adam Rolls, Mister Liam Honeychurch and the Defence Science and Technology (DST) Group during the setup and execution of the experimental work.

Last but not least; I would like to thank my wife Apsara, my parents and my brother for their unwavering love and support for me in pursuing my dreams. To them I dedicate this thesis.

This page intentionally left blank.

Abstract

The hydrodynamic interaction between two vessels operating in close proximity can affect their safety and handling, especially if the vessels are significantly different in size, for example when a tug is assisting a large ship. During such operations, the drift-angle of the tug and lateral distance between the vessels are frequently varied to ensure accurate course keeping and safety. This can result in unsteady hydrodynamic interaction effects induced on the vessels, which in turn can adversely affect their ability to maintain course and safety, especially for the smaller tug. Hence, knowledge of the hydrodynamic loads acting on the tug under these conditions is of significant practical value to the tug operator in order to avoid collision, capsizing or being run over. However, there are limited comprehensive studies to date characterising the interaction behaviour on a tug manoeuvring in close proximity to a large ship.

This project investigates the hydrodynamic interaction behaviour acting on a tug during ship-assist manoeuvres in order to establish safe operational envelopes using full scale validated Computational Fluid Dynamics (CFD) simulations. The investigation included quantifying the interaction effects on the tug due to changes in the vessel speeds, the longitudinal and lateral location relative to the ship, the drift-angle of the tug, and the relative size between the vessels.

The CFD model was validated at model-scale using experiments performed in the model test basin at the Australian Maritime College (AMC), which were then extended to represent full-scale operations. Thus, the scaling effects and non-dimensionalisation approach used to characterise the hydrodynamic behaviour for vessels of different sizes, ratios, and separations were investigated and verified. Different numerical approaches (CFD and potential flow solvers), and simulation conditions and settings within the respective approaches were also examined. The findings were used to identify guiding principles to achieve accurate numerical simulation results for hydrodynamic interaction effects during tug-ship operations.

The operational implications on a tug during ship-assist manoeuvres are discussed based on the hydrodynamic interaction data obtained through the CFD simulations. The hydrodynamic interaction data is consolidated into Hydrodynamic Interaction Region Plots (HIRP), which are non-dimensionalised based on the size and speed of the vessels and can thus be used by tug operators to determine the actual interaction forces and moments on a tug for different drift angles and locations relative to the ship for a given forward speed. This enables tug operators to determine the safe operational envelopes specific to the vessels in question and their prevailing conditions.

In future studies, the results of this project can be integrated into ship/tug handling simulators by replacing their existing interaction modules using new algorithm developed through non-linear regression analysis of the data consolidated within the HIRPs developed in this work.

This page intentionally left blank.

Table of Contents

List of Figures

List of Tables

Nomenclature

BR	Breadth Ratio, B_s/B_t
B_s	Breadth of the tanker ship (m)
B_t	Breadth of the tug (m)
C_F	Frictional resistance coefficient
C_N	Yaw moment coefficient
C_P	Dynamic pressure coefficient, $C_P = (P - P_\infty)/q$
C_T	Drag coefficient
C_X	Longitudinal force coefficient
C_Y	Lateral force coefficient
D	Depth of the water (m)
DR	Displacement Ratio, ∇_s/∇_t
F_{rD}	Froude Number (Depth), $F_{rD} = u/\sqrt{g\ D}$
F_{rs}	Froude Number (Tanker ship Length), $F_{rs} = u/\sqrt{g\ L_s}$
F_{rt}	Froude Number (Tug Length), $F_{rt} = u/\sqrt{g\ L_t}$
g	Acceleration due to gravity (9.81 m s^{-2})
L_m	Length waterline of the model scale tanker ship (m)
L_{OA}	Length overall of the vessels (m)
L_s	Length waterline of the tanker ship (m)
L_t	Length waterline of the tug (m)
N	Yaw moment acting on tug (N m)
N_I	Yaw moment acting on the interacting tug, chapter 5 (N m)
N_o	Yaw moment acting on the open water tug, chapter 5 (N m)
P	Pressure (pa)
P_∞	Free-stream reference pressure (pa)
q	Dynamic pressure (pa), $q = \rho\ V^2/\ 2$
R_e	Reynolds number, $R_e = uL/\nu$
R_F	Frictional resistance on ship model in chapter 1 (N)
R_G	Mesh convergence ratio, $R_G = \epsilon_{21}/\epsilon_{32}$
R_T	Total resistance on ship model in chapter 1 (N)

S_s	Wetted surface area of the tanker ship (m^2)
S_t	Wetted surface area of the tug (m^2)
T	Draft of the vessels (m)
u	Fluid flow velocity (m s^{-1})
V	Velocity of ship models in chapter 1 (m s^{-1})
X	Longitudinal force acting on tug (N)
X_I	Longitudinal force acting on the interacting tug, chapter 5 (N)
X_o	Longitudinal force acting on the open water tug, chapter 5 (N)
Y	Lateral force acting on tug (N)
Y_I	Lateral force acting on the interacting tug, chapter 5 (N)
Y_o	Lateral force acting on the open water tug, chapter 5 (N)
y^+	Non-dimensional wall distance of first inflation layer
Δx	Non-dimensionalised longitudinal-distance between vessels
δx	Longitudinal distance between vessels (m)
Δy	Non-dimensionalised lateral distance between vessels
Δy_{ship}	Non-dimensionalised lateral distance between vessels calculated as a ratio of the tanker breadth in chapter 4
Δy_{tug}	Non-dimensionalised lateral distance between vessels calculated as a ratio of the tug breadth in chapter 4
δy	Lateral distance between vessels (m)
δy_{cl}	Lateral distance between the centrelines of the vessels in chapter 4 (m)
δy_m	Lateral distance between the midships of the vessels in chapter 4 (m)
	Change in the results between the fine and medium mesh
	Change in the results between the medium and coarse mesh
ρ	Density of water (kg m^{-3})
θ	Drift angle of the tug (Degrees)
	Fluig Kinematic viscosity (kg m^{-1} s^{-1})
∇_s	Volumetric displacement of the tanker ship (m^{-3})
∇_t	Volumetric displacement of the tug (m^{-3})

Abbreviations

AMC	Australian Maritime College
CFD	Computational Fluid Dynamics
DNV	Det Norske Veritas
DT	Dry Transom
EFD	Experimental Fluid Dynamics
GL	Germanischer Lloyds
HIRP	Hydrodynamic Interaction Region Plot
ITTC	International Towing Tank Conference
LVDT	Linear Voltage Displacement Transducer
MAIB	Marine Accident Investigation Branch
MARAD	Maritime Administration, USA
MARIN	Maritime Research Institute Netherland
MCA	Maritime Coastguard Agency, United Kingdom
PF	Potential Flow
RANS	Reynolds Averaged Navier-Stokes
RKE	Realizable Two Layer k-ε turbulence model
SA	Spalart-Allmaras turbulence model
SST	Shear Stress Transport turbulence model
WT	Wet Transom

This page intentionally left blank.

Chapter 1

Thesis Introduction

This chapter discusses the research question, project outcomes, methodology employed to achieve the outcomes, limitations, and novel aspects of the work carried out. It includes a brief description of the related issues and past work on hydrodynamic interaction effects induced on tugs during ship-assist manoeuvres.

1.1 Introduction

Tug assistance is particularly significant when ships with limited manoeuvring capabilities are handled in restricted waters. In such manoeuvres, tugs are either used during the transit of larger ships to or from a berth, or during their mooring and unmooring operations (Hensen, 2003). Due to growing marine traffic in restricted waterways and harbour waters, tugs are exposed to dangers such as collision, grounding, girting, and being run-over by larger ships (Hensen et al., 2013). In addition, hydrodynamic interaction between the vessels can adversely affect the handling and safety of attending tugs. Interaction forces change with vessel type, width of fairway, and drift angle between them (Hensen, 2012). These forces and their effects become prominent when the vessels are significantly dissimilar in size and are operating in close proximity during tight manoeuvres similar to that shown in Figure 1.1. Although experienced tug operators may know that interaction forces differ between types of vessels, the safety envelop for each of these cases is much harder to determine.

Figure 1.1: A tug operating near the bow of a car carrier during a ship-assist manoeuvre (Hensen et al., 2013).

"Dangers of interaction" is a guidance note prepared by the Maritime and Coastguard Agency of the United Kingdom (MCA, 2001) to draw the attention of ship owners, ship operators, pilots, and tug operators to the effects of hydrodynamic interaction on vessel manoeuvrability. It states that when vessels manoeuvre at close quarters for operational reasons, the greatest potential danger exists when there is a large difference in size between the two vessels, and is mostly experienced when a ship is being attended by a tug. The Marine Accident Investigation Branch (MAIB, 2011) report strongly suggests mariners familiarise themselves with the "Dangers of Interaction" guidelines in order to become aware of potentially dangerous situations caused by hydrodynamic interaction effects. Hensen et al., (2013) surveyed 160 pilots, tug masters and ship captains about their awareness of interaction effects during these manoeuvres, and the accuracy of ship manoeuvring simulators replicating these effects. Around 30% of the tug masters questioned had faced critical situations due to interaction effects during ship-assist manoeuvres and 40% emphasised the dissimilarity between interaction effects in training simulators and in real manoeuvres. Just as it is important to have simulator training for those who operate ships in critical manoeuvres, it is essential that the interaction effects are accurately determined by simulator algorithms. Ship handling simulators use interaction effect prediction algorithms developed using data collected via either experimental, theoretical, or computational based methods.

The first experimental investigation to appear in the literature was conducted by Taylor, (1909) using scaled models towed in pairs abreast one another and at locations ahead or astern. Since this was the first time such an experiment had been undertaken, the apparatus used was of an improvised nature. The suction or repulsion forces on the vessels were measured, and Taylor introduced preliminary data for researchers to extend in future studies. Newton, (1960) carried out a series of model-scale experiments and full-scale trials to determine the interaction effects between ships on parallel courses in deep water. He concluded that it is possible to use model-scale experiments as a guiding tool to predict interaction effects induced on vessels during close quarter manoeuvres. However, he could not verify the possibility of using model-scale experiments to predict the effects on vessels of widely differing size and form, since the full-scale and model-scale ships he investigated were of similar size ratio.

Dand (1975, 1978, and 1995) carried out captive model experiments to determine the physical causes of interaction and their effects on tugs during ship-assist manoeuvres. The findings of these studies are still used for tug-ship interaction prediction, when both ship and tug are advancing on parallel courses in close proximity to each other. However, his conclusion was formed by results obtained from one of a number of manoeuvres encountered by a tug during ship-assist manoeuvres, and thus it is difficult to generalise it to tugs operating at different drift angles and in different locations. Vantorre et al., (2002) conducted physical model-scaled tests to determine ship interaction effects in head-on and overtaking encounters for similar and dissimilar size vessels. The test results generated were used to create a mathematical model to improve the quality of the interaction effects predicted within ship manoeuvring simulators. They identified a need for further experiments to simulate the interaction effects when ships of different sizes and types operate in close proximity.

Jong, (2007) studied the interaction forces and moments on a ship with tugs attending at different drift angles. He investigated the level of influence of the forces exerted by a tug on a ship, depending on the tug's distance from the ship, its angle, and its position along the ship's length. Although the findings were valuable for such operations, the hydrodynamic interaction effects acting on tugs by larger ships were not thoroughly discussed in his study. Geerts et al., (2011) assessed the hydrodynamic interaction forces acting on a tug sailing freely in the vicinity of the bow of a large container ship. The overview of model topology in the towing tank used in their study is shown in Figure 1.2. They performed a series of model-scaled tests during which a model tug was towed together with a model ship. The test results were then incorporated into a simulation program to assess the steering action required to maintain the tug's position. The simulations were used to identify the most suitable location for a tug to be positioned relative to a larger ship during a towline passing operation within the bow area of the latter. This again represents only one of many manoeuvres that a tug may undergo during ship-assist operations.

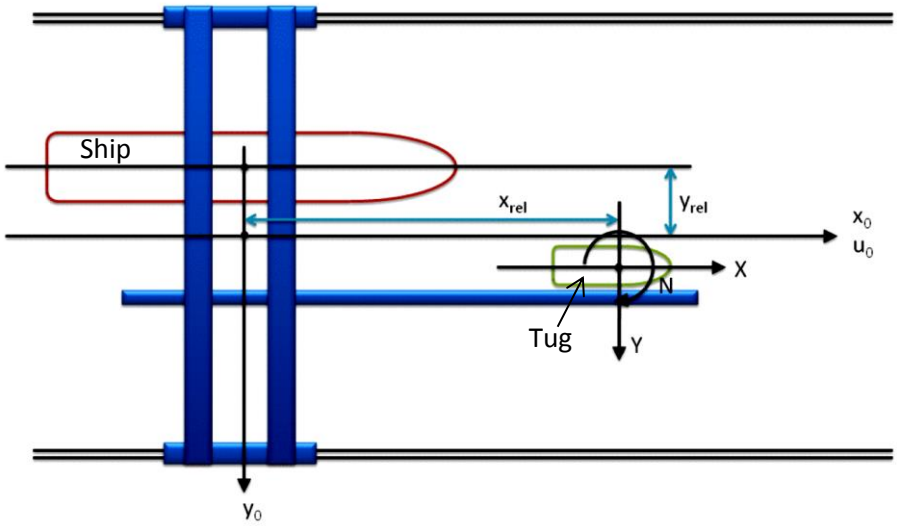

Figure 1.2: Overview of model topology utilised by Geerts et al., (2011) in the towing tank to investigate interaction forces and moments acting on a tug sailing freely in the vicinity of the bow of a large container ship.

A number of researchers have investigated the capabilities of theoretical methods to predict interaction effects, thus reducing the need for expensive experimental work. Tuck and Newman, (1974) performed the pioneering theoretical investigations into ship-to-ship interactions, with their results being fairly consistent with the experimental results presented by Newton, (1960). Yeung, (1978) also carried out a theoretical study using slender body theory on the hydrodynamic interaction between two bodies moving in shallow water, comparing the theoretical results for ship-tug interaction against Dand, (1975) experimental data. Yeung, (1978) noted that although the general behaviour of the experimental curves was predicted by the theoretical analysis, the peak force and moment values were significantly underestimated, particularly when the tug was in the stern region of the larger ship.

Kuniji et al., (1984) developed a mathematical model to predict manoeuvring motions of ships operating at low speeds in restricted waters. The model aimed to express the hydrodynamic forces on ships by combining the open water characteristics of the hull, propeller, and rudder. They suggested further attention was needed to determine the effectiveness of the mathematical model to solve the hydrodynamic interaction effects induced on ships due to assisting tugs, because most of the time ships that are manoeuvring

at low speeds need tug assistance. Takashina, (1986) conducted a similar study to develop a mathematical model to predict the manoeuvring motion of ships during tug assist operations. The results of that mathematical model were then compared against free running model test data for typical ship and tug manoeuvres and were found to provide satisfactory agreement. This study however did not discuss the hydrodynamic effects induced on the tug by the larger ship.

In addition to this kind of theoretical work, researchers have conducted numerical simulations to determine interaction effects between vessels operating in close proximity. A comparative Computational Fluid Dynamics (CFD) study of the interaction between a tug and a large tanker sailing in parallel courses at low speeds was undertaken by Fonfach et al., (2011). They analysed the interaction effects acting on a tug using inviscid flow, turbulent viscous flow, inviscid free surface flow, and viscous free surface flow theories using CFD. According to their findings, CFD with viscous and free surface effects showed better agreement with the experimental data than the other numerical models. However, their study was limited to only a tug operating parallel to a larger ship and located at a few locations relative to the latter.

Figure 1.3: Escort tug *Foss America* escorting a ship: Picture taken by Robert Allan Ltd. (Brendan, 2009).

Brendan, (2009) carried out a CFD-based study to predict the performance of an escort tug (see Figure 1.3). This study solely focused on the drag force acting on a tug when operating freely with different drift angles in open water, without the presence of a large ship. Therefore, effects due to hydrodynamic interaction between the vessels were not included.

Sorensen et al., (2009) revealed that when a tug is operating near a large ship, complex pressure conditions can significantly effect the reliability of training simulator predictions. Subsequently, they improved the mathematical model of tugs within their simulator using a complex ship-to-ship interaction module between the ship and the tug. Simonsen et al., (2011) conducted a numerical study on a subset of cases taken from physical model-scale tests conducted to study quasi-steady ship-to-ship interaction effects (Figure 1.4). In this study, the tug was located in the midship region of a tanker with the tug's drift angle varying from 0 to 60 degrees, concluding that CFD is a promising tool for ship interaction studies. However, in actual operations the tug may experince drift angles greater than 60 degrees, and will operate at locations other than the midship.

Figure 1.4: The experimental set-up of Simonsen et al., (2011) to study quasi-steady ship-ship interaction effects. The tug is located midship of the larger ship, with a drift angle of zero degrees.

Due to the high computational power and the meshing time required for CFD methods, relatively simple potential flow double body theory was identified by Pinkster and Bhawsinka, (2013); Sutulo and Soares, (2009) as the best method for online interaction effect predictions. Sutulo and Soares, (2009) and Sutulo et al., (2012) developed a potential flow double-body panel code to estimate interaction effects in real time on commonly used computer hardware. The results obtained with the code were validated against model-scale experimental data obtained in deep and shallow water towing tanks for a tug operating near a larger ship in parallel operations. The results illustrated the potential of the double-body panel method to predict interaction effects. However this method was unable to accurately predict the sway force at small horizontal clearance, which was expected to be more pronounced than predicted for non-parallel operations.

In summary, it is seen that existing numerical and experimental studies on interaction effects on tugs during ship-assist operations are rather limited in addressing the range of manoeuvres and situations encountered by tugs during such operations. This includes limited work in investigating the interaction effects on tugs operating in different locations relative to the ship and at different drift angles in order to gain a more generalised view of the interaction behaviour. In addition, the solution approaches available in the literature lack clear guidance on their applicability for such studies. This study therefore investigates the hydrodynamic interaction effects induced on tugs that are operating at various locations and angles during ship-assist manoeuvres, using CFD and Potential Flow (PF) methods that are validated through captive model experiments. The results are used to quantify the interaction effects on the tug's operational envelope when operating around a larger ship during ship-assist manoeuvres.

1.2 Research Objective

The aim of this project is to investigate the hydrodynamic behaviour of a tug when interacting with a larger ship during ship-assist manoeuvres. This is done by examining the tug's hydrodynamic interaction effect coefficients for a range of relative positions and drift

angles between the two vessels at two common speeds during ship-assist manoeuvres using numerical and experimental techniques.

The motivation behind this study is to quantify the hydrodynamic interaction that influences a tug's ability to safely manoeuvre in close proximity to a ship, as well as identifying a safe operating envelop. Thus, the specific research question for this project is:

What are the adverse hydrodynamic interaction effects induced on a tug, and what is the safe operating envelope to minimise these effects while manoeuvring in close proximity to a larger ship?

To answer the above question, the project focuses on the following four outcomes:

1. A review of the literature on hydrodynamic interaction and its influence on the behaviour of multiple vessels operating in close proximity.
2. Development and validation of a numerical simulation model to capture the hydrodynamic characteristics of a tug operating in close proximity to a large ship.
3. Analysis of the hydrodynamic interaction behaviour on a tug operating at different relative positions, drift angles and velocities alongside a larger ship, including the effects of the relative size between the two vessels.
4. Develop Hydrodynamic Interaction Region Plots (HIRPs) using the data obtained through full-scale simulations in order to quantify safe operating envelopes for tugs partaking in ship-assist manoeuvres.

1.3 Research Methodology

In order to establish confidence in the accuracy of the findings, the study was carried out in four phases using a staged approach.

Phase 1: Comparative numerical simulations to evaluate the capability of Potential Flow (PF) and Reynolds Averaged Navier Stokes (RANS) based CFD methods to predict the hydrodynamic interaction effects on a tug.

It is evident from the literature that PF solvers are used to simulate real-time interaction effects within ship handling simulators. However, a number of researchers (Doctors, 2006; Doctors & Beck, 2005; Falter, 2010; Fonfach et al., 2011; Lindberg et al., 2012; Mantzaris, 1998; Pinkster & Bhawsinka, 2013; Shin et al., 2008; Zhou et al., 2012) have questioned the accuracy of the PF methods that are currently used. Therefore, the first phase of this study was a comparative model-scale numerical simulation study employing the Rankine-source panel code-based software Futureship® (DNV GL Maritime, 2014) and the CFD software StarCCM+® (CD-Adapco, 2015) to identify their suitability for interaction effect studies.

Phase 2: Verification and Validation of the CFD model used to simulate hydrodynamic interaction induced on a tug by a larger ship during ship-assist manoeuvre.

Following the establishment of RANS-based CFD as the investigation tool for tugs with non-streamlined hull shapes, the CFD simulation models underwent a verification and validation process. One of the major challenges faced in CFD modelling is that the results can vary significantly depending on the computational grid and the numerical model settings. This phase therefore investigated modelling techniques and the accuracy of CFD generated interaction forces and moments acting on a tug hull operating at different drift angles and locations along a tanker hull. The CFD results were validated using the model-scale experimental results.

Phase 3: Extrapolate CFD model-scale results to full-scale.

This phase investigated a suitable correlation technique to non-dimensionalise the lateral distance between vessels of dissimilar sizes and a scaling option for interaction effect studies. It focused on the interaction effects on a tug operating around the forward shoulder of a tanker at different lateral distances during ship-assist operations. The findings enable the interaction effects determined for one ship-to-tug ratio to be used to predict the

safe operating distances for different ship-to-tug ratios, using the non-dimensionalisation method presented.

Phase 4: Analysis of the hydrodynamic interaction effects on a tug at different relative positions and drift angles to the ship, including the influence of varying relative sizes between the two vessels.

This investigation provides the safe operating envelopes for tugs to reduce adverse hydrodynamic interaction effects induced by larger ships during ship-assist manoeuvers. The investigations were conducted using verified CFD simulation models. The location and the drift angle of the tug were changed along the longitudinal and transverse perimeter of a tanker to replicate widely used real world ship-assist scenarios. The simulations were performed at two Froude numbers that represent the most common minimum and maximum vessel operational speeds during such manoeuvres. The results of these simulations were used to develop a number of HIRPs that signify safe operating envelopes for tugs during ship-assist manoeuvers.

1.4 Geometries and scales

This study aims to investigate the interaction behaviour between a generic stern drive tug and a MARAD-F series tanker (Reoseman, 1987) under full-scale conditions. Such measurements however, are difficult to obtain using actual vessels due to difficulties associated with the availability and accessibility of vessels, associated cost, risk of collision and the difficulty of maintaining appropriate environmental conditions throughout the experimental programme. Therefore, experimental captive model-scale tests are used to validate the CFD models in this study. This enables the validated CFD models to be used for the analysis of interaction under full-scale conditions. An analysis of the validity and reliability of extending the CFD simulation from model-scale to full-scale conditions is also presented.

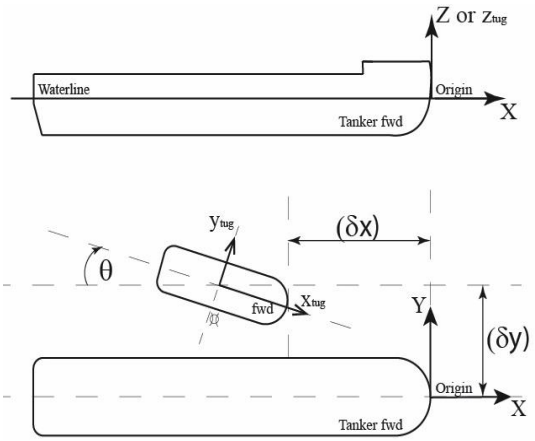

Figure 1.5: Local (tug) and global coordinate systems and vessel locations.

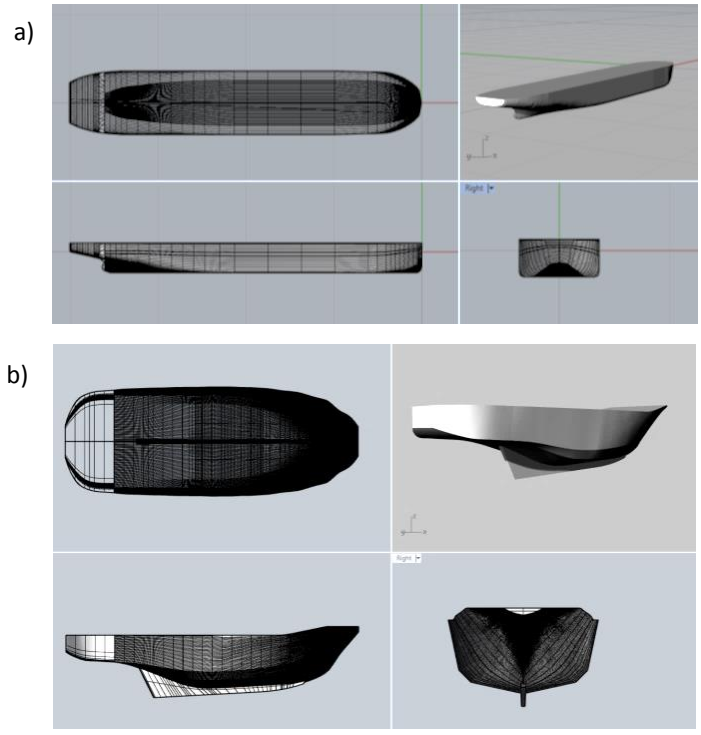

Figure 1.6: 3D hull forms: (a) MARAD-F series tanker, (b) stern drive tug.

The hydrodynamic forces and moments presented in this study are based on the local coordinate system of the vessels illustrated in Figure 1.5. The three dimensional model-scale hull form geometries were developed using the commercial software Rhinoceros® (Figure 1.6). The induced interaction forces and moments are investigated as a function of the relative position, drift angle, size, and speed of the two vessels in order to characterise the interaction behaviour. The dimensions of the vessels are given in the relevant chapters.

1.5 Limitations of the investigation

The current study focuses only on the fixed configuration of the vessels, thus there is no relative motion between them. The rationale for utilising this method is that when a tug assists a larger ship, the tug uses a rope to connect with the large ship requiring both vessels to travel at approximately the same speed. In addition, during ship escort manoeuvres, tugs usually travel alongside the ship at the same speed (Hensen, 2003). The test speeds used to investigate the interaction behaviour on the tug correspond to two speeds, the minimum and maximum operating speeds (3 knots and 6 knots full-scale) commonly encountered during ship-assist manoeuvres (Hensen, 2003).

In the experimental and numerical investigations, the models had to remain fixed in all degrees of freedom. This allowed the hydrodynamic interaction between the bare hulls of the vessels to be the focal point of the study, thus enabling modifications to the unadulterated interaction effect module operational within ship handling simulators (Kongsberg Maritime, 2012; Pinkster & Bhawsinka, 2013). The results of this work can in future be compared against fully appended configurations of the two vessels in order to quantify the contribution of the appendages to the interaction behaviour.

1.6 Novel Aspects

There are four areas in which this project provides original contributions to the field.

- The work represents a pioneering study that investigates and quantifies the hydrodynamic interaction effects between full-scale tugs and ships at various tug drift angles and at different longitudinal and lateral relative locations. While there are a few numerical studies characterising this interaction, these studies were conducted at model-scale (Geerts et al., 2011; Simonsen et al., 2011) with the vessels operating in parallel headings at limited locations (Fonfach, 2010). The study of Simonsen et al., (2011) investigated the interaction effects acting on a tug drifted up to 60 degrees,

positioned at the midship region of a tanker. However, in real operations tugs may operate at larger drift angles and at different relative locations. The current study investigates full-scale hydrodynamic interaction predictions for a range of drift angles up to 90 degrees, with the tug operating at a number of locations along the length of the tanker and at five different lateral separations. The results enable the generation of comprehensive HIRPs for ship-assist scenarios that is a major contribution to such operations.

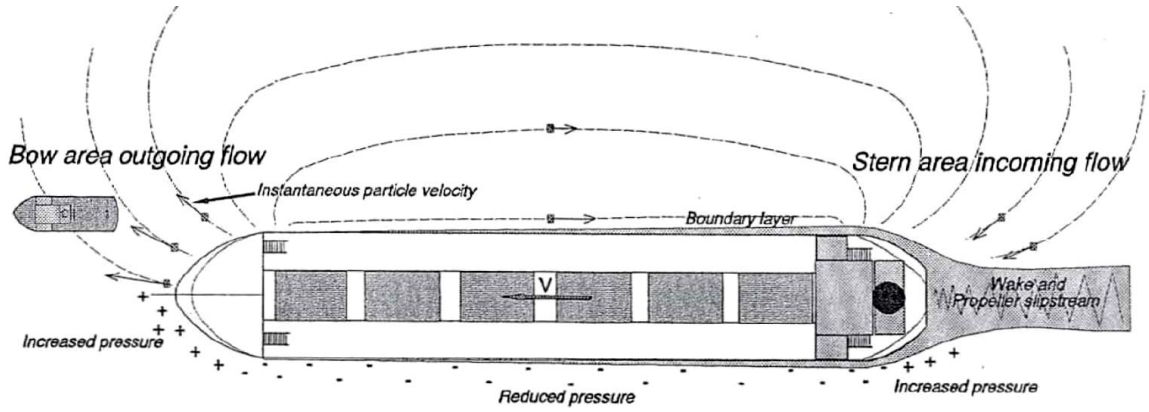

Figure 1.7: Flow field around a large ship affecting a tug operating in close proximity (Hensen, 2003). (+) indicates positive pressure and (-) indicates negative pressure.

- When a vessel moves through the water, it creates a bow wave and a high positive pressure field around the bow that can greatly influence interaction effects on a tug operating in close proximity (see Figure 1.7). This is an area that has very little information in the literature. Geerts et al., (2011) investigated the hydrodynamic interaction effects acting on a tug sailing freely in the vicinity of the bow of a tanker. However, the interaction effects due to larger tug drift angles and smaller lateral separations between the vessels were not investigated. This study investigates the hydrodynamic interaction effects on a tug operating in the bow wave region of a ship through various ship-tug breadth ratios and at different lateral separations. It is further extended to investigate the effects on the tug due to the high pressure field generated around the ship's stern, a research area that has little published data.

- To date, most of the numerical and experimental hydrodynamic interaction studies on ship-assist manoeuvers have been carried out at model-scale. It is therefore difficult to establish how well these results represent full-scale interaction behaviour. This is further exacerbated by a lack of proven methodologies for non-dimensionalising the relative distances between the two vessels, affecting the comparison of model and full-scale interaction effect data, as well as that between vessels of dissimilar size ratios. This study investigates a suitable correlation technique to non-dimensionalise the lateral distance between vessels of dissimilar sizes, and a scaling option for interaction effect studies.

- CFD simulations are increasingly being adopted as a tool to determine the interaction effects in ship-assist manoeuvres. However, most of the studies available in the public domain lack comprehensive verification and validation studies. This research investigates modelling techniques and the accuracy of CFD generated interaction forces and moments acting on a tug at different drift angles, as and at different lateral and longitudinal locations along a tanker. This includes a comprehensive verification and validation study, which includes numerical and experimental uncertainty analysis in accordance with proven standards and guidelines (ITTC, 2002a, 2002b; Roache, 1998; Stern et al., 2001; Wilson et al., 2001).

1.7 Thesis Outline

This thesis follows a “Chapterised Thesis” structure, where Chapters 2 to 6 comprise of separate scientific papers. The structure of the thesis is outlined below.

Chapter 1: The introductory chapter clarifies the research question, project outcomes, and the methodology employed to achieve the outcomes. It also includes a brief discussion of the issues and past work on the hydrodynamic interaction between vessels, especially during tug assist operations.

Chapter 2: Examines the ability of PF solvers to predict interaction effects acting on an un-appended transom stern tug operating in close proximity to a tanker during ship-assist manoeuvres. The investigation had both vessels operating at the same speed in parallel courses. The validation process consisted of a comparison between the results from PF solvers, CFD simulations, and experimental measurements. When the flat transom of the tug was above the water level creating a dry transom flow, the PF solver showed very good agreement with experimental and CFD results. However, it failed to do so for wet transom conditions, especially at higher Froude numbers. This led to the selection of CFD simulations supplemented by experimental measurements for the remainder of the study.

Chapter 3: Investigates the accuracy of CFD predicted interaction forces and moments acting on a tug hull at different drift angles, and lateral and longitudinal locations relative to a tanker hull. Validation of the simulations was carried out against experimental measurements obtained in a model test basin. It showed that the quality of the mesh model, including those in the near wall region and in areas of separation; the simulation settings; and the turbulence model have a significant influence on the accuracy of the computational results.

Chapter 4: Explores a suitable correlation technique for non-dimensionalising the lateral distance between vessels of dissimilar sizes, as well as providing a scaling option for interaction effect studies. It focuses on the interaction effects on a tug operating around the forward shoulder of a tanker at different lateral distances during ship-assist operations. The findings enabled the interaction effects determined for one ship-to-tug ratio to be used to predict the safe operating distances for vessels of different ship-to-tug ratios.

Chapter 5: Investigates the safe operating envelopes for tugs to use to mitigate adverse hydrodynamic interaction effects induced by larger ships during ship-assist manoeuvres. The drift angle of the tug, as well as the relative location of the tug along the longitudinal and lateral perimeter of a tanker was varied to replicate widely used real world tug operational scenarios. The simulations were performed at two Froude numbers that represent the most common minimum and maximum vessel operational speeds during such manoeuvers. The results of these simulations were used to identify critical areas for tugs to avoid during ship-

assist manoeuvers. The midship region of a large ship was deemed the safest region, while the forward and aft regions were identified as the most critical regions for a tug to operate within.

Chapter 6: This chapter expands on the work presented in Chapter 5 conducting a comparative numerical and experimental study to investigate interaction effects on a tug operating within the midship, forward and aft regions of a large ship at varying drift angles and lateral separations. The non-dimensionalised interaction effects were used to create HIRPs to identify the variation of the coefficients with respect to the tug's drift angle and its location relative to the ship. The HIRPs enable tug operators to identify safe operating envelopes for tugs to approach the midship, forward and aft regions of large vessel during tug assist manoeuvres.

Chapter 7: The concluding chapter provides an overall summary of the project, bringing together the findings of the individual chapters. It also provides final comments on the findings and outcomes, as well as discussing the implications of the findings and the respective contributions. It finally discusses limitations of the study and possible future work.

Appendices:

Appendix I Outlines the experimental and numerical uncertainty analysis.

Appendix II Provides information and transport equations for the RANS modelling and turbulence models used in this study.

Appendix III Provides the details of hull models used in this study.

Appendix IV Illustrates the experimental set-up used in the validation programme.

This page intentionally left blank.

Chapter 2

Accuracy of Potential Flow Methods to Solve Hydrodynamic Interaction

This chapter has been published in the International Journal on Marine Navigation and Safety of Sea Transportation. The citation for the research article is:

Jayarathne, N., Ranmuthugala, D., Chai, S. & Fei, G. (2014), 'Accuracy of Potential Flow Methods to Solve Real-time Ship-Tug Interaction Effects within Ship Handling Simulators', *International Journal on Marine Navigation and Safety of Sea Transportation*, vol. 8, no. 4, pp. 497-504.

ABSTRACT

The hydrodynamic interaction effects between two vessels that are significantly different in size operating in close proximity can adversely affect the safety and handling of these vessels. Many ship handling simulator designers implement Potential Flow (PF) solvers to calculate real-time interaction effects. However, these PF solvers struggle to accurately predict the complicated flow regimes that can occur, for example, as the flow passes a wet transom hull or one with a drift angle. When it comes to predicting the interaction effects on a tug during a ship-assist, it is essential to consider the rapid changes in the tug's drift angle, as the hull acts against the inflow creating a complicated flow regime. This chapter investigates the ability of the commercial PF solver, Futureship®, to predict the accurate interaction effects acting on tugs operating at a drift angle during ship handling operations through a case study. This includes a comparison against Computation Fluid Dynamics (CFD) simulations and captive model tests to examine the suitability of the PF method for such duties. Although the PF solver can be tuned to solve streamlined bodies, it needs further improvement to deal with hulls at drift angles.

2.1 Introduction

Tug boats play a significant role when ships incapable of slow manoeuvres are handled in restricted waters. Ships and their attending tugs are exposed to dangers such as collision, grounding, girting, and run-overs when operating in close proximity in restricted waterways. Furthermore, the hydrodynamic interaction forces and moments can adversely affect the handling and safety of the attending tugs. Hensen (2012) showed that the interaction effects change with ship type, width of fairway, and the drift angles of the vessels; which can cause even experienced tug masters difficulties with identifying safe operating envelopes for their tugs during such manoeuvres. In addition, Hensen (2012) stated that these effects become prominent when the vessels are significantly dissimilar in size and operated in close proximity during tight manoeuvres. Hensen et al. (2013) questioned 160 tug masters with regard to their awareness of the interaction effects during such manoeuvres. Around 30% of the tug masters had faced critical situations due to unexpected ship-to-ship interaction effects in actual ship-assist manoeuvres.

Ship handling simulators use empirical and semi-empirical methods, theoretical and numerical methods, or Potential Flow (PF) methods to predict interaction effects (Sutulo & Soares, 2009). With the exception of the PF method, the others require an interaction effect coefficients database to solve mathematical models implemented into the simulators, with the database developed and validated by empirical and numerical techniques. For example, Vantorre et al. (2002) conducted physical model tests to determine the ship interaction effects in head-on and overtaking encounters of similar and dissimilar ships. The test results were used to create a new mathematical model to improve the quality of the interaction effects within ship manoeuvring simulators.

Researchers such as Sutulo and Soares (2009), Sutulo et al. (2012) and Pinkster and Bhawsinka (2013) employed PF solvers to predict the interaction effects as an alternative to the excessive work and high cost involved in developing a coefficient based model. Currently only the relatively simple PF double-body panel method is utilised to provide estimates of the interaction forces and moments in real time within simulators (Sutulo et al., 2012).

Pinkster and Bhawsinka (2013) developed a computer program to estimate and validate the interaction effects using the simulator operated by the Maritime Research Institute Netherlands (MARIN). The PF double-body method was employed within their computer program for multi-body cases involving ships and port structures. Real time interaction forces and moments were fed into the simulator using high speed computers to solve the flow equations. However, the final results were found to be highly sensitive to the initial conditions, which were tedious to set-up.

Sutulo et al. (2012) developed a PF double-body panel code on the basis of the classic Hess and Smith (Hess & Smith, 1964, 1967) method to estimate interaction effects in real time on commonly used computer hardware. The results obtained with the code were validated against experimental data obtained in deep and shallow water towing tanks for a tug operating near a larger vessel. The results illustrated the potential of the PF double-body panel method for predicting interaction effects, while highlighting the lack of accuracy in predicting the sway forces at small horizontal clearances. It was expected to be more pronounced in non-parallel operations, similar to those encountered during tugs assisting ships. Fonfach et al. (2011) did experimental and numerical investigations to explore the contribution of various factors to interaction effects, which were not accounted for by the PF method. They revealed substantial influence of free-surface effects on the accuracy of predicted interaction effects.

Many researchers (Doctors, 2006; Doctors & Beck, 2005; Eliasson & Olsson, 2011; Mantzaris, 1998; Mierlo, 2006; Pranzitelli et al., 2011) have investigated the capabilities of PF methods to study various hull shapes, especially transom stern hulls with free surface. Pranzitelli et al. (2011) studied the free-surface flow around a semi-displacing transom stern motor-yacht advancing steadily in calm water using both a PF method and Computational Fluid Dynamics (CFD), and comparing them to Experimental Fluid Dynamics (EFD) results. It was found that the results generated from the PF method were substantially different because of the inability of its panels to ‘roll-down’ and intersect with each other during iterations. The researchers concluded that the presence of the free-surface can make more complicated discretisation, resulting in numerical problems for complex geometries, such as for transom stern hulls.

Considering the interaction effects on a tug during ship-assist, the rapid changes of tug drift angle cause a large portion of the downstream wake due to the hull to be characterised by a bluff body flow in a similar manner to a wet transom flow, as shown in Figure 2.1. Thus, it is essential to select a flow solver that can accurately solve such conditions during real-time predictions. Therefore, this study aims to examine the accuracy of the drag force prediction by a PF solver in wet transom conditions, as a case study to investigate its suitability for use in complicated real-time interaction effects analysis of tugs operating at a drift angle.

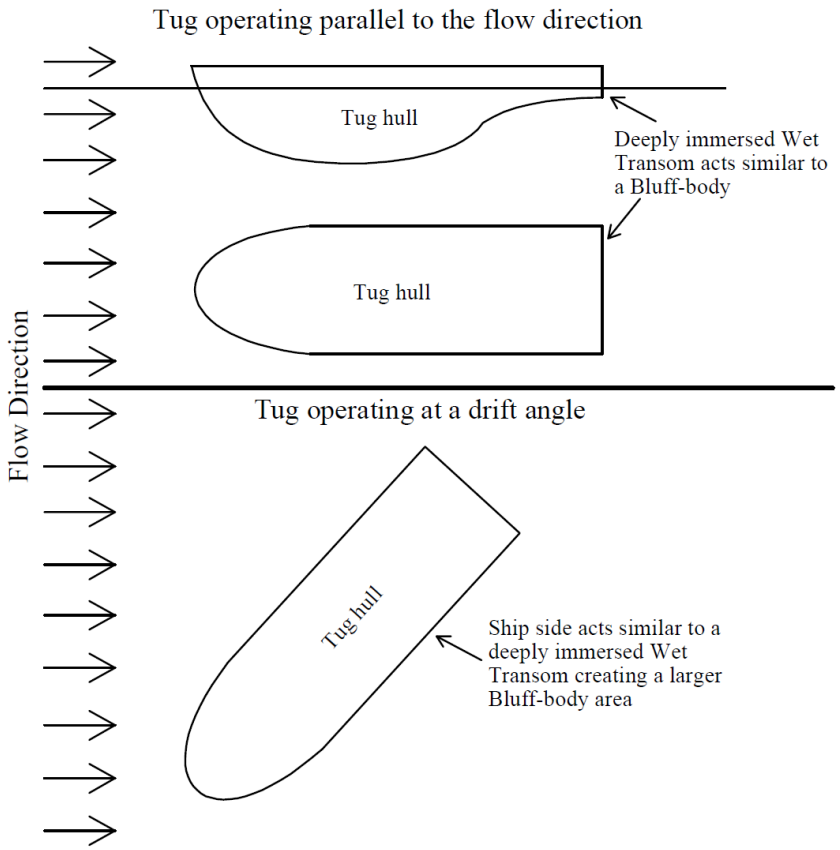

Figure 2.1: Tug operating parallel to the flow (top) and operating at a drift angle (bottom).

In order to employ a PF solver for real-time interaction effect prediction, it must be capable of solving the nonlinear free surface effects and incorporate viscous resistance into the analysis. The PF package Futureship®, which meets the above requirements was available at the Australian Maritime College (AMC) and thus it was utilised in this study. FS-Flow® is the module used within Futureship® for Rankine-Source panel code analysis (DNV GL Maritime, 2014). FS-Flow® solves the boundary value problem of potential theory including the

nonlinear free-surface. The PF approach assumes that the fluid is inviscid and the flow is irrotational around the bodies. Hence, FS-Flow® is equipped with a separate module capable of calculating the viscous resistance in terms of a friction line in combination with the wetted hull surface. Therefore, the dynamic forces, static forces, and viscous forces acting on the bodies are included in the final results, although the fluid is considered as inviscid within PF. The total resistance and its components obtained from the PF solver was then compared against captive model experiments and CFD results generated by the commercial CFD code StarCCM+® to investigate the possibility of using the PF software for future analysis of interaction effects.

2.2 Numerical Analysis

The set-up and relevant features of the two commercial software packages, FS-Flow® and StarCCM+®, are provided below.

2.2.1 Hull form and coordinate system

A 1:20 scaled hull model of the AMC's 35 m training vessel MV Bluefin was utilised in this study. The particulars of the full and model-scale hulls are given in Table 2.1. The two test conditions analysed to investigate the effects of transom generated complex flow regimes were:

- dry transom with a model draft of 0.17 m; and
- wet transom with a model draft of 0.18 m.

Table 2.1: Main Particulars of the Hull Form.

Main Particulars	Unit	Full-scale	Model-scale
Length Waterline	m	32.150	1.608
Wetted Surface area	m^2	384.15	0.96
Dry Transom Draft	m	3.48	0.17
Wet Transom Draft	m	3.60	0.18

A three-dimensional model-scale hull form was developed using the commercial software Rhinoceros® 5.0V and imported into the two packages. The coordinate system for the analysis is shown in Figure 2.2. The flow velocity vector was in the positive X direction while the horizontal plane through the origin was considered as the free surface.

2.2.2 Domain and Mesh in FS-Flow®

Flow velocities ranged from 0.34 m/s to 1.04 m/s in model-scale, acting along the positive X direction, with the vessel allowed to trim and heave during the analysis. The free surface had a rectangular shape, with the inlet boundary at a distance equal to the scaled model waterline length (L_m) upstream of the origin, the outlet boundary at $3L_m$ downstream from the origin, and a total domain width of $1.1L_m$. The dimensions were selected to match those of the AMC towing tank, except for the length, which was shorten to reduce the computational effort without adversely affecting wake resolution. The mesh configuration is illustrated in Figure 2.2, which was developed in FS-Flow®.

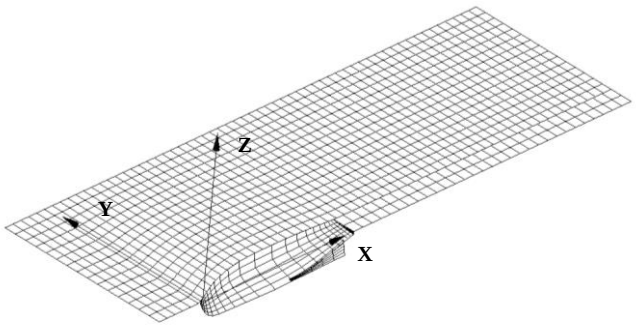

Figure 2.2: Coordinates system and Ship Model with Free surface in FS-Flow®.

The mesh independence study was conducted through mesh refinements without affecting the stability of the solver. The drag coefficient at a forward speed of 1.04 m/s was tested for dry transom condition for the models with different panel numbers to obtain an appropriate mesh. This approach provided sufficiently accurate results while maintaining low computational effort. The finest mesh investigated had 4220 panels; while a 3490 panel mesh was selected as a suitable mesh for steady-state simulations as its predictions were within 1.5% of that for the finest mesh (see Figure 2.3).

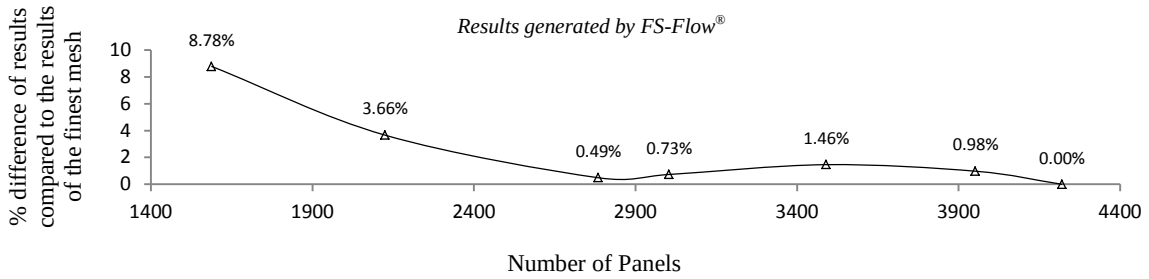

Figure 2.3: Absolute % difference of Drag Coefficient against finest panel mesh for the FS-Flow® model.

2.2.3 Set-up and Mesh in StarCCM+®

StarCCM+® uses a finite volume technique to solve the Reynolds Averaged Navier-Stokes (RANS) equations (CD-Adapco, 2015). In order to directly compare the CFD and EFD results, the width and depth of the AMC towing tank were replicated in the numerical fluid domain, although the length was reduced to 10.0 m to decrease the mesh load while ensuring the pressure and wake fields generated by the hull were sufficiently resolved within the domain. In addition, since the flow around the hull is symmetrical about the centerline, only the starboard half of the hull was modeled in order to reduce the computational domain and thus the associated computational effort. The vessel was fixed in all degrees of freedom, using trim and heave conditions obtained from the captive model test results. The computations were performed using hexahedral trimmed mesh generated by StarCCM+®. Following a mesh independence study (Figure 2.4), a mesh with approximately 3.5 million cells was selected for the investigation as the percentage difference reduced to below 0.5% beyond this size mesh.

The near wall spacing on the vessel is defined using the dimensionless distance (y^+) measured from the wall surface to the edge of the first layer. The resolution of the boundary layer was estimated by prescribing the number of inflation prism layers, the growth rate, and the first node distance from the wall (y^+) reflected by the non-dimensional distance value (y^+), as defined in Equation 2.1.

$$y' = L_m \times y^+ \times \sqrt{80} R_e^{\frac{-13}{14}} \quad (2.1)$$

where L_m is the waterline length of the model hull and R_e is the length-based Reynold's number.

The minimum total thickness of the inflation layers around the hull was matched to 2 times Prandtl's 1/7th power law theoretical estimate of turbulent boundary layer thickness over a flat plate, i.e. 2×0.16 L_m / $R_e^{1/7}$ (Leong, 2014; White, 2003). The y^+ study was conducted between y^+~1 to y^+~100 with the k-ω Shear Stress Transport (SST) turbulence model, which change from the low Reynolds number wall treatment model to the empirical-based wall function formulation around y^+=10. From Figure 2.5 it is seen that the % variation of the drag coefficient is approximately 5% at a y^+ of 30. Thus, y^+~30 was selected as a compromise between accuracy and solver time. However, it should be noted that this y^+ value is acceptable for longitudinal flow, but too high for oblique flow which would require a y^+ less than 1 (Leong et al., 2014). Customised anisotropic refinement was applied to the free-surface region (Figure 2.6) to resolve the wave field around the hull.

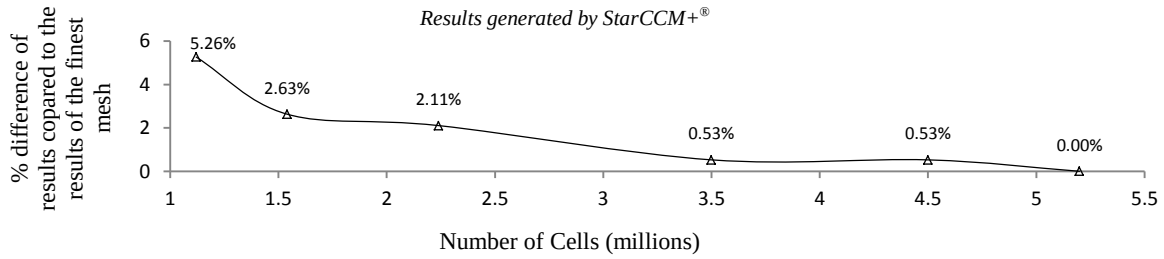

Figure 2.4: CFD grid independent study: Absolute % difference of Drag Coefficient against finest mesh.

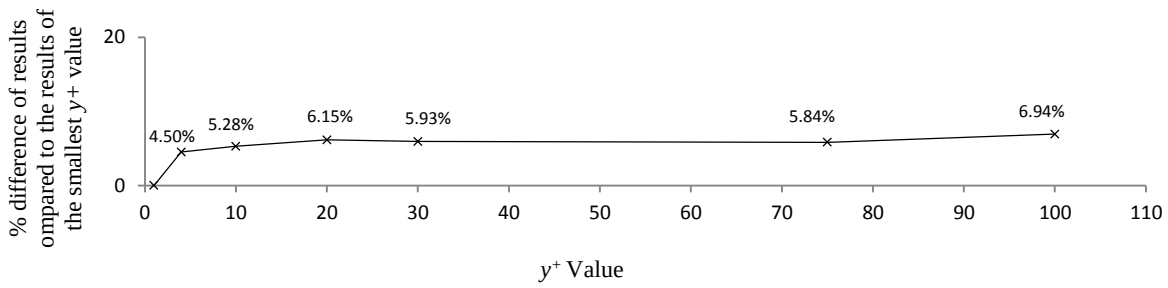

Figure 2.5: CFD near wall mesh (y^+) study: % difference of Drag Coefficient against y^+~1 mesh.

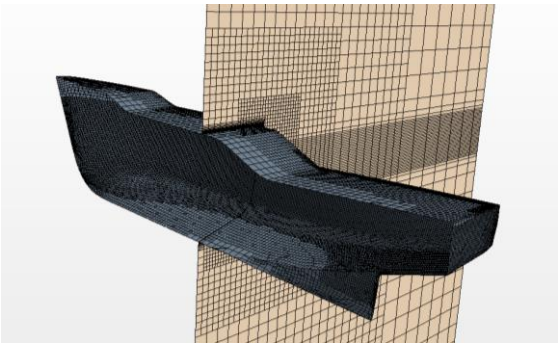

Figure 2.6: Hexahedral 3.5 million cells mesh used in StarCCM+®.

Simulations were treated as implicit unsteady, conducted for 25 s durations with a 0.024 s time step and 10 inner iterations. The free surface was modelled using the Euler Multiphase and the volume of fluid technique, with the inflow considered as a flat wave having a particular velocity. The drag force acting on the vessel was calculated for similar speeds and drafts as used in the PF-based simulations.

2.3 Experimental Set-up

Captive scaled model experiments were performed in AMC's 100 m (length) x 3.55 m (width) x 1.5 m (depth) towing tank (Figure 2.7). The scaled hull model, which was allowed to trim and heave, was attached below the towing carriage using one strain gauge and two Linear Voltage Displacement Transducers (LVDTs). Experiments were conducted using the two different drafts for the hull model. At the lower draft, i.e. 0.17 m, the transom was in the dry condition, while at the higher draft, i.e. 0.18 m, it was wet. Both conditions were tested at speeds ranging from 0.34 m/s to 1.04 m/s in model-scale.

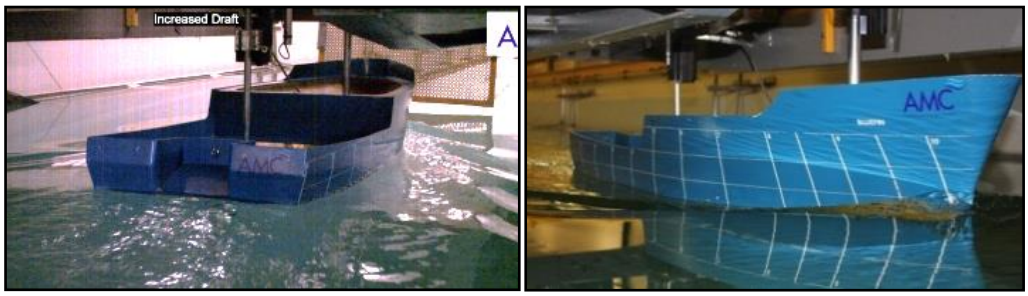

Figure 2.7: Experimental testing in AMC Towing Tank; Stern view (Left), Bow view (Right).

2.4 Results and Discussion

2.4.1 Drag coefficient and Friction coefficient

The drag forces obtained from the numerical and experimental work were non-dimensionalised to obtain the drag coefficient *(C_T)* as shown in Equation 2.2. The frictional resistance coefficients *(C_F)* given in Equation 2.3, obtained from the numerical results were compared against the ITTC correlation line. The latter was developed based on the Hughes version of a flat plate friction line incorporating a shape factor of 0.1194 is given in Equation 2.4 (ITTC, 2011a).

$$C_T = \frac{R_T}{\frac{1}{2}\rho S V^2} \tag{2.2}$$

$$C_F = \frac{R_F}{\frac{1}{2}\rho S V^2} \tag{2.3}$$

$$ITTC\ correlation\ line = \frac{0.075}{(\log_{10} \mathrm{R_e} - 2)^2} \tag{2.4}$$

The computing resource used to perform the PF computations were 8 CPU cores, with a total RAM of 8GB. It took an average of 90 seconds to solve one case in PF solver. For CFD simulations a High Performance Cluster (HPC) was utilised. The average time for a CFD simulation was 3 hours with 24 CPU cores.

2.4.1.1 Dry transom with a model draft of 0.17m

In this condition the transom remained dry above the waterline, giving a streamlined water-plane. The non-dimensionalised drag force results from EFD, PF code FS-Flow® (PF), and CFD are plotted against the Length Froude number (F_r) in Figure 2.8. ITTC (2002) guidelines were used to estimate the EFD uncertainty, which is 11.8%, plotted on the figure using error bars.

The numerical and EFD results have a similar trend except at the lowest F_r, where the numerical models tend to over-predict. This may be due to the inaccurate prediction of

laminar to turbulent transition region on the scaled experimental model. However, the PF and CFD remain similar even at low F_r, with the maximum difference between the PF and CFD results being 15%, while the maximum difference between the PF and EFD results is 7.2%, except at the lowest F_r, as discussed previously.

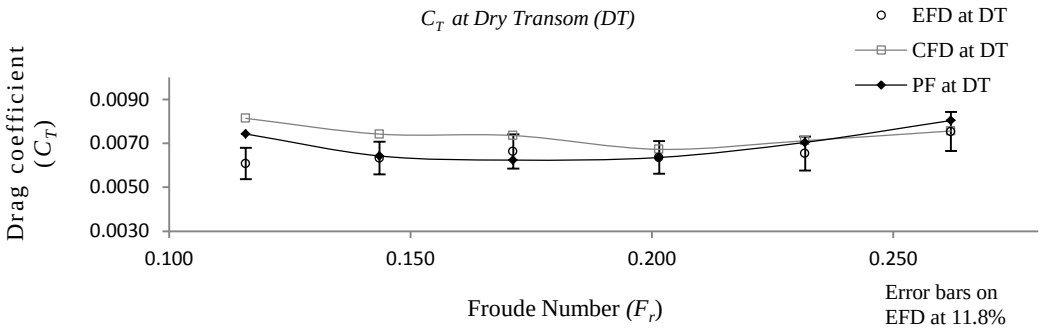

Figure 2.8: C_T comparison for dry transom condition. EFD uncertainty estimated using ITTC 2002 guidelines.

The results indicate that the viscous module integrated within FS-Flow® has good prediction capability. In order to verify its accuracy, the frictional resistance coefficients (C_F) obtained from the PF and CFD simulations were compared against the ITTC correlation line as shown in Figure 2.9. The C_F from the PF method correlates well with the ITTC line with a maximum difference of 5%, whereas the CFD values are slightly below the ITTC prediction with an average difference of 15%. A finer mesh with different turbulence models and a smaller y^+ may improve the CFD results. This was not carried out in this chapter since its aim was to investigate the accuracy of the PF solver. The results of the finer mesh and smaller y^+ are presented in Chapter 3. From Figure 2.8 it is clear that the PF solver in FS-Flow® is suitable to solve flow around well streamlined hull geometries.

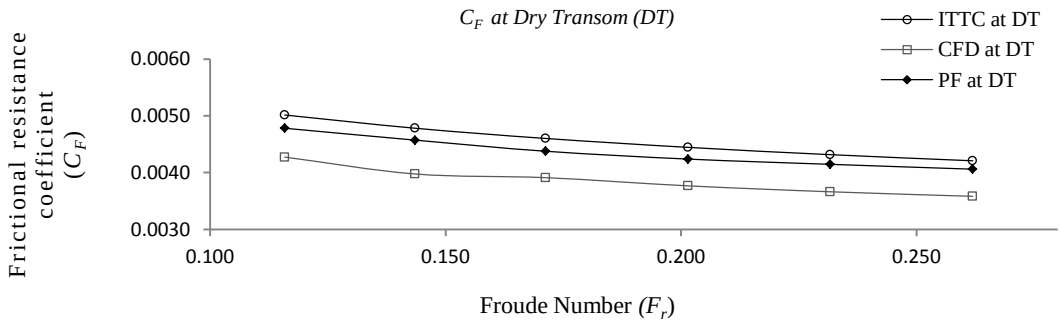

Figure 2.9: C_F comparison for dry transom condition.

2.4.1.2 Wet transom with a model draft of 0.18m

In order to test FS-Flow®'s ability to solve wet transom conditions, the model was tested at the higher draft. The non-dimensionalised EFD, CFD, and PF drag forces in this condition are plotted against F_r in Figure 2.10.

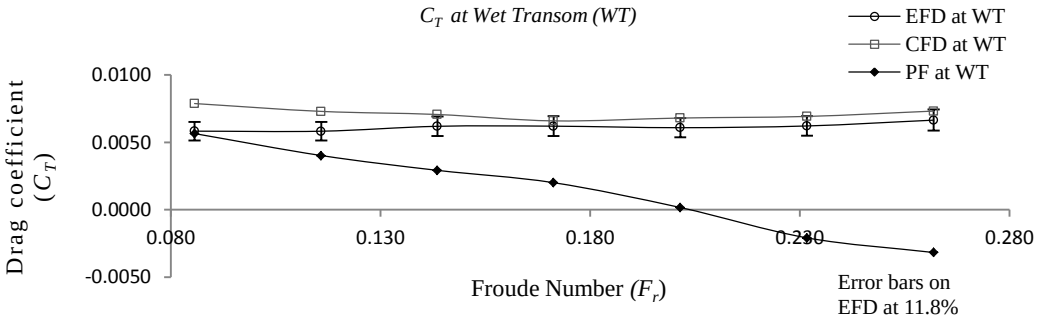

Figure 2.10: C_T comparison for wet transom condition. EFD uncertainty estimated using ITTC 2002 guidelines.

It is evident that the CFD and EFD results are in good agreement throughout the F_r range. However, the PF results, although relatively close to the EFD at low F_r, significantly under predict C_T as F_r increases. Interestingly, the direction of C_T changes sign around F_r of 0.2, implying the drag force on the vessel acts opposite to the flow direction, a physical impossibility. Since the total drag is made up of viscous, pressure, and wave making components, it is necessary to decompose the resistance into the different components to identify the real cause for this discrepancy.

First considering the viscous drag force, a comparison was made between the results obtained by the PF solver, the CFD shear force, and the ITTC correlation line, presented in Figure 2.11. It is apparent that the viscous force generated by PF is in agreement with the ITTC correlation line, which is similar to the results obtained in the dry transom conditions previously discussed in section 2.4.1.1.

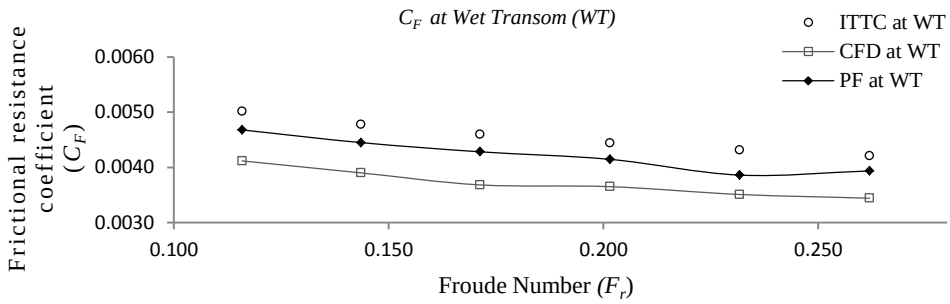

Figure 2.11: C_F comparison for Wet Transom condition

2.4.2 Wave pattern and pressure contours

Since the results discrepancy was not related to the viscous effects, the residuary components were next investigated, especially since the error increased significantly with F_r. Thus, the free surface wave patterns generated by the PF and CFD simulations, as well as photographs of the wave patterns from the EFD work at a speed of 1.04 m/s were compared to identify the influence of wave making resistance. Figure 2.12 provides the PF, CFD and EFD wave patterns for wave heights between ±0.03 m.

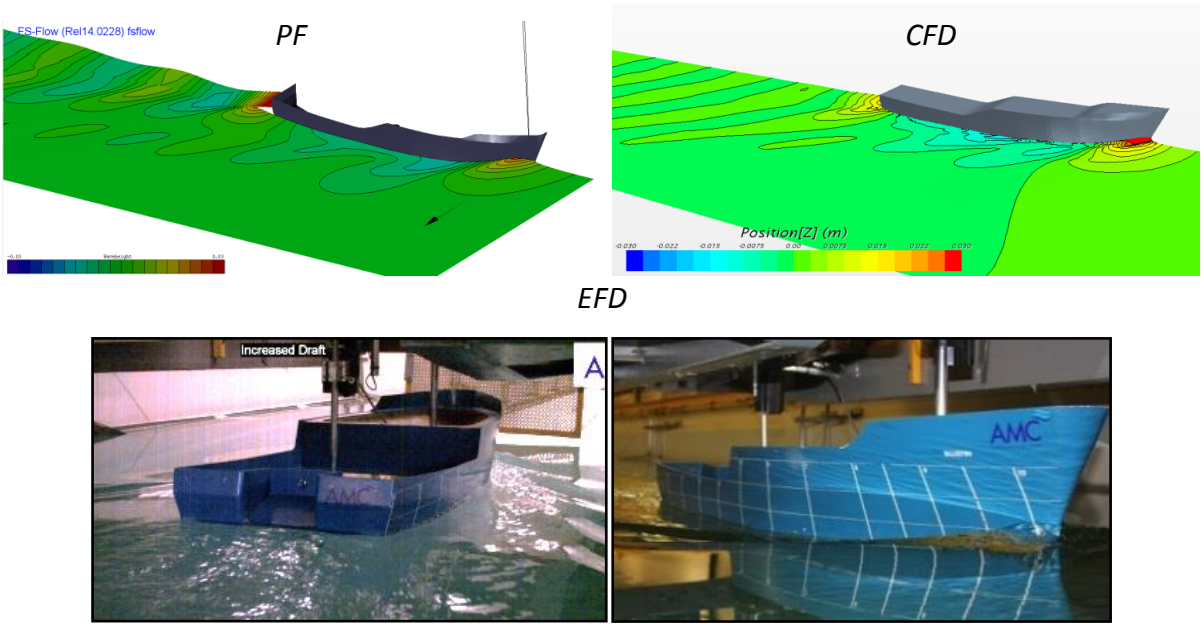

Figure 2.12: Free surface waves heights in PF, CFD and EFD.

It is clearly seen from these plots that the waves generated by PF are not in agreement with

those obtained from EFD and CFD. Notable, the stern wave generated by PF is the highest in magnitude, whereas as expected, the CFD predicts the bow wave to be the largest wave, similar to the EFD results in Figure 2.7. The inaccurate wave pattern predicted by the PF simulations will create a high pressure region at the stern of the hull, which can result in a negative drag force. In order to verify this, the Dynamic Pressure Coefficient (C_P) generated by PF was examined and is shown in Figure 2.13 (a).

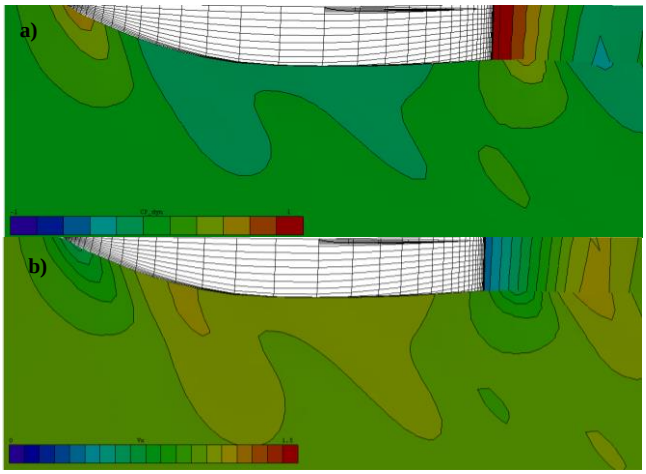

Figure 2.13: a) Dynamic Pressure Coefficient and b) Velocity contour generated by PF

As suspected, the PF code has a high positive pressure region at the stern due to the weakness in predicting the velocity component in y-direction within the transom mesh. This creates a very low horizontal velocity at the transom as shown in Figure 2.13(b), and hence a corresponding high pressure region creating negative drag force on the vessel. Since this unrealistic result occurred due to the wet transom, it was decided to check the drag force generated by the PF code without the transom mesh (Figure 2.14) at a 0.18 m draft, with the results plotted against the F_r in Figure 2.15.

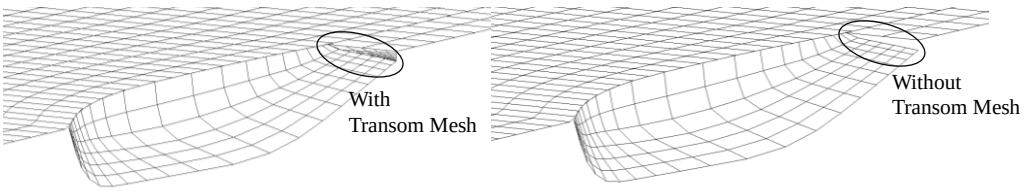

Figure 2.14: PF hull with (Left) and without (Right) transom mesh

2.4.3 Results without Transom Mesh

It is interesting to note that when the transom mesh is omitted from the hull, the accuracy of the drag force predicted by the PF simulation is appreciably improved showing good agreement with the EFD and CFD results (Figure 2.15). Removing the transom mesh mitigated the error attributed to insufficient resolution of the large pressure gradient on the hull and poor numerical conditioning of the pressure integration (Doctors, 2006; Doctors & Beck, 2005; Maki, 2006; Saha & Tarafder, 2013; Tarafder et al., 2009).

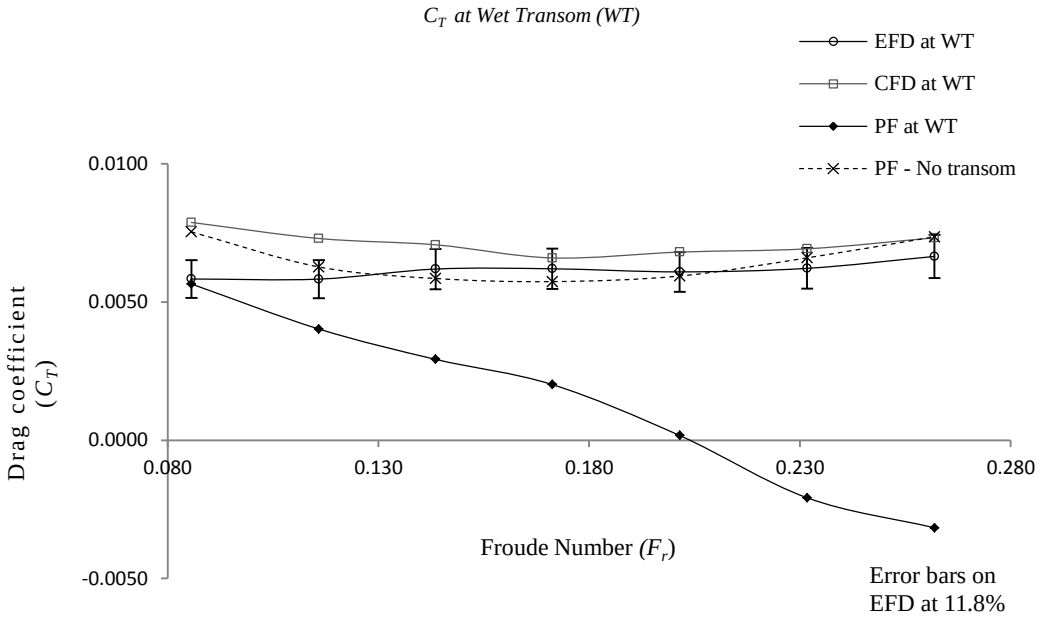

Figure 2.15: Comparison for wet transom condition, including the PF results without the transom mesh.

Thus, it is important to investigate the possibility of utilising this finding to conduct interaction effects analysis during ship handling operations. During such operations, tugs can dramatically change their drift angle to maintain the course of the ship. If the PF code is used to solve such cases, a suggested panel generation scheme is shown in Figure 2.16.

As illustrated in Figure 2.16, when the drift angle changes, the downstream side of the tug hull is characterised by the bluff body effect, similar to that of a wet transom situation as discussed previously in Section 2.4.1.2. However, unlike the wet transom situation, in this

case the leeward side represents a large portion of the vessel's side hull. Thus, if the downstream transverse mesh panels are removed, a significant part of the hull mesh would be omitted. The removal of the transverse mesh panels would then results inaccuracy and stability issues within the PF simulation if it is used for solving interaction effects on drifted vessels.

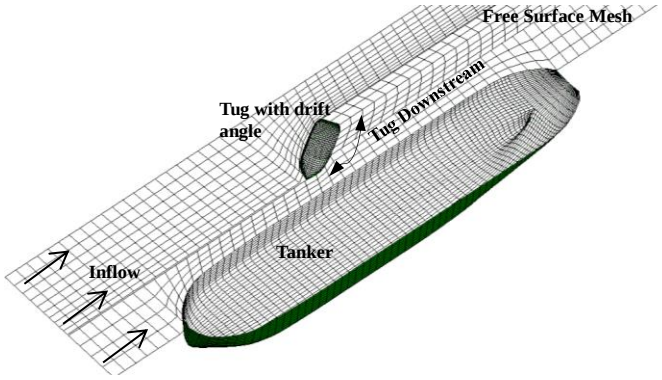

Figure 2.16: Ship handling Operation: Panel generation in PF.

2.5 Conclusion

In this chapter the drag forces acting on a transom stern hull operating under wet and dry transom conditions were investigated using PF, CFD, and EFD methods. The aim was to identify the accuracy of the PF method to determine real-time interaction effects acting on a tug operating in close proximity to a tanker within ship handling simulators. For the dry transom flow, the PF solver showed very good agreement with the EFD and CFD results. However, it failed to do so for the wet transom condition, especially at higher F_r. Further investigations revealed that these discrepancies were due to the PF solver's weaknesses in predicting the flow velocity around the transom, which is at near right angles to the flow direction.

It was identified that if FS-Flow® is used to estimate drag forces on wet transom hulls of tugs operating parallel to the flow, it is necessary to omit the transom stern mesh panels. Thus, it is suitable to estimate the forces acting on well streamlined bodies across the length based F_r range, including the viscous effects. However, this is not feasible when the tug is at a drift

angle, as the mesh panels affected will represent one full side of the vessel, thus adversely affecting the mesh domain. Therefore, it was identified that the investigated PF solver, FS-Flow®, is limited in its ability to predict real-time interaction effects within ship handling simulators, especially in manoeuvrers such as ship-assist operations.

Currently the authors are conducting CFD studies to predict the offline interaction effects acting on a tug with varying drift angles operating in close proximity to a large tanker, with validation through EFD. The quantified results will be then used to feed into AMC's ship handling simulator via a database in order to predict real-time interaction effects.

Chapter 3

Accuracy and the Modelling Techniques of RANS based CFD Simulations for Hydrodynamic Interaction Prediction

This chapter has been reviewed and accepted for publication in the Journal of Marine Science and Technology. The citation for the research article is:

Jayarathne, N., Ranmuthugala, D., Leong, Z.Q., Fei, G. & Chai, S. (2017), 'Numerical and Experimental Prediction of Hydrodynamic Interaction Effects Acting on Tugs during Ship Manoeuvres', *Journal of Marine Science and Technology* (Accepted for publication).

ABSTRACT

The role of tugs is significant when assisting ships with limited manoeuvring capabilities. Hence, knowledge of the hydrodynamic interaction effects that act on a tug under these operations is of great practical value for the tug master in order to avoid damage, collision, or capsizing. Computational Fluid Dynamics (CFD) simulations are increasingly being adopted as a tool of analysis for determining the interaction effects in such vessel manoeuvres. However, one of the major challenges faced in CFD, is that the results can vary greatly depending on the numerical model settings. This chapter investigates modelling techniques and the accuracy of CFD generated interaction forces and moments acting on a tug hull operating at different drift angles, and at lateral and longitudinal locations along a tanker hull against Experimental Fluid Dynamics (EFD) data.

3.1 Introduction

The role of tugs is significant when assisting ships with limited manoeuvring capabilities at slow speeds in restricted waters. However, the hydrodynamic interaction between these vessels can adversely affect the handling and safety of the much smaller tugs, which in extreme cases can lead to the latter capsizing or colliding. “Dangers of interaction” (MCA, 2001) is a guidance note prepared by the Maritime Coastguard Agency in the United Kingdom to draw the attention of ship owners, pilots, and ship and tug masters to the effects of hydrodynamic interaction on vessel manoeuvrability. It states that when vessels are being manoeuvred at close quarters for operational reasons, the greatest potential danger exists when there is a large difference in size between the two vessels and it is most commonly experienced when a ship is being attended by a tug (MCA, 2001).

The Marine Accident Investigation Branch (MAIB, 2011) report strongly suggests mariners to familiarise themselves with the ‘Dangers of interaction’ guidelines in order to be alert to dangerous situations caused by hydrodynamic interaction effects during these operations. One aspect of the training to meet these requirements is the use of appropriate simulators for those who operate ships and tugs, to familiarize themselves with interaction effects during critical manoeuvres. For these simulators to replicate actual behaviour, it is essential that the interaction effects are accurately determined by mathematical models to provide seafarers with realistic experiences. However, the pursuit of accuracy should not affect the ability to provide real-time responses within simulators. Thus, many studies such as: Vantorre et al., (2002), Sorensen et al., (2009), Falter, (2010), Geerts et al., (2011), Lindberg et al., (2012), Sutulo et al., (2012), Pinkster and Bhawsinka, (2013) have been carried out to improve predictions of the interaction effects in simulators, without adversely affecting their accuracy and real-time responses.

Sutulo et al., (2012) identified Potential Flow (PF) theory as one of the best methods for the prediction of real time interaction effects within simulators. They conducted model-scale experiments to measure the interaction effects acting on an azimuth stern drive tug operating in close proximity to a conventional tanker. These tests were conducted in both

shallow and deep water using a tug model placed in various heading angles and positions around the tanker model. However, only those where the vessels were parallel to each other (referred to as parallel operations) were compared and discussed against the PF code results in their study. The results illustrated the capability of the PF method to predict interaction effects, while highlighting a lack of accuracy in predicting the lateral force and yaw moment at small horizontal clearances, which was expected to be more pronounced in non-parallel operations, i.e. vessels with different drift angles. These findings were supported by work carried out by the authors in Jayarathne et al., (2014) through comparative numerical and experimental investigations that identified inaccuracies in the forces along the hull calculated by PF methods for a tug with a transom stern hull. The study also showed that the results obtained through Reynolds Averaged Navier-Stokes (RANS) based Computational Fluid Dynamics (CFD) simulations were in good agreement with experimental measurements.

A CFD-based study of the interaction between a tug and a large tanker sailing in parallel was undertaken by Fonfach et al., (2011). They used inviscid flow, turbulent viscous flow, inviscid free surface flow, and viscous free surface flow theories with Standard Spalart-Allmaras (SA) and Shear Stress Transport (SST) turbulence models in their study. The target cell size near the tug was maintained as 0.0025 times the tug length. They observed large discrepancies in the results predicted by all flow models at small lateral clearances, especially for the lateral force. Due to time constraints, the authors did not conduct a mesh convergence study in their investigation, thus the accuracy of the selected turbulence model and the near wall cell size cannot be verified with the available data. Nevertheless, their results showed that the CFD model with both the viscous and free surface effects had better agreement with experimental data compared to the other flow theories utilized.

Simonsen et al., (2011) did a CFD-based study on a subset of cases taken from model-scale experiments studying quasi-steady ship-to-ship interaction effects. A tug was located at a number of longitudinal and transverse positions alongside a tanker for parallel operations. However, it was locked near the midship of the tanker for the drifted tug analysis, with the tug angle varying from 0 to 60 degrees. The authors had done a semi-systematic refinement for the initial CFD grid and checked the trend of the solution, with the non-dimensional wall

distance of first inflation layer (y^+) on the no-slip surfaces for the simulations maintained at between 1 and 30 with the SST turbulence model. Their CFD results showed poor agreement with the experimental data for the lateral force acting on the tug at selected tug drift angles. The cause of the error was inconclusive as the study did not quantify the experimental or numerical uncertainties.

In this way, a number of researchers have used experimental and CFD methods to predict forces and moments acting on tugs during ship handling. However, their investigations have covered only limited operational scenarios including parallel operation and limited drift angles at fixed locations relative to the larger vessel. Furthermore, the numerical and experimental uncertainties were not clearly quantified when making comparisons against experimental work. Therefore, the causes of the discrepancies between CFD and the experimental data are hard to identify. This chapter extends the above findings by investigating the capability of CFD to predict the interaction effects acting on tugs during ship handling at parallel and drifted operations at different lateral and longitudinal locations along a tanker (i.e. the larger vessel). The CFD simulation results generated by StarCCM+® for different tug-ship combinations were compared against captive model-scale test results obtained via a series of experiments conducted in the Model Test Basin at the Australian Maritime College (AMC). Finally, the chapter explores the effect of the CFD modelling factors, such as the turbulence model, application of y^+ in the near-wall mesh, and the quality of the mesh model on force and moment predictions.

3.2 Numerical Simulations

3.2.1 Selection of Ship Models

For the study of tug-ship interaction, the CFD simulations consisted of generic model-scale hulls of a stern drive tug and a MARAD-F series tanker with a length ratio of 1:2.4 between

the two vessels. The vessel particulars are given in Table 3.1 and the coordinate system for the analysis is shown in Figure 3.1.

Table 3.1: Principal dimensions of the selected hull forms.

Main Particulars	Unit	Tanker		Tug	
		Full-scale	Model-scale	Full-scale	Model-scale
Length Overall	m	75.60	4.20	31.16	1.732
Length Waterline	m	72.00	4.00	28.46	1.581
Breadth	m	13.12	0.729	11.50	0.639
Draft	m	4.42	0.246	3.55	0.197
Scale	-	1	1/18	1	1/18

Throughout the analysis the tug was located on the port side of the tanker, with a range of lateral distances (δy) and longitudinal locations (δx) as shown in Figure 3.1.

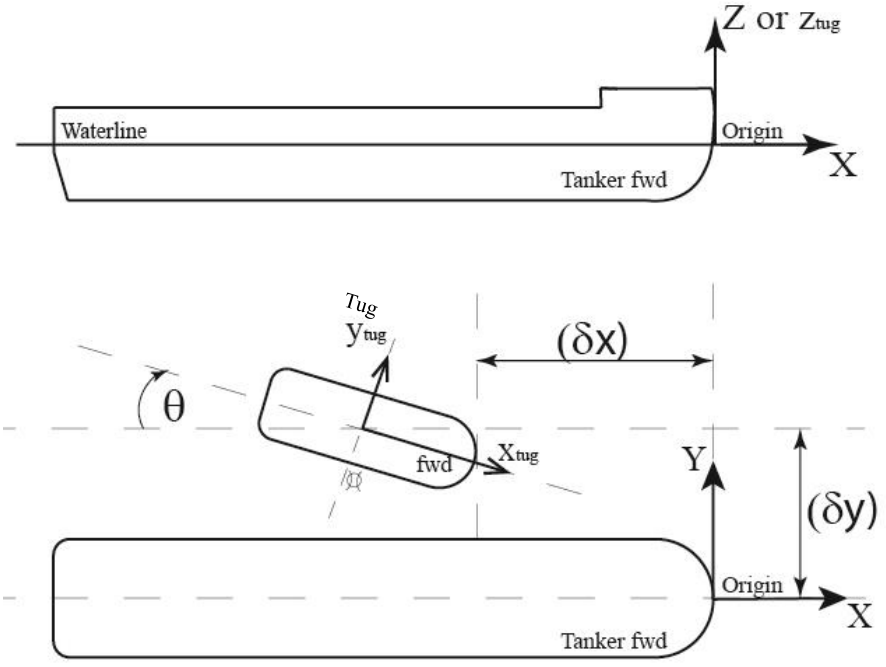

Figure 3.1: Local (tug) and global coordinate systems and vessel locations.

The three-dimensional model-scale hull form geometries were developed using the commercial software Rhinoceros® 5.0V as shown in Figure 3.2 and imported into StarCCM+®.

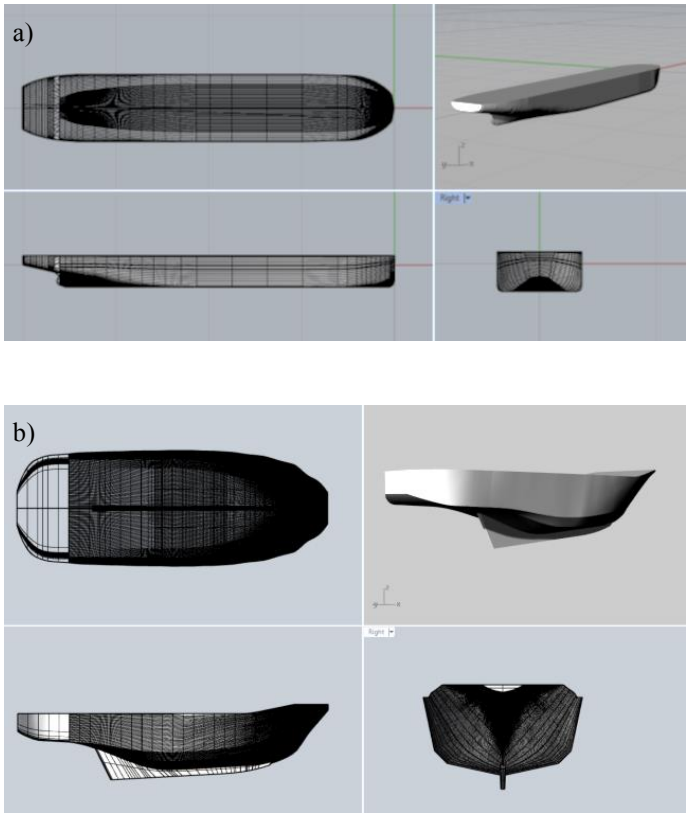

Figure 3.2: 3D hull forms: (a) MARAD-F series tanker, (b) stern drive tug.

3.2.2 Non-Dimensionalisation of Results

The hydrodynamic longitudinal force (*X*), lateral force (*Y*), and yaw moment (*N*) acting on the tug were non-dimensionalised for CFD and EFD comparisons based on the volumetric displacements of the hulls using Equations 3.1 to 3.3 as previously employed in similar studies (Fonfach et al., 2011; Simonsen et al., 2011; Sutulo & Soares, 2009).

$$C_X = \frac{2X}{u^2 \nabla_t^{1/3} \nabla_s^{1/3} \rho} \tag{3.1}$$

$$C_Y = \frac{2Y}{u^2 \nabla_t^{1/3} \nabla_s^{1/3} \rho} \tag{3.2}$$

$$C_N = \frac{2N}{u^2 \nabla_t^{1/3} \nabla_s^{1/3} L_t \rho} \tag{3.3}$$

The lateral (Δy) and longitudinal locations (Δx) of the tug were also non-dimensionalised using tanker dimensions as defined in Equations 3.4 and 3.5 respectively (Fonfach et al., 2011; Simonsen et al., 2011; Sutulo & Soares, 2009).

$$\Delta y = \frac{\delta y}{B_s} \tag{3.4}$$

$$\Delta x = \frac{\delta x}{L_s} \tag{3.5}$$

3.2.3 Numerical Set-up

The finite volume based StarCCM+® package was used to solve the RANS equations employing three different turbulence models, i.e. Realizable Two Layer k-ε (RKE), Shear Stress Transport (SST), and Spalart-Allmaras (SA) (CD-Adapco, 2015). However, for the mesh sensitivity study, only the SST turbulence model was utilized. The implicit unsteady simulations were carried out with the free surface modelled as an Euler Multiphase, using the Volume of Fluid technique (CD-Adapco, 2015). For the accuracy of results, it is important to establish a suitable grid after evaluating the effects of the total thickness of inflation layers around the tug and y^+ of the first inflation layer. Leong et al., (2014) verified that the thickness of the inflation layers around a body should be at least 1.5 times of Prandtl's 1/7th power law (1.5x0.16L_t/$Re_{Lt}^{1/7}$) estimate of the turbulence boundary layer thickness over the surface length (White, 2003). Thus in this study, the total thickness of the boundary layer was maintained as 2.0 times Prandtl's 1/7th power law estimate, and the inbuilt prism layer mesher (CD-Adapco, 2015) was used to generate high quality near wall cells with y^+~ 0.5.

Both the tanker and tug geometries were locked in all degrees of freedom throughout the analysis. The upstream end of the domain was considered as a velocity inlet, the downstream end as a pressure outlet, the side and bottom surfaces as walls, and the top boundary was also considered as a velocity inlet (Figure 3.3). The latter significantly increases the simulation's stability and reduces the simulation time, while maintaining the

same degree of accuracy for free-surface simulations compared to a slip wall boundary (CD-Adapco, 2015; Tezdogan et al., 2015). The depth of the water during the experiments was maintained at 0.8 m, which was replicated in the CFD simulations. The water depth to draft ratios for the tanker and tug were 3.25 and 4.06 respectively, which represent the deep water condition as outlined in PIANC, (1992).

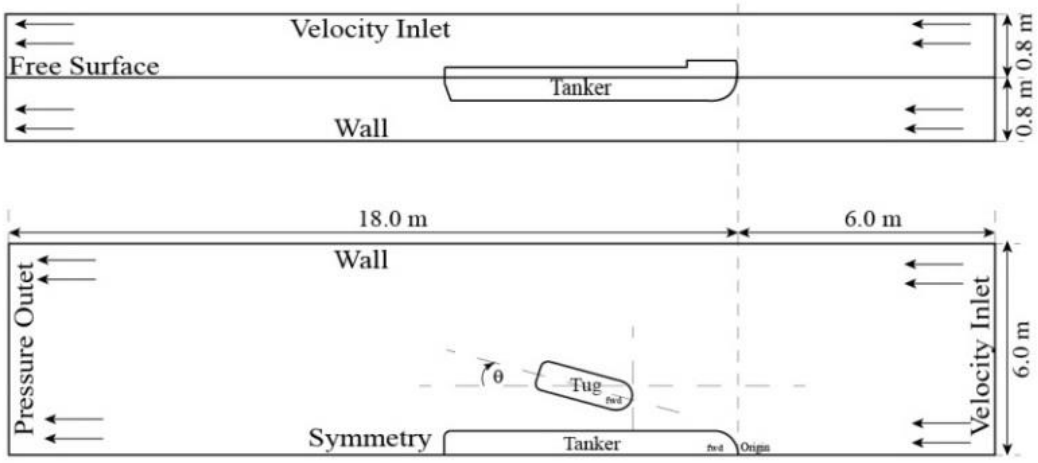

Figure 3.3: Computational domain used in StarCCM+® simulations.

Fonfach, (2010) and Fonfach et al., (2011) used a symmetry plane modelling technique for their studies of interaction effects to significantly reduce the computational effort by reducing a large number of cells. A similar approach was also employed in this study with only the Port half of the tanker modelled, with the use of a symmetry plane to reduce computational effort. To check the effect of the symmetry plane on the interaction predictions, compatible simulations were carried out using two different domains, one consisting of the complete tanker hull and the other the half tanker hull with the symmetry plane. The meshing scheme and solver settings were kept identical to the current simulation setup for both cases. The tug drift angles of zero, 15 and 30 degrees were investigated using the two different computational domains. The lateral separations of Δy_{ship}= 2.190 and 2.276 were investigated at 0.41 m/s speed while maintaining the tug at $\Delta x = 0$ longitudinal location. The maximum difference between the forces and moments on the tug obtained for the two simulation domains were within 0.5% of each other, and this was deemed acceptable for the current study. Therefore, all simulations for the study were conducted

with the half tanker hull with the symmetry plane domain. The trimmed cell mesher (CD-Adapco, 2015) was used to generate unstructured, rigid, hexahedral fixed cells within the simulation domain. Cell sizes were refined using the volumetric control option in certain areas around the tug and the free surface to ascertain a progressively refined grid to capture the complex flow features.

All the CFD cases were simulated in double precision mode with the variables of interest converging to four significant figures over 50 iterations to mitigate the truncation error. For the CFD simulations, due to the presence of turbulence stimulators in the experiments, a fully turbulent wall treatment model was used. See Gui L. et al., (2000); Olivieri A. et al., (2001); Shi Xun et al., (2010); Yoon H., Longo J., et al., (2015); Yoon H., Simonsen C.D., et al., (2015) for similar work, and Section 3.4.2 for additional information on the turbulence stimulators employed. No overset mesh was employed since there was no relative motion between the vessels.

3.3 Verification Study

The verification conducted consisted of mesh sensitivity, y^+, and turbulence model studies. These are described below.

3.3.1 Mesh Sensitivity Study

For the mesh sensitivity study, the tug was kept at the midship region of the tanker (Δx = 0.5) with zero degree drift angle and lateral separation of Δy = 1.25. The surface mesh size was systematically varied, while keeping the SST turbulence model with the y^+ at a constant value of 0.5 to investigate the effect of mesh resolution on the interaction results. Nine meshes were generated by carrying out mesh refinement, especially on the vessel hull surfaces in the pressure interaction region between the vessels and in the forward and aft regions around the vessels. The best mesh was selected by analysing the longitudinal and lateral forces, and yaw moment acting on the tug and comparing them against those

obtained for the mesh consisting of the finest elements as shown in Figure 3.4. As seen in Figure 3.4, for the 7.9 million element mesh, the forces and moment were within 4% of the finest (13.5 million) mesh, with further refinement causing very little change in convergence. As a conservative measure the 8.94 million element mesh was selected (Figure 3.5) for the remainder of the study, which had a maximum deviation of less than 2% from the 13.5 million mesh for both forces and yaw moment. A detailed numerical uncertainty analysis in line with the ITTC, (2002a) is also provided in Appendix I to further justify the usage of the selected mesh.

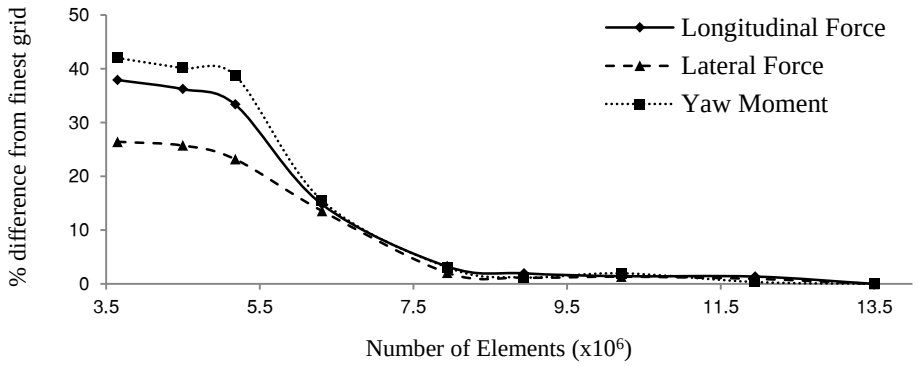

Figure 3.4: Percentage (%) difference from the finest 13.5 million elements mesh for the predicted forces and moment, with varying mesh element size.

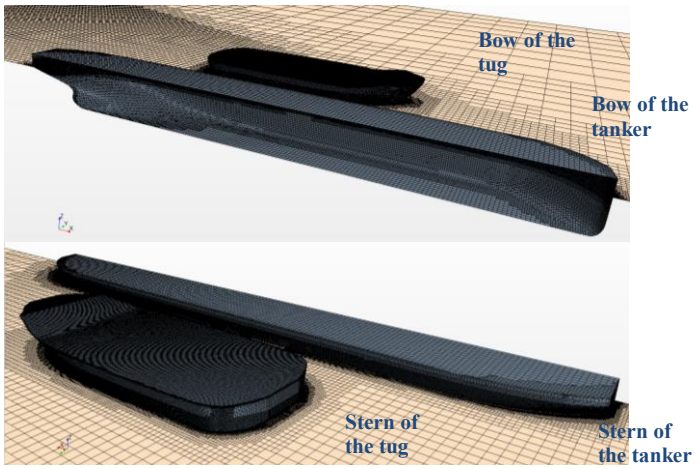

Figure 3.5: Selected 8.94 million element mesh grid.

3.3.2 y^+ and the Turbulence model study

Using the 8.94 million mesh, various combinations of y^+ and turbulence models were tested, as shown in Table 3.2, at both the parallel and tug at 30 degree drifted operations. When using turbulence models it was important to select models that were suitable for the task at hand as they are optimized for different situations. Three distinct turbulence models i.e. RKE, SST, and SA were investigated in this section along with a y^+ ranging from 0.1 to 100 to identify the most suitable turbulence model and y^+ combination for ship-tug interaction simulations. All three turbulence models were selected with all y^+ wall treatment options provided within StarCCM+®. This enabled the turbulence model to automatically switch between the wall function approach, if the near wall cell lay within the logarithmic region ($y^+ > 30$) or resolving into the viscous sub-layer, if the cells were closer to the surface ($y^+ < 5$). If the value lay within the buffer region ($5 < y^+ < 30$), the wall treatment mathematically blended the linear and logarithmic solutions to predict the wall shear stress.

Table 3.2: The y^+ and turbulence model combinations tested for parallel and 30 degree drifted tug operation simulations.

Grid Number	y^+	Turbulence Models used		
		SST	SA	RKE
1	0.1	✓	✓	✓
2	0.5	✓	✓	✓
3	1	✓	✓	✓
4	1.5	✓	✓	✓
5	2	✓	✓	✓
6	5	✓	✓	✓
7	10	✓	✓	✓
8	20	✓	✓	✓
9	30	✓	✓	✓
10	50	✓	✓	✓
11	100	✓	✓	✓

As seen in Table 3.2, 33 different cases were evaluated to determine the best combination for two test conditions, i.e. tug parallel, and drifted at 30 degrees to the tanker. The results from the simulations were non-dimensionalised and plotted separately for parallel and

drifted operations under longitudinal and lateral forces, and yaw moment for evaluation as shown in Figure 3.6 and Figure 3.7. For the parallel tug operations (Figure 3.6), the forces and moment predictions using all three turbulence models when y^+<1 were found to be within 2.5% of the values obtained for the smallest y^+ of 0.1. However, for 1<y^+<5, the deviation of the longitudinal forces for all three turbulence models increased to 6%, with the trend continuing until the y^+ approached 30, when the deviation dropped back to around 5% for the RKE turbulence model. Further increases in y^+ increased the deviation of the predicted longitudinal forces for all three turbulence models.

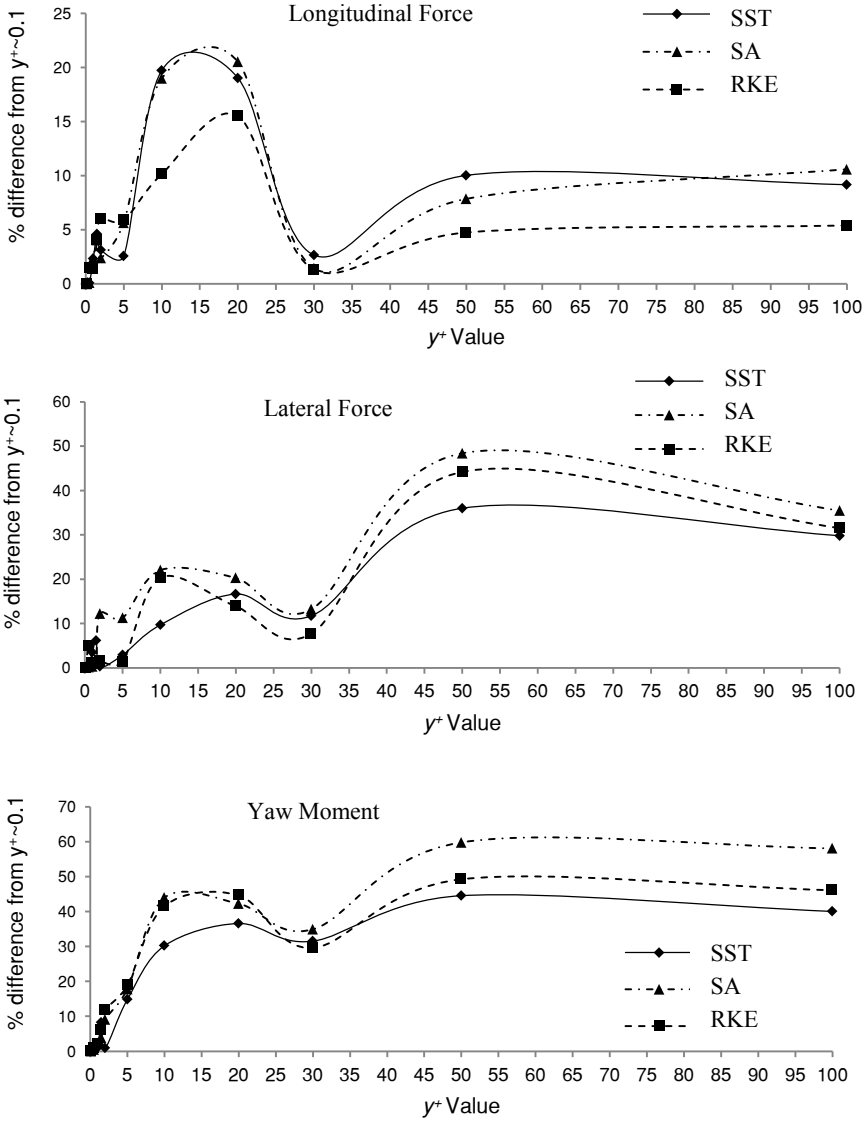

Figure 3.6: Percentage (%) difference from the simulation using the smallest y^+ value (0.1) for the predicted longitudinal and lateral forces, and yaw moment, with varying y^+ values for parallel tug and tanker operation for the three different turbulence models.

Similarly, the percentage difference in the predicted lateral forces increased to around 12.25% within the initial y^+ range of 5. Among the three turbulence models, the SA model showed this largest deviation of up to y^+~5, which was 12.25%, while the SST and RKE turbulence models showed maximum deviations of 6.19% and 4.98% respectively. When the y^+ further increased, the % difference of the longitudinal and lateral forces decreased as y^+ approached 30, with the maximum difference found at 9.31%, for the lateral force predicted by the RKE model. This sudden decrease was possibly due to the turbulence models switching automatically to the wall function as the y^+ moved from the buffer region to the logarithmic region. Beyond a y^+ of around 35, the results significantly deteriorated.

It is evident that when the near wall cell lies within the buffer region ($5< y^+<30$), all turbulence models showed larger % deviations. This agrees with the finding presented by Salim and Cheah, (2009), that when the first node is within the buffer region, neither the wall function approach nor the wall modelling approach can provide results with sufficient accuracy. Thus, the results obtained for the tug and tanker parallel operations confirm that the least deviated results are obtained when $y^+<1$, i.e. when the sub layer is resolved, although a y^+~30 provided reasonable accuracy through the use of the wall function. The buffer region of $5< y^+<30$ did not provide satisfactory results with any of the three turbulence models used in this study.

The yaw moment displayed a similar pattern to the longitudinal and lateral forces, i.e. for $y^+<1$ the maximum difference was 2.25% for the SA turbulence model, and this increased to 18.9% when y^+ reached 5. Further increase in the y^+ value increased the deviation beyond 30% for all three turbulence models, with a temporary dip back to 30% at y^+~30 due to the models switching to the wall function as discussed above. Thus, it's clear that only for the $y^+<1$ condition does the longitudinal and lateral forces, and yaw moment predictions fall within acceptable margins. The least deviation within that $y^+<1$ region was using the SST turbulence model, while the SA model gave the largest error. StarCCM+® guidance on the use of turbulence models states that the SA model is best for mild separation flows such as flow past a wing (CD-Adapco, 2015). However, the flow past the transom stern of the tug model resulted in severe flow separation due to the blunt body at the trailing edge creating wakes and disturbed flow, as confirmed by the authors in Jayarathne et al., (2014).

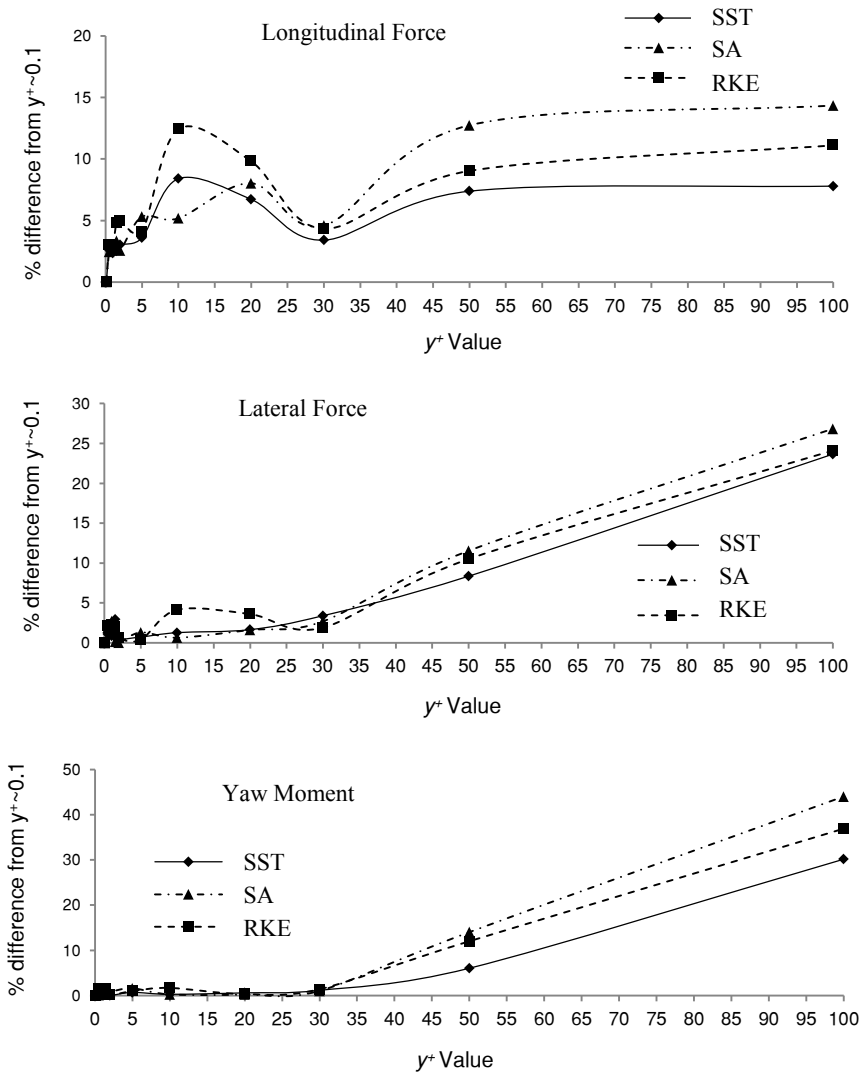

Figure 3.7: Percentage (%) difference from the simulation using the smallest (0.1) y^+ value for the predicted longitudinal and lateral forces, and yaw moment, with varying y^+ value for 30^0 drifted tug and tanker operation for the three different turbulence models.

Figure 3.7 illustrates the forces and moment predictions when the tug was drifted by 30 degrees to the tanker. As seen in the plots, the longitudinal forces for y^+<1 show a maximum % deviation of 2.87% from the results for a grid with a y^+ of 0.1, which was for the SA turbulence model. As the y^+ value was increased within the viscous sub-layer, i.e. 1< y^+<5, the maximum % deviations for the three models increased, with the SA model being the highest again at 5.31%. For 5<y^+<30, i.e. within the buffer region, the % deviation increased, with the maximum being 12.43% for the RKE model. As per the recommendation by StarCCM+® (CD-Adapco, 2015), the RKE two-layer formulation works with either Low-Reynolds number type grids, i.e. y^+~1 or wall-function type grids, i.e. y^+ around 30. Thus,

when the y^+ is within the buffer region, the deviation was larger than those experienced in other regions. At y^+~30, the % deviations were significantly reduced to around 5%, which then rapidly increased as the y^+ increased to 100.

The lateral force prediction differences were similar to the longitudinal force differences for all three turbulence models, showing a maximum of 2.72% for the SA model when 1< y^+. An increased y^+ value amplified the deviation for all turbulence models, with the expected dip at y^+~30. Yaw moment differences were less distinguishable for smaller y^+ values. However, the maximum % difference of moments was found in the RKE model for 1<y^+, which was 1.56%. While the deviation increased within the logarithmic region (i.e. y^+>30), the differences increased significantly beyond 30% for all three turbulence models.

Among the three turbulence models tested, the SST model showed the least deviation in most of the cases, especially when considering the lateral forces and when the tug was drifted, creating complicated flow behaviour with flow separations and circulations. In addition, for all models the least % deviations were experienced when y^+<1. Therefore, the SST turbulence model with a y^+~1 was selected to proceed further in this study. This ensured the results were consistent with the equations solved into the viscous sub layer to predict any adverse pressure gradient and flow separations. The wall function model did not show sufficient accuracy when the y^+ was within the buffer region (i.e. 5<y^+<30).

3.4 Validation Study

Keeping the verified simulation model as a base model, a series of compatible model-scale numerical simulations and experimental investigations were carried out in order to compare the CFD simulation results with the experimental results.

3.4.1 Numerical (CFD) simulations

Using the same model-scale tug and tanker used for the verification study, a new series of simulations were carried out for different Δx and Δy (see Equations 3.4 and 3.5) values and different tug drift angles with the SST turbulence model and y^+~1. Two flow velocities were used for the study, i.e. at model-scale speeds of 0.41 m/s and 0.62 m/s.

The selected cases for the study are given in Table 3.3, with each case replicated within the CFD simulations and the experimental program. Due to limitations in the experimental arrangement, at a tug drift angle of 8.4 degrees it was not possible to place the tug at a Δy separation of 1.34, since it would collide with the model carriage support pillars (see Figure 3.9 and Appendix IV) used to tow the models. Similarly for the 16.8 degrees drift angle it was only possible to have a Δy separation of 1.09 since Δy separations of 1.24 and 1.34 coincided with the model carriage support pillars.

Table 3.3: Cases investigated for the CFD and experimental comparison study.

Simulation Case Number	Tug Drift Angle θ (degrees)	Δx (non-dimensionalised)	Δy (non-dimensionalised)
1	0	0.6	1.09
2	0	0.6	1.24
3	0	0.6	1.34
4	0	1.0	1.09
5	0	1.0	1.24
6	0	1.0	1.34
7	0	1.2	1.09
8	0	1.2	1.24
9	0	1.2	1.34
10	8.4	0.6	1.09
11	8.4	0.6	1.24
12	8.4	1.0	1.09
13	8.4	1.0	1.24
14	8.4	1.2	1.09
15	8.4	1.2	1.24
16	16.8	0.6	1.09
17	16.8	1.0	1.09
18	16.8	1.2	1.09

3.4.2 Experimental Investigation

In order to compare the results generated through CFD, corresponding cases were replicated through captive model experiments in AMC's 35 m (length) x 12 m (width) x 1.0 m (depth) Model Test Basin shown in Figure 3.8. The depth of the water in the Model Test Basin was maintained at 0.8 m and the water temperature was between 17 and 18 degrees Celsius during the experiment.

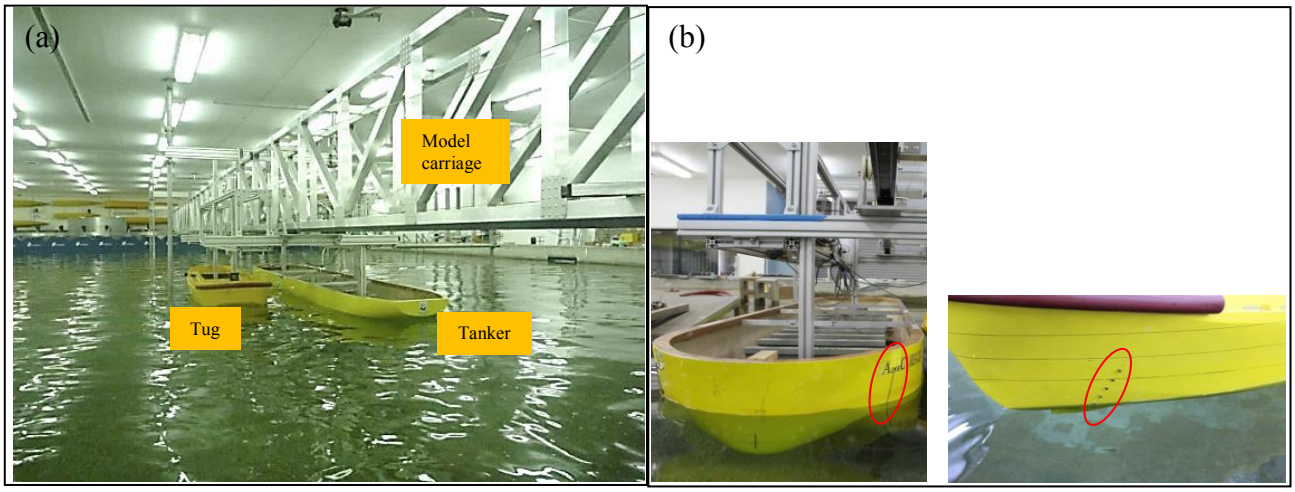

Figure 3.8: (a) Experimental set-up for interaction between vessels in AMC's Model Test Basin (b) Turbulence simulators used on the models: left image wire on tanker model and right image studs on tug model.

The scaled tanker and tug models were fixed in all degrees of freedom during the study. The tanker model was attached without any strain gauges or sliders below the model carriage connection box, which was used to guide the models. However, the tug model was attached on to the model carriage connection box using two load cells as shown in Figure 3.9, to measure the longitudinal and lateral forces, and to calculate the yaw moment. Experiments were conducted at the fully loaded drafts of both hulls, with all cases tested for two different speeds of 0.41 m/s and 0.62 m/s in model-scale (see Table 3.4). Both models were attached together to the model carriage, thus moving forward at the same speed with no relative motion between them. The models were fitted with turbulence stimulators in the form of a wire for the tanker model and studs for the tug model to generate a fully turbulent boundary layer along the hull of the vessels. Locations of the studs were

calculated based on the ITTC, (2011b) guidelines and are shown for the two models in Figure 3.8 (b).

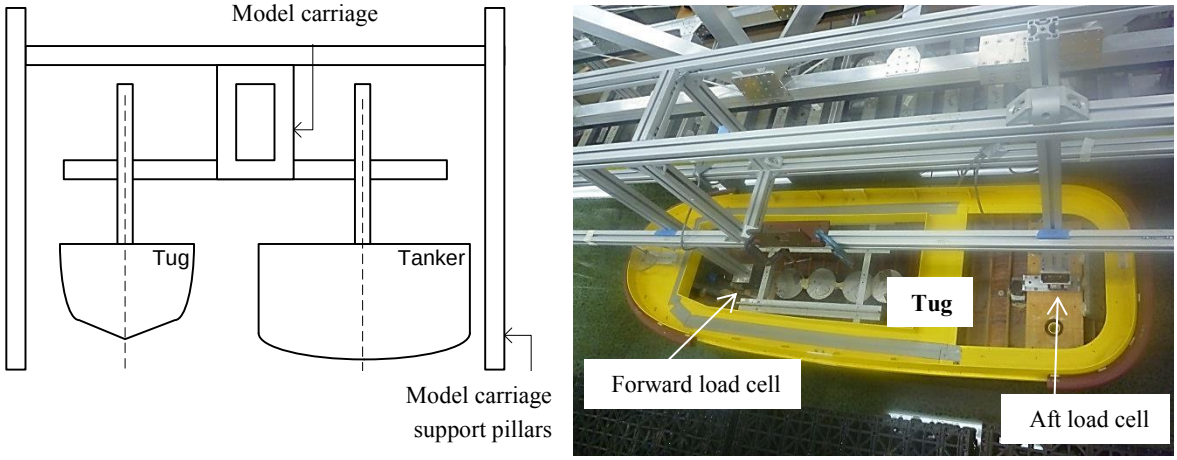

Figure 3.9: (a) Schematic of the experimental set-up in AMC's Model Test Basin (b) Load cells attached on to the tug. Additional pictures and sketches of the model carriage are given in Appendix IV.

Table 3.4: Speed regimes tested during validation study.

Speed of vessels			Froude Number based on	
Model-scale (m/s)	Full-scale (m/s)	Full-scale (knot)	Tug length	Tanker length
0.41	1.74	3.4	0.10	0.07
0.62	2.62	5.1	0.15	0.10

3.5 Discussion

The longitudinal and lateral forces, and yaw moment results obtained from the 36 CFD simulations and their equivalent 36 experimental runs were plotted in six different groups to facilitate the analysis, as outlined in Table 3.5. The uncertainty analysis conducted in accordance with ITTC, (2002b) for the experimental measurements are presented in Appendix I.

Table 3.5: Results analysis groups.

Drift Angle (Deg)	Group Number	Speed (m/s)	Cases from Table 3.3
0	1	0.41	1 to 9
0	2	0.62	1 to 9
8.4	3	0.41	10 to 15
8.4	4	0.62	10 to 15
16.8	5	0.41	16 to 18
16.8	6	0.62	16 to 18

3.5.1 Parallel Operation - Drift Angle of 0 degrees (Groups 1 and 2)

Figure 3.10 shows the results for the longitudinal and lateral forces, and yaw moment coefficients for the cases in Group 1, when the hulls were parallel and at a forward speed of 0.41 m/s.

The differences between the CFD and experimental results lay well within the uncertainty margins of the experiments. The maximum differences between CFD and experimental longitudinal force, lateral force, and yaw moment were found to be 7.7%, 8.8%, and 13.4% respectively. Furthermore, when comparing the CFD and experimental flow behaviour in Figure 3.11, it was observed that the free surface between the vessels and around the stern of the tug for the CFD and experimental work show similar flow behaviour, including wave intersection between the vessels.

Figure 3.12 shows the three coefficients for Group 2, i.e. at the relative positions as in Group 1 but at a 0.62 m/s forward speed. At 0.62 m/s, the difference between CFD and experimental longitudinal force, lateral force, and yaw moment were 9.9%, 11.3% and 13.2% respectively. These differences were within the experimental uncertainty margin and the trends of the longitudinal and lateral forces were similar to the plots at the speed of 0.41 m/s. However, the maximum yaw moments were experienced at different longitudinal separations, at Δx = 1.2 for 0.41 m/s and at Δx = 0.6 for 0.62 m/s. It is noted that when the flow speed increased, the tanker's bow wave was more prominent and its effect on the tug

increased. Thus, yaw moment was larger at Δx = 0.6 at a speed of 0.62 m/s, in comparison to the Δx = 1.2. In contrast to this, for both speeds the lowest yaw moments were experienced when the tug was around the midship region of the tanker (i.e. Δx = 1.0), similar to the findings of Dand, (1975), which discussed the interaction effects acting on a tug when it overtakes a larger ship.

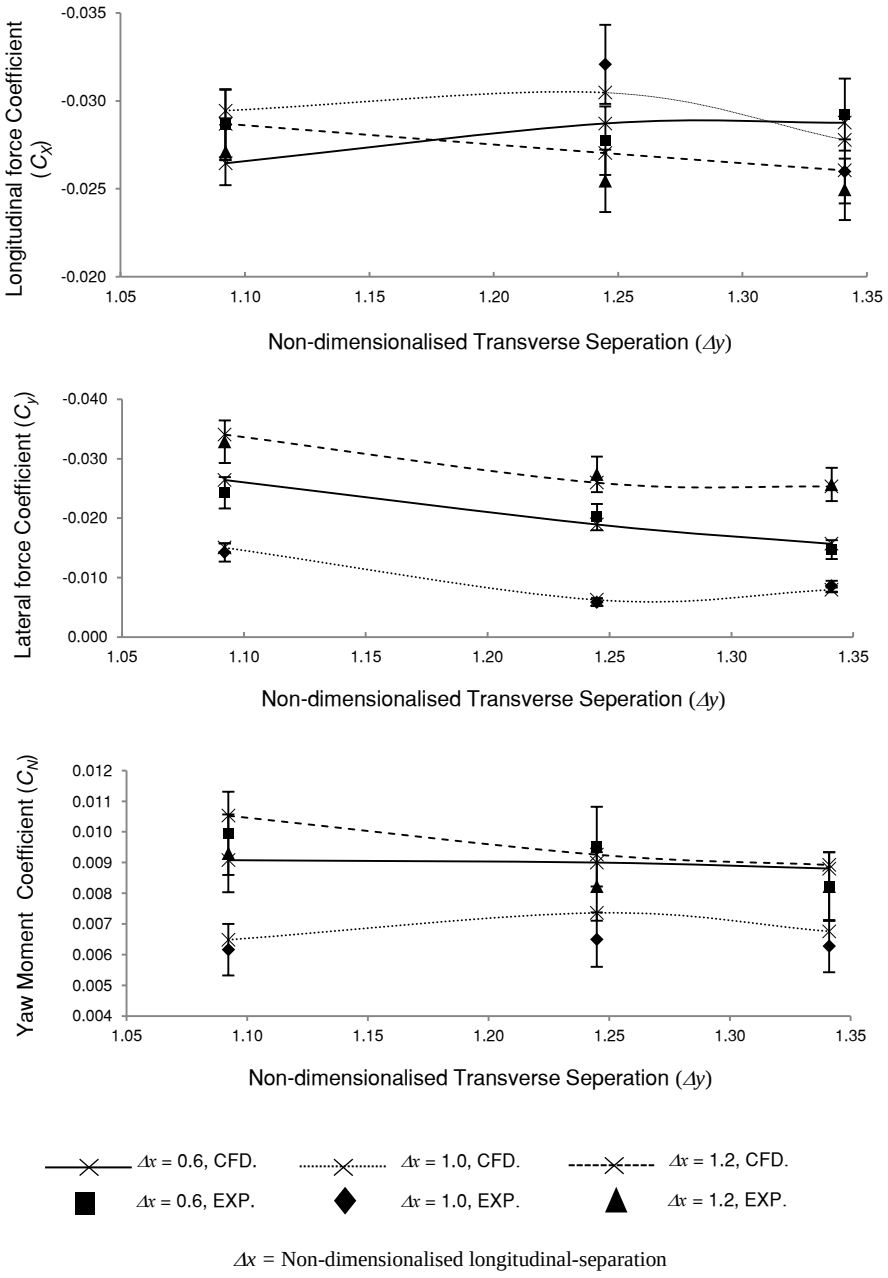

Figure 3.10: CFD and experimental comparison of longitudinal and lateral forces, and yaw moment coefficients acting on the tug when parallel to the tanker and moving forward at a common speed of 0.41 m/s (Group 1).

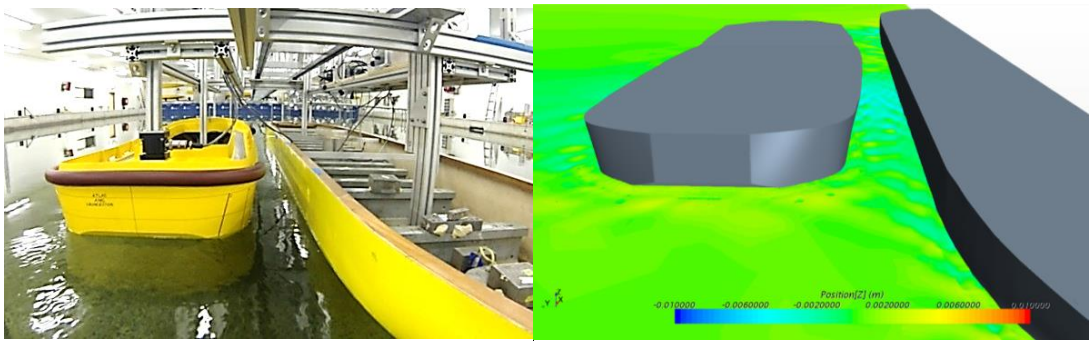

Figure 3.11: Experimental and CFD free surface at a common forward speed of 0.41 m/s at Δx = 1.2, Δy = 1.09, and $\theta = 0$ degree. Free surface legend is in meters

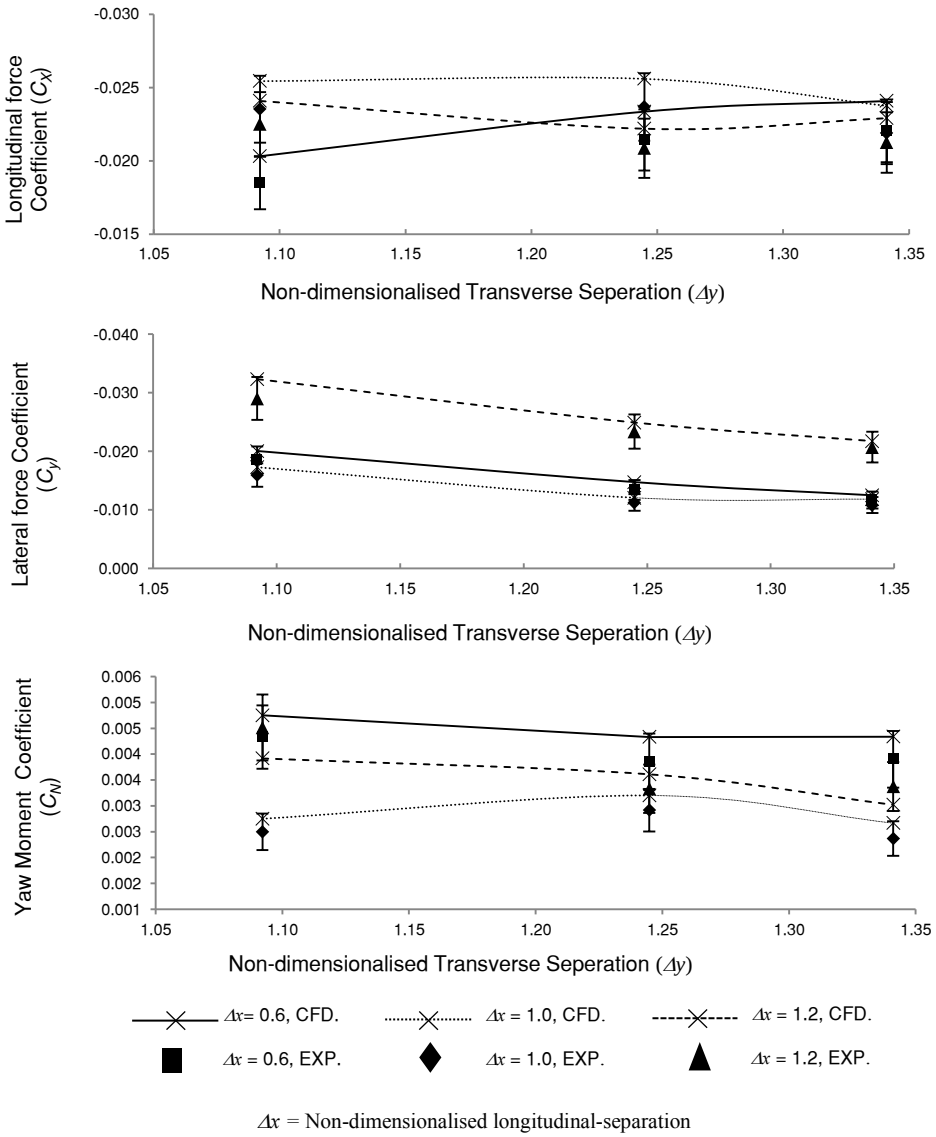

Figure 3.12: CFD and experimental comparison of longitudinal and lateral forces, and yaw moment coefficients acting on the tug when parallel to the tanker and moving forward at a common speed of 0.62 m/s (Group 2).

3.5.2 Drift Angle of 8.4 degrees (Groups 3 and 4)

The results for Group 3 and Group 4, which represents the 0.41 m/s and 0.62 m/s speeds respectively, at a tug drift angle of 8.4 degrees, are illustrated in Figure 3.13 and Figure 3.14 respectively.

As seen in Figure 3.13, the difference between the CFD and the experimental results were 12.5% for the longitudinal force coefficient, 13.6% for the lateral force coefficient, and 14.4% for the yaw moment coefficient, with all CFD predictions lying within the experimental uncertainties outlined in Appendix I.

As illustrated in Figure 3.14, the differences between CFD and experimental results increased when the speed of the vessels was increased to 0.62 m/s in the Group 4 cases. These are shown in Figure 3.15, with the increased % differences being: longitudinal force coefficient 14.7%, lateral force coefficient 16.3%, and yaw moment coefficient 17.6%. Thus at 0.62 m/s, the CFD predictions were slightly beyond the experimental uncertainty margin by 1.4%, 0.5% and 2.5% respectively. Simonsen et al., (2011) also experienced a similar mismatch between CFD and experimental results at larger drift angles, concluding that the CFD had good qualitative agreement with the experimental results. Yet, if the expected precision limit of the results is high, the causes for these differences have to be thoroughly investigated.

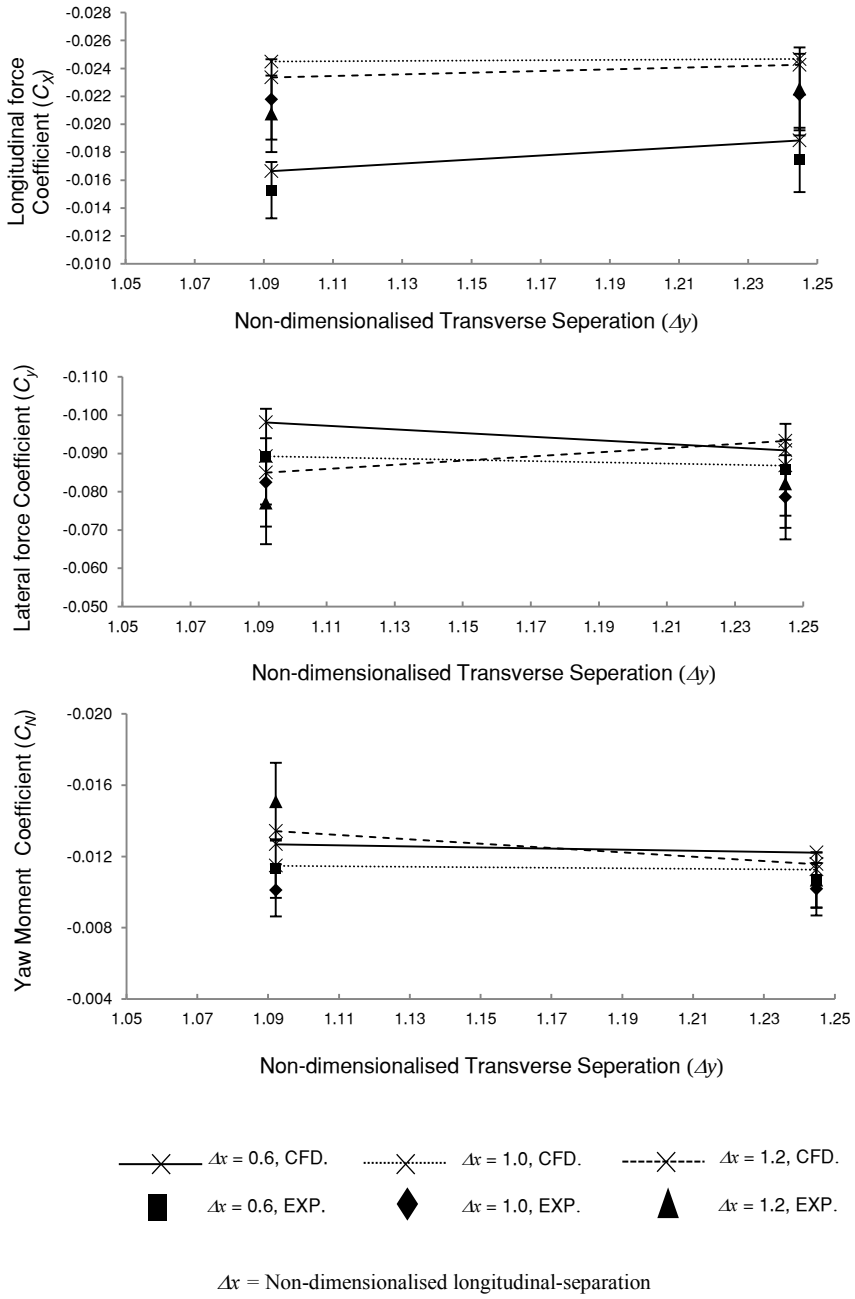

Figure 3.13: CFD and experimental comparison of longitudinal and lateral forces, and yaw moment coefficients acting on the tug when drifted 8.4 degrees to the tanker and moving forward at a common speed of 0.41 m/s (Group 3).

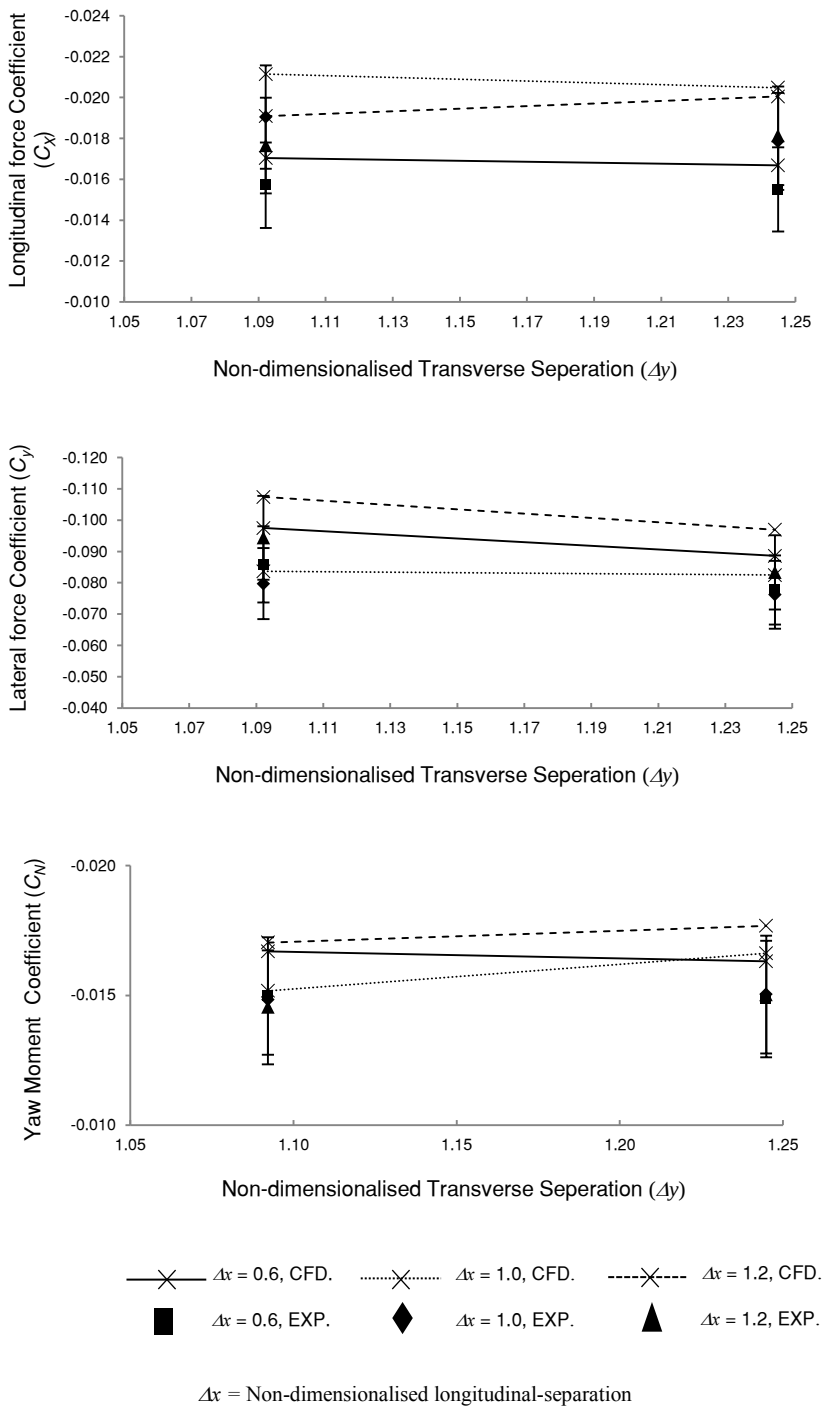

Figure 3.14: CFD and experimental comparison of longitudinal and lateral forces, and yaw moment coefficients acting on the tug when drifted 8.4 degrees to the tanker and moving forward at a common speed of 0.62 m/s (Group 4).

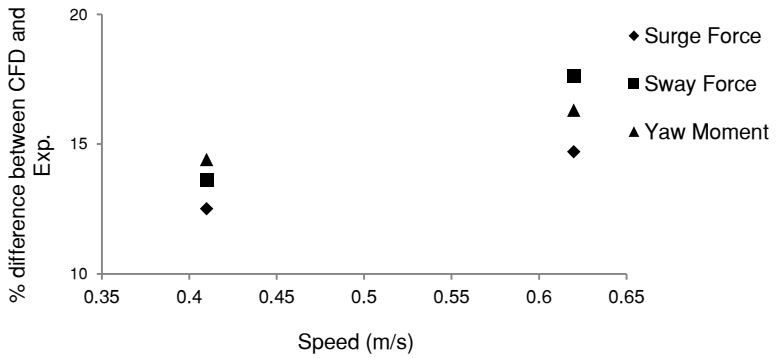

Figure 3.15: Percentage (%) difference between the CFD simulations and Experimental investigation results for tug with 8.4 degrees drift angle at 0.41 m/s and 0.62 m/s speeds.

Figure 3.16 shows the comparison of the flow behaviour predicted by the CFD and that observed during the equivalent experimental run.

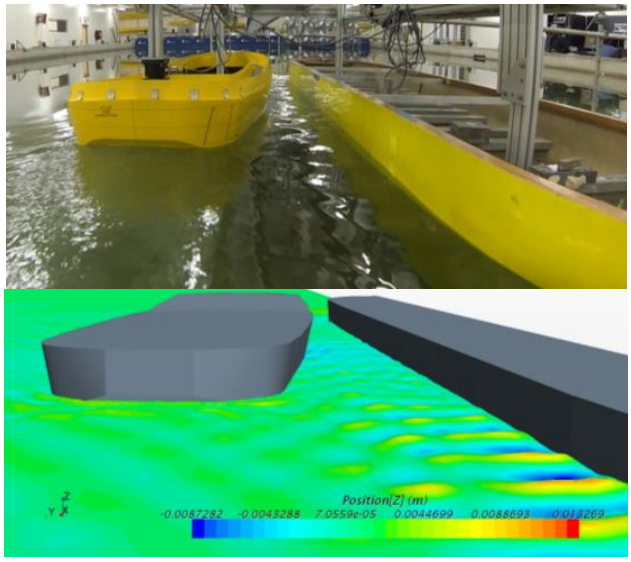

Figure 3.16: Experimental and CFD free surface at a common forward speed of 0.41 m/s at Δx = 1.0, Δy = 1.01, and $\theta = 8.4$ degrees. Free surface legend is in meters.

3.5.3 Drift Angle of 16.8 degrees (Groups 5 and 6)

Finally the results for Group 5 and Group 6 for the tug drifted by 16.8 degrees were analysed. Due to the limitations of the towing rig used for the experiments, only one transverse separation (Δy = 1.09) was considered for this drift angle. However, longitudinal

location was changed to similar locations (Δx = 0.6, 1.0, 1.2) as with Groups 1 to 4, and the tests were conducted for similar common speeds of 0.41 m/s and 0.62 m/s. The longitudinal and lateral forces, and yaw moment coefficient results for the two groups were plotted against the common speeds in Figure 3.17.

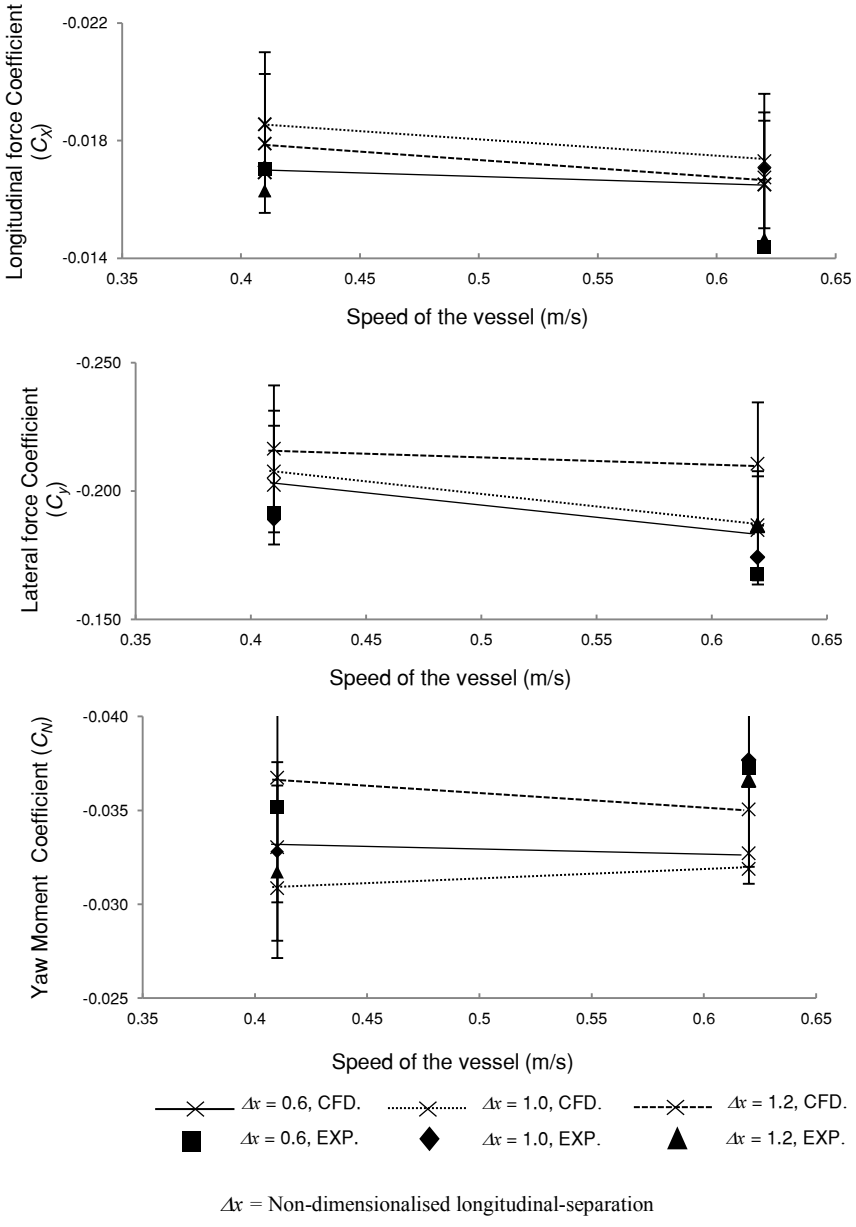

Δx = Non-dimensionalised longitudinal-separation

Figure 3.17: CFD and experimental comparison of longitudinal and lateral forces, and yaw moment coefficients acting on the tug when drifted at 16.8 degrees to the tanker and moving forward at common speeds of 0.41 m/s and 0.62 m/s, lateral separation Δy of 1.09, and varying longitudinal separations Δx (Groups 5 and 6).

At this drift angle, the differences between the CFD and experimental results at 0.41 m/s for the longitudinal force and lateral force coefficients were 9.8% and 12.6% respectively, while the difference for the yaw moment coefficient was 14.4%. As the speed was increased to 0.62 m/s the differences between the CFD predictions and the experimental results increased to 13.8%, 12.9% and 15.8% respectively. Similar to the Group 4 results discussed earlier, they were marginally beyond the level of experimental uncertainty by 0.6%, 1.5% and 1.3% respectively.

Thus, it is seen that with the increasing Froude number, CFD prediction showed a slight deviation away from the experimental results. However, doubling the drift angle from 8.4 to 16.8 degrees showed little change in the difference between the CFD and the experimental results. Consequently, this error was deemed as being dependent on the Froude number rather than the drift angle. Nevertheless, it is necessary to investigate similar operations with larger Froude numbers to identify the real cause of this deviation. However, the current study is limited to investigating interaction effects on tugs when assisting ships entering or leaving ports, where the tugs operate within their lower speed range, typically around 3 to 6 knots, and thus at smaller Froude numbers, as speeds beyond 6 knots become too high for effective tug assistance (Hensen, 2003). Therefore, the verified CFD parameters within this study were deemed suitable for predicting the interaction effects of the tug-ship interaction scenarios considered at typical ship-assist operational speeds.

3.6 Conclusion

This chapter outlines a comparative numerical and experimental study conducted to investigate the suitability of RANS-based CFD simulations for predicting the interaction effects acting on a tug during ship-assist operations. It includes investigating the selection of appropriate turbulence models and boundary layer modelling on the simulation results. Three distinct turbulence models (i.e. RKE, SST, and SA) and y^+ ranging from 0.1 to 100 were included within this interaction prediction study to identify the most appropriate turbulence model and y^+ combination. The uncertainties for EFD data for parallel vessel operations

were quantified using ITTC, (2002b) at 7%, 9.4%, and 7% for longitudinal force, lateral force, and yaw moment respectively.

It was shown that for $y^+ \leq 1$ the SST turbulence model offered good agreement with the experimental measurements for both the parallel and drifted tug manoeuvre test cases at the speed range tested (i.e. Froude number 0.10 to 0.15 based on tug length). For the cases within the $1 < y^+ < 5$ range, the RKE results closely followed the SST results with a maximum difference of around 2%. Within this region, the SA turbulence model showed the largest discrepancy among the three turbulence models, at around 12%. This confirms that the SA model is best for mild separation flows, such as flow past a wing at low angle of attack. For tugs, with a submerged transom stern, a highly separated flow is created, resulting in instability and accuracy issues in the numerical modelling.

The region $5 < y^+ < 30$ does not provide good results with any of the three turbulence models used in this study due to inaccurate blending of the linear and logarithmic solutions to predict the wall shear stress. If the computational resources are limited, then a y^+ at 30 can provide a reasonable result with the wall function model. A $y^+ > 30$ was found to be inadequate for the investigation of interaction effects due to the large resultant deviations found in this study.

When the tug was drifted to higher angles, i.e. 8.4 degrees and 16.8 degrees, the CFD predictions with the SST turbulence model and $y^+ \leq 1$ were greater than the EFD uncertainties by 2.5%. Furthermore, it was found that the major cause for the increased discrepancies was the increased Froude number, and not the drift angle. However, for ship-assist operations the Froude numbers will be relatively low due to operational limitations on the speeds and thus the selected turbulence model and y^+ combination were found to be acceptable for interaction effect studies.

Based on this, the use of SST turbulence model with smaller y^+ values will be used to further extend this study. This will involve simulations of more tug and tanker combinations by increasing the tug's drift angle up to 90 degrees and changing its location throughout the tanker length and beyond to quantify the interaction effects under different scenarios and

identify safe tug operational envelopes when operating in proximity to a large vessel. In addition, the current models will form the basis to develop full-scale simulation models and also to investigate tugs and tankers having relative motion, to identify the interaction effects when a tug is approaching a tanker underway during rope handling operations.

Chapter 4

Effects of Lateral Separation and Relative Size of Vessels on Hydrodynamic Interaction

This chapter has been reviewed and accepted for publication in the Transactions Royal Institution of Naval Architects: Part A1- International Journal of Maritime Engineering. The citation for the research article is:

Jayarathne, N., Ranmuthugala, D., Leong, Z.Q. & Fei, G. (2017), 'Non-Dimensionalisation of Lateral Distances Between Vessels of Dissimilar Sizes for Interaction Effect Studies', *Transactions RINA: Part A1- International Journal of Maritime Engineering.* (Accepted for publication)

Chapter 4 has been removed for copyright or proprietary reasons.

It has been published as: Jayarathne, N., Ranmuthugala, D., Leong, Z., Fei, J., 2017. Non-dimensionalisation of lateral distances between vessels of dissimilar sizes for interaction effect studies, Transactions RINA: Part A1- International journal of maritime engineering, 159, 429

Chapter 5

Safe Tug Operations during Ship-Assist Manoeuvres

This chapter has been submitted for publication in the Journal of Navigation and at the time of writing is under review. The citation for the research article is:

Jayarathne, N., Ranmuthugala, D., Leong, Z. Q. (2017), 'Safe Tug Operations during Ship-Assist Manoeuvres', *The Journal of Navigation (Under Review)*.

ABSTRACT

The hydrodynamic interaction effects on a tug operating in close proximity to a larger vessel can result in significantly dangerous situations for the tug. To date most studies focus on the interaction effects between the vessels when they are operating in parallel, which represent only one of many practical ship-assist manoeuvres. It is therefore necessary to investigate a wide range of tug-ship combinations to obtain a detailed understanding of these effects. This chapter discusses the hydrodynamic interaction effects on a tug operating at various relative positions and drift angles to a larger ship, both moving together at the same forward speed. The hydrodynamic effects were determined using Computational Fluid Dynamics (CFD) simulations that were validated using captive model test data. The range of manoeuvres discussed in this chapter provides a comprehensive overview of the hydrodynamic interaction effects on a tug enabling tug operators to identify safe operating envelopes for their vessels.

5.1 Introduction

Tugs play a significant role when assisting large ships with limited manoeuvring capabilities at slow speeds in restricted waters, such as in harbour and canals. However, the hydrodynamic interaction effects due to interacting pressure fields around the vessels can have a significant impact on their safety and handling during such manoeuvres. The adverse hydrodynamic effects are more severe for the attending tugs as they are much smaller in size in comparison to the assisted ships (Hensen et al., 2013). The Maritime Coastguard Agency (MCA) in the United Kingdom states that when vessels are being manoeuvred at close quarters for operational reasons, the greatest potential danger exists when there is a large difference in size between the two vessels, such as when a ship is being attended by a tug (MCA, 2001). Thus, it is vital to make tug operators aware of adverse interaction effects that can occur during such vessel manoeuvres by quantifying the relevant effects through comprehensive research studies.

To date, most of the studies on vessel interaction have been carried out for similar sized vessels (Chen & Fang, 2001; Falter, 2010; Fortson, 1974; Lataire et al., 2012; Lu et al., 2009; Newton, 1960; Tuck & Newman, 1974; Zou & Larsson, 2013), with only a small number focusing on dissimilar sized vessels operating in close proximity (Dand, 1975; Fonfach et al., 2011; Geerts et al., 2011; Jong, 2007; Simonsen et al., 2011; Vantorre et al., 2002). Dand, (1975) carried out scaled-model experiments on tug-ship interaction to determine the physical causes of interaction and the resulting effects. This approach is still useful for tug-ship interaction prediction when both vessels are advancing on parallel courses. However, parallel operation is only one of many manoeuvres encountered in practical operating conditions. Vantorre et al., (2002) conducted physical scaled model tests to determine ship interaction effects for head-on and overtaking encounters of similar and dissimilar vessels in parallel. The study conducted by Fonfach et al., (2011) also used a tug operating in parallel to a tanker to predict interaction effects acting on tugs.

Contrary to previous studies, Geerts et al., (2011) assessed the hydrodynamic interaction effects on a tug with small drift angles (between -5 to 10 degrees) operating in close

proximity to a container ship moving forward at the same speed. Their study was however, limited to a tug operating at the bow area of the ship and to a few drift angles that tugs may operate at during ship-assist manoeuvres. Simonsen et al., (2011) conducted a study to predict the interaction effects acting on a drifted tug located at various longitudinal and lateral locations to a larger ship. However, the tests were conducted only for a tug located in the midship region of the ship at limited tug drift angles (zero to 60 degrees), thus providing a limited set of data.

As stated above, research studies available in the public domain do not explicitly address the interaction behaviour between a tug and a ship operating at different ship locations and tug drift angles. Therefore, it is difficult to establish how well these results represent the overall interaction behaviour of a tug during real ship-assist manoeuvres. Thus, there is a need to investigate possible tug-ship combinations during ship-assist manoeuvres to comprehend the significance of the hydrodynamic interaction effects on tugs.

This chapter presents the results of full-scale CFD simulations conducted to investigate the interaction effects on a tug operating at different longitudinal and lateral locations relative to a tanker. At each location the tug's drift angle was varied from zero to 90 degrees. Simulations were conducted for two full-scale speeds, i.e. 3 knots and 6 knots, representing the widely used minimum and maximum ship-assist manoeuver speeds (Hensen, 2003). Selected CFD simulation results were validated at model-scale against experimental measurements obtained in the Model Test Basin at the Australian Maritime College (AMC). Previous work by Jayarathne et al., 2017a compared the interaction effects acting on a tug operating in close proximity to ships of varying sizes in order to correlate model-scale and full-scale interaction effects. The results showed good agreement between non-dimesionalised interaction effects for differently scaled vessels, thus providing confidence to use full-scale CFD simulations in this study. The findings of this study are important for tug operators in order to understand the safe operating envelopes for their vessels safely during close quarter ship-assist manoeuvres.

5.2 Case Study

The interaction effects induced on a tug in close proximity to a larger ship was investigated through CFD and experimental work using a generic hull form of a stern drive tug and a MARAD-F series tanker hull form. The main particulars of the full-scale tug and tanker are given in Table 5.1.

The longitudinal force (*X*), lateral force (*Y*), and yaw moment (*N*) acting on the tug for different cases were measured and non-dimensionalised using volumetric displacements in accordance with Equations 5.1 to 5.3 (Fonfach et al., 2011, Jayarathne et al., 2017b, Simonsen et al., 2011) respectively. The forces were measured in the global coordinate system; while the yaw moment was defined about the tug-local coordinate system (see Figure 5.1).

$$C_X = \frac{2X}{u^2 \nabla_t^{1/3} \nabla_s^{1/3} \rho} \tag{5.1}$$

$$C_Y = \frac{2Y}{u^2 \nabla_t^{1/3} \nabla_s^{1/3} \rho} \tag{5.2}$$

$$C_N = \frac{2N}{u^2 \nabla_t^{1/3} \nabla_s^{1/3} L_t \rho} \tag{5.3}$$

Table 5.1: Principal particulars of the selected full-scale tug and tanker hull forms.

Principal Particulars	Unit	Tanker	Tug
Length Overall	m	210.00	31.16
Length Waterline	m	200.00	28.46
Breadth	m	36.45	11.50
Draft	m	12.30	3.55
u_1	m s^{-1}	1.54	1.54
F_{r1}	-	0.035	0.092
u_2	m s^{-1}	3.09	3.09
F_{r2}	-	0.070	0.185

The approaches used to non-dimensionalise the lateral and longitudinal distances are given in Equations 5.4 and 5.5 respectively. Justification for the use of these terms were published previously by the authors in Jayarathne et al., (2017a) . Table 5.2 provides a summary of the cases investigated in this study.

$$\Delta y = \frac{\delta y}{B_s} \tag{5.4}$$

$$\Delta x = \frac{\delta x}{L_s} \tag{5.5}$$

Table 5.2: Parameter range for the cases investigated in this study.

Parameter	Range	Increment
δx (m)	20.00 to -220.00	10.00
Δx	-0.10 to 1.10	0.05
δy (m)	1.00 to 72.90	18.22
Δy	0.03 to 2.00	0.25
θ (degrees)	0 to 90	15 degrees

5.3 CFD Simulation

Validated CFD models previously developed by the authors (Jayarathne *et al*., 2016, 2017a, and 2017b) were employed to analyse the case studies discussed above. The CFD simulations were modelled using the commercial CFD software StarCCM+®, a finite volume method based CFD package, utilising an unstructured hexahedral mesh approach. The CFD simulations employed the Reynolds Averaged Navier-Stokes (RANS) based Shear Stress Transport (SST) model for the analysis. The free surface of the domain was modelled as an Eulerian Multiphase using the Volume Of Fluid (VOF) technique, with the implicit unsteady simulation technique. The free surface was dependent on the VOF flat wave, with a 0.5 of volume fraction implying that a computational cell is equally filled with air and water. The mesh within the free surface region was refined in order to enable the variations in volume fraction to be more accurately captured. A second-order convection scheme was used to

accurately capture sharp interfaces between the phases. The nominal total inflation layer thickness of two times Prandtl's 1/7th power law (2x0.16L_t/$Re_{Lt}^{1/7}$) turbulent boundary layer thickness estimate (Leong et al., 2014; White, 2003) was used to model the inflation layers around the vessels. As investigated previously by the authors Jayarathne et al. (2017b), a SST turbulence model with the tug's near wall mesh spacing i.e. y^+, maintained at around 1. This in turn helped to resolve the boundary layer all the way to the wall with a finer mesh to accurately capture any separation and improve the accuracy of the results.

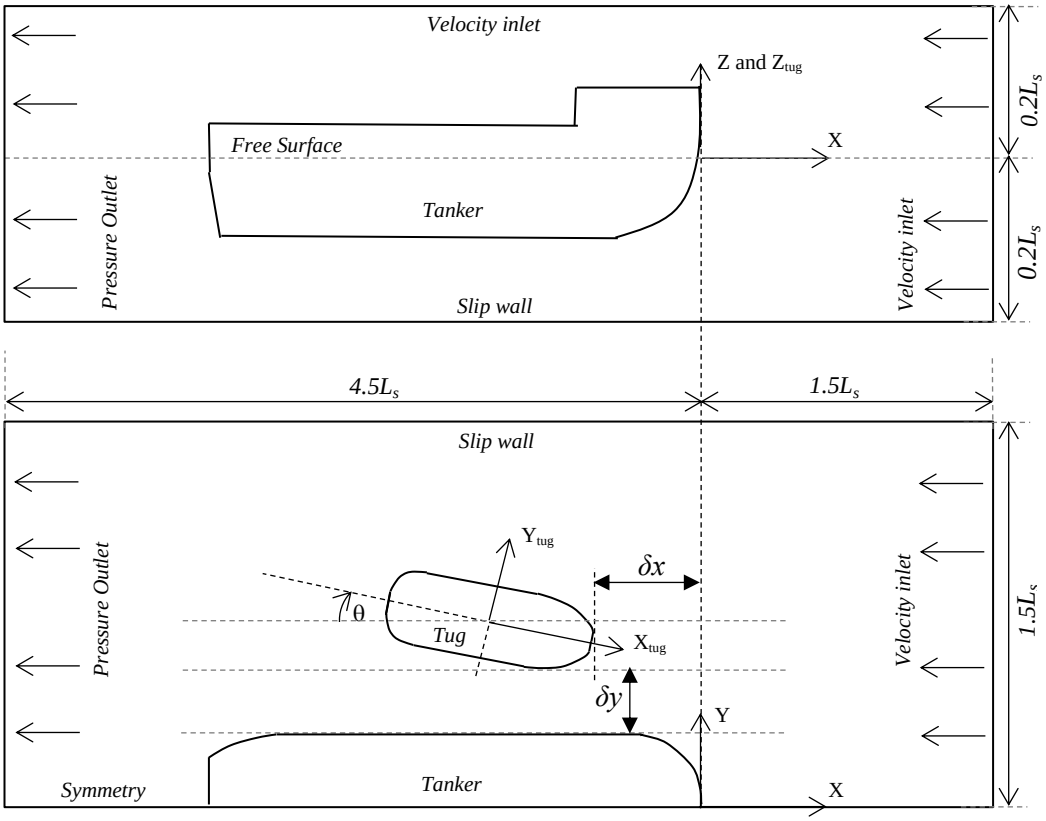

Figure 5.1: Computational domain used in CFD simulations showing coordinate systems, boundaries and relative distances. Top – side view showing tanker. Bottom – plan view showing local (tug) coordinate system and global coordinate system with vessel locations.

Throughout the analysis, the tug was located on the port side of the tanker. Model scale CFD simulations replicated the experimental captive model test conditions to aid validation of the former. Both the tanker and tug geometries were fixed (i.e. zero degrees of freedom) for all of the cases investigated. The upstream end and top boundaries of the domain were kept as inlet boundaries and the downstream end defined as a pressure outlet (see Figure 5.1). As recommended by CD-Adapco, (2015), the velocity inlet at the top boundary was

used in preference to a slip wall boundary to reduce the simulation convergence time without affecting the accuracy of the results. The use of the velocity inlet boundary condition at the top prevents the fluid from 'sticking' to the walls as well as creating a blockage. Thus, it avoids the occurrence of a pressure gradient between the fluid and the wall, as would be the case if a slip-wall boundary condition was used (Tezdogan et al., 2015).

5.4 Experimental Set-up

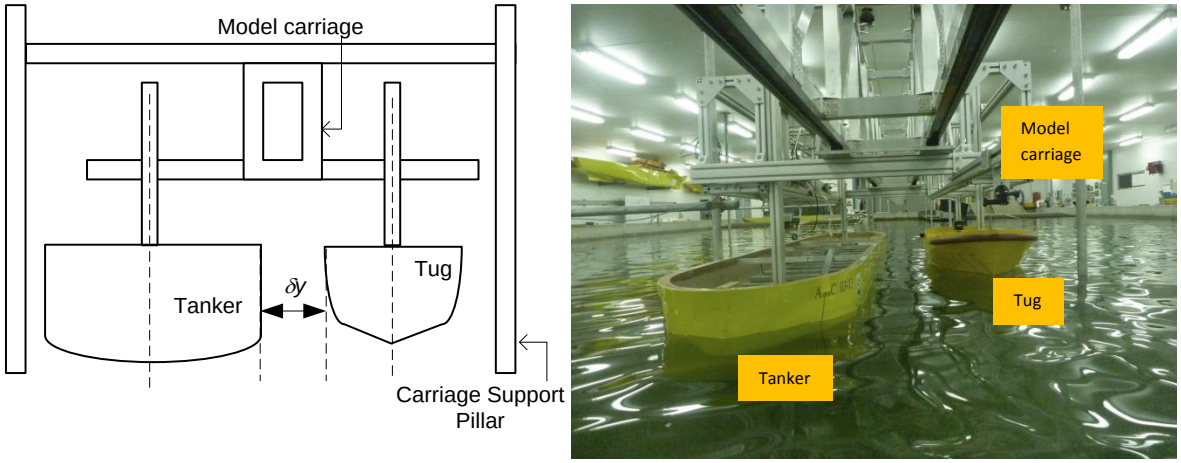

Figure 5.2: Left: Schematic of the experimental set-up in AMC's Model Test Basin. Right: Experimental set-up in AMC's Model Test Basin.

In order to validate the CFD simulations, a series of captive model experiments were conducted in the AMC Model Test Basin to measure the experimental interaction effect on the tug operating in close proximity to a tanker. The dimensions of the Test Basin are 35 m (length) x 12 m (width) x 1.0 m (depth), with the experimental set-up shown in Figure 5.2. The model-scale tanker and tug models were fixed in all degrees of freedom in a similar configuration to that in the CFD simulations, with no relative motion between them. As the forces and moment acting on the tanker were not measured, it was directly attached to the model carriage, while the tug was attached using two strain gauges in order to record the forces acting on it. The experiments were conducted at the fully loaded drafts of both hulls at two model-scale speeds of 0.41 m/s and 0.62 m/s. Experimental uncertainty limits were calculated in accordance with the ITTC, (2002b), giving 7%, 9.4%, and 7% for the measured

longitudinal force, lateral force, and yaw moment respectively (see Jayarathne et al., (2017b) and Appendix I for details on the uncertainty estimation).

5.5 CFD Verification and Validation

The verification and validation studies for the CFD predictions and non-dimensionlisation convention (Equations 5.1 to 5.5) of the interaction effects for vessels of different sizes and scales are described in detail by the authors in Jayarathne *et al*., (2016, 2017a, and 2017b) and in Appendix I. Only a summary is presented in this section. For the verification and validation purpose, the tug was located near the bow of the tanker (i.e. Δx = 0) and Δy = 2.190 and 2.276 lateral separations at a forward speed of 1.74 m/s (tug length based Froude number of 0.104 were used). Froude scaling was used for measuring the dynamic parameters.

To quantify the simulation uncertainty based on the mesh resolution for the model-scale and full-scale predictions, the Richardson Extraplotion method outlined in ITTC, (2002a) was used. Mesh models for both scales at three different resolutions (see Table 5.3): fine (see Figure 5.3), medium and coarse were created, with an approximate mesh refinement ratio of √2. The mesh refinement was carried out on the vessel surfaces and in the pressure and wake regions around the vessels.

Table 5.3: Mesh resolution of the simulations used for the sensitivity study (M – Millions).

Mesh (Number)	Fine (1)	Medium (2)	Coarse (3)
Model Scale	7.2 M	4.8 M	3.5 M
Full Scale	14.6 M	10.9 M	7.6 M

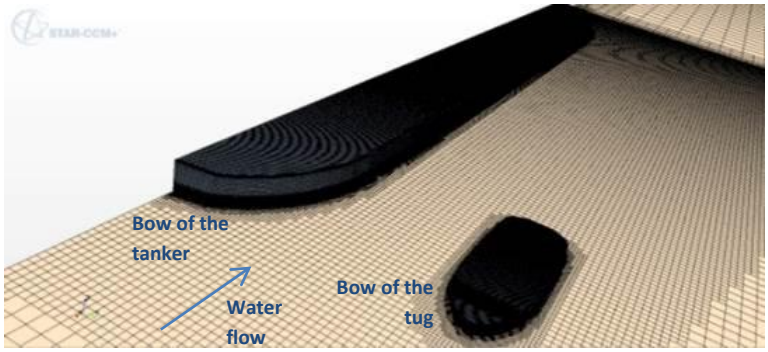

Figure 5.3: Selected Full Scale Mesh – 14.6 Million Cells.

Table 5.4 presents the error percentage estimates compared to the Richardson extrapolated values (Stern et al., 2001). The model-scale CFD and model-scale experimental interaction effect coefficients were in good agreement, with the difference being less than the experimental uncertainty, i.e. less than 7%, 9.4%, and 7% of the longitudinal force, lateral force, and yaw moment respectively (Jayarathne et al., 2017b). Furthermore, the model-scale and full-scale interaction effect coefficients predicted by the CFD simulations were in good agreement with the maximum difference between them less than 8% (Jayarathne et al., 2017b). Thus it provides confidence in the use of full-scale results and the non-dimensional conventions presented in this study.

Table 5.4: Relative error percentage estimates of the longitudinal and lateral forces and the yaw moment with respect to the Richardson extrapolated values.

Interaction Effect	Percentages (%) of the relative error estimates								
	Longitudinal Force Coefficient			Lateral Force Coefficient			Yaw Moment Coefficient		
Mesh Number	1	2	3	1	2	3	1	2	3
Model scale	0.43	1.44	4.78	1.96	3.89	7.55	1.21	2.53	5.24
Full Scale	0.41	2.10	6.87	2.09	5.99	9.12	3.56	6.64	13.25

5.6 Discussion

This section discusses the longitudinal force, lateral force and yaw moment induced on the tug due to the hydrodynamic interaction. It is divided into four sub-sections to improve the clarity of the large number of interaction data presented. The first two sections present the interaction effects on the tug at two tug drift angle (θ) ranges, i.e. zero to 45 degrees, and 60 to 90 degrees respectively, in comparison to that of an open-water tug (i.e. no interaction). The last two sections discuss the effects of Froude number and the lateral separation on the interaction effects respectively.

5.6.1 Interaction effects at a tug drift angle between 0 to 45 degrees

The force and moment coefficients on the tug when it is at non-dimensionalised lateral distances (Δy) of 0.50 and 1.00 and at a drift angle between zero and 45 degrees are presented in Figure 5.4. From the figure it is seen that when the tug is within the forward (i.e. -0.10 < Δx < 0.00), midship (i.e. -0.55 < Δx < -0.45), and aft (i.e. -1.00 < Δx < -0.90) regions of the tanker, there are significant changes in the result trends.

As seen in Figure 5.4, when the tug is in the forward region of the tanker (i.e. -0.10 < Δx < 0.00), the longitudinal force coefficients are slightly greater than the coefficients of the open-water tug. This is because the tug is in the 'resistance barrier' (Dand, 1975) created by the tanker's bow pressure region, where the pressure on the windward side of the tug is increased. Thus, there is an increase in its longitudinal force. At the forward region of the tanker, when the tug is drifted, it experiences a reduction in lateral force and yaw moment in comparison to the open-water tug, due to the tanker's high bow pressure region that 'pushes' the forward section of the tug away from the tanker.

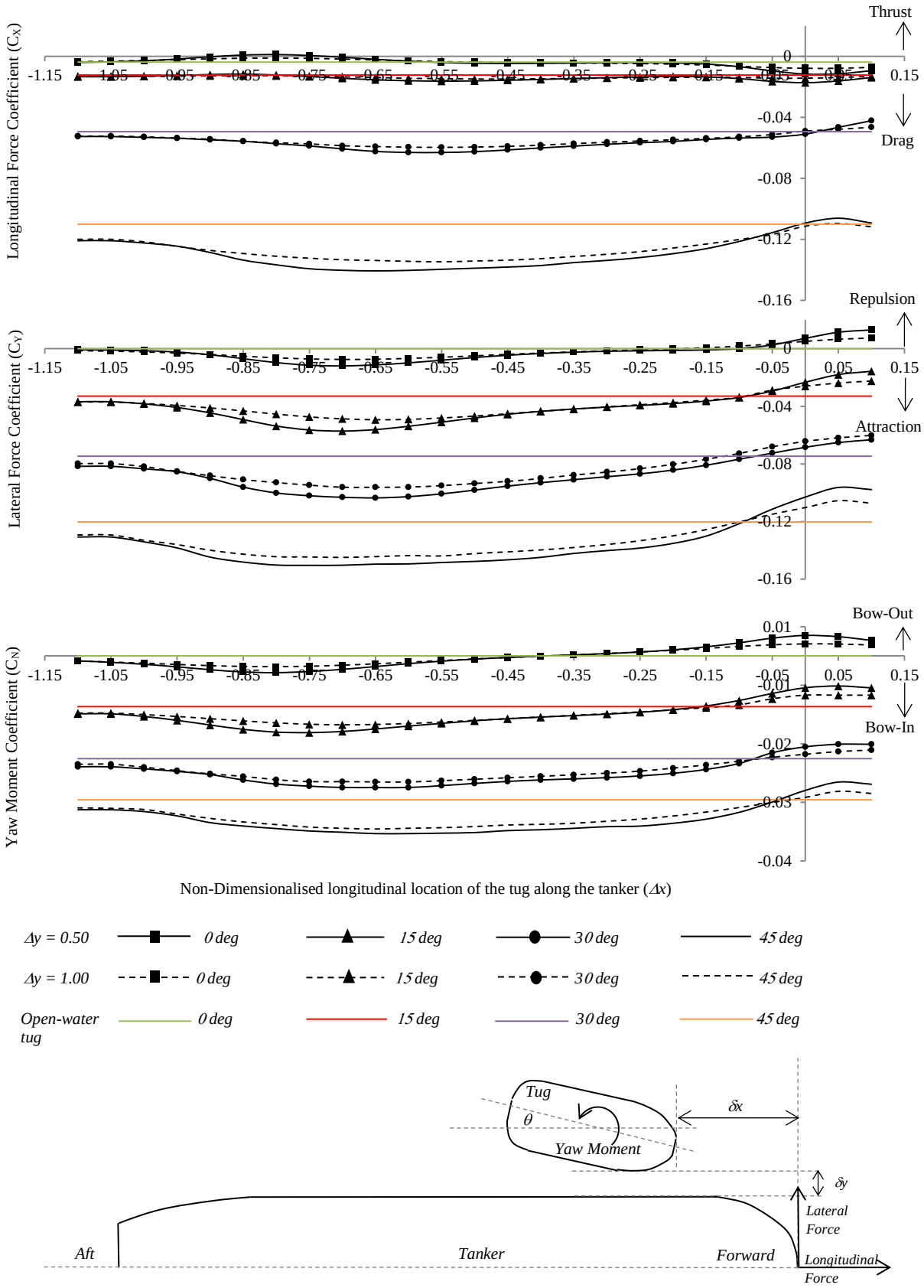

Figure 5.4: CFD predicted forces and moment coefficients for a tug operating at the non-dimensionalised lateral separations (Δy) of 0.50 and 1.00 from the tanker, at tug drift angles (θ) of 0, 15, 30 and, 45 degrees, in comparison to an open-water tug.
Δx is the non-dimensionalised longitudinal separation.

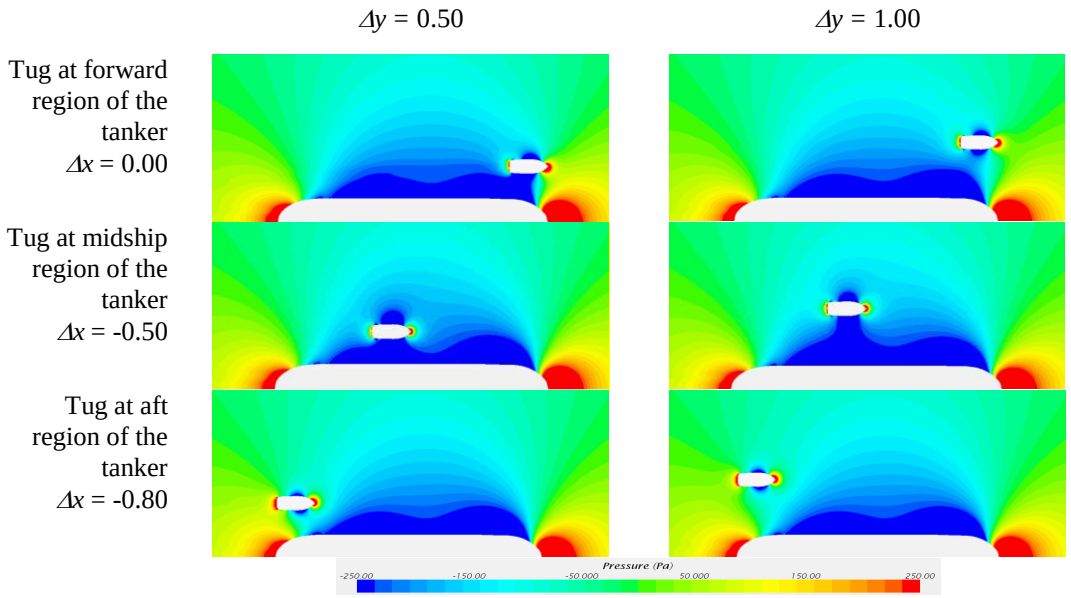

Figure 5.5: CFD pressure plots for the tug operating at the non-dimensionalised lateral separation (Δy) of 0.50 and 1.00 from the tanker, at tug drift angles (θ) of zero degrees. Δx is the non-dimensionalised longitudinal separation.

When the tug is forward of the tanker's bow, i.e. $\Delta x > 0.00$, its longitudinal force is slightly reduced at 30 and 45 degree drift angles compared to the open-water condition. However, the lateral force and yaw moment are having similarity to that on the tug located in $-0.10 < \Delta x < 0.00$ region. As the tug moves toward the midship region of the tanker, the longitudinal force, the lateral attraction force and the bow-in yaw moment coefficients are gradually increased. At all of the drift angles, the magnitudes of the coefficients are higher than the open-water tug. These effects are due to the low pressure field around the tanker's midship region, which attracts the tug. However, the attraction force distribution along the tug is biased towards the forward section due to the significant difference in pressure in that region, thus resulting in a bow-in yaw moment (see Figure 5.5).

When the tug reaches the aft region of the tanker, there is a gradual decrease in the longitudinal force, lateral attraction force and bow-in yaw moment coefficients, due to the tug's interaction with the tanker's aft pressure recovery region (see Figure 5.4). As seen in Figure 5.4, at zero and 15 degree drift angles the longitudinal drag force coefficient on the interacting tug is lower than the open-water tug when Δx is between 0.7 and 0.9. This is mainly due to the influence of pressure recovery region at the stern of the tanker, which creates a reduction in pressure gradient along the tug's length. When the tug moves past

this region, the coefficients at all the angles gradually recover to the magnitudes of the open-water condition as it moves away from the region of the tanker's pressure influence. In summary, as shown in Figure 5.4, the trends in the force and moment coefficients at all longitudinal locations are found to be rather similar between the drift angles examined. Thus, although the influence of the interaction increases over larger drift angles, the trends in the force and moment coefficients remain fairly consistent. It is also noted that the difference in the force and moment coefficients between open-water and interacting tugs are fairly small when the drift angle is less than 15 degrees.

5.6.2 Interaction effects at a tug drift angle between 60 to 90 degrees

Figure 5.6 shows the forces and moment coefficients for an open-water and an interacting tug when it is at non-dimensionalised lateral distances (Δy) of 0.50 and 1.00 and at drift angles of 60, 70, and 90 degrees. At the tanker's forward region ($-0.10 < \Delta x < 0.00$), the tug experiences significantly higher longitudinal force to that experienced in the open-water condition. The lateral attraction force and bow-in yaw moment coefficients are also higher compared to the open-water tug condition, although the differences are significantly less than the longitudinal force coefficient.

When the tug is at the tanker's midship region, a tug drift angle of 60 degrees has the largest variation in forces and moment coefficients between the open-water and interacting tugs. At drift angles of 75 and 90 degrees the forces and moment coefficients of the tug in the midship region are more consistent. When the tug is located in the tanker's aft region (i.e. $-1.00 < \Delta x < -0.90$), a relatively large variation in the forces and moment coefficients is observed compared to the open-water tug condition. The reason for these significant variations is the tanker's pressure recovery region that affects the pressure distribution around the tug, similar to the observation discussed in Section 5.6.1 for the lower drift angles. Another significant observation is that the lateral force on the tug at a drift angle of 90 degrees is a repulsion force, contrary to the other angles that generate an attraction force. Interestingly comparing the lateral force coefficient, in Figures 5.4 and 5.6, shows that the attraction force increases as the drift angle increases to about 45 degrees and it then reduces culminating as a repulsion force when the drift angle is close to 90 degrees.

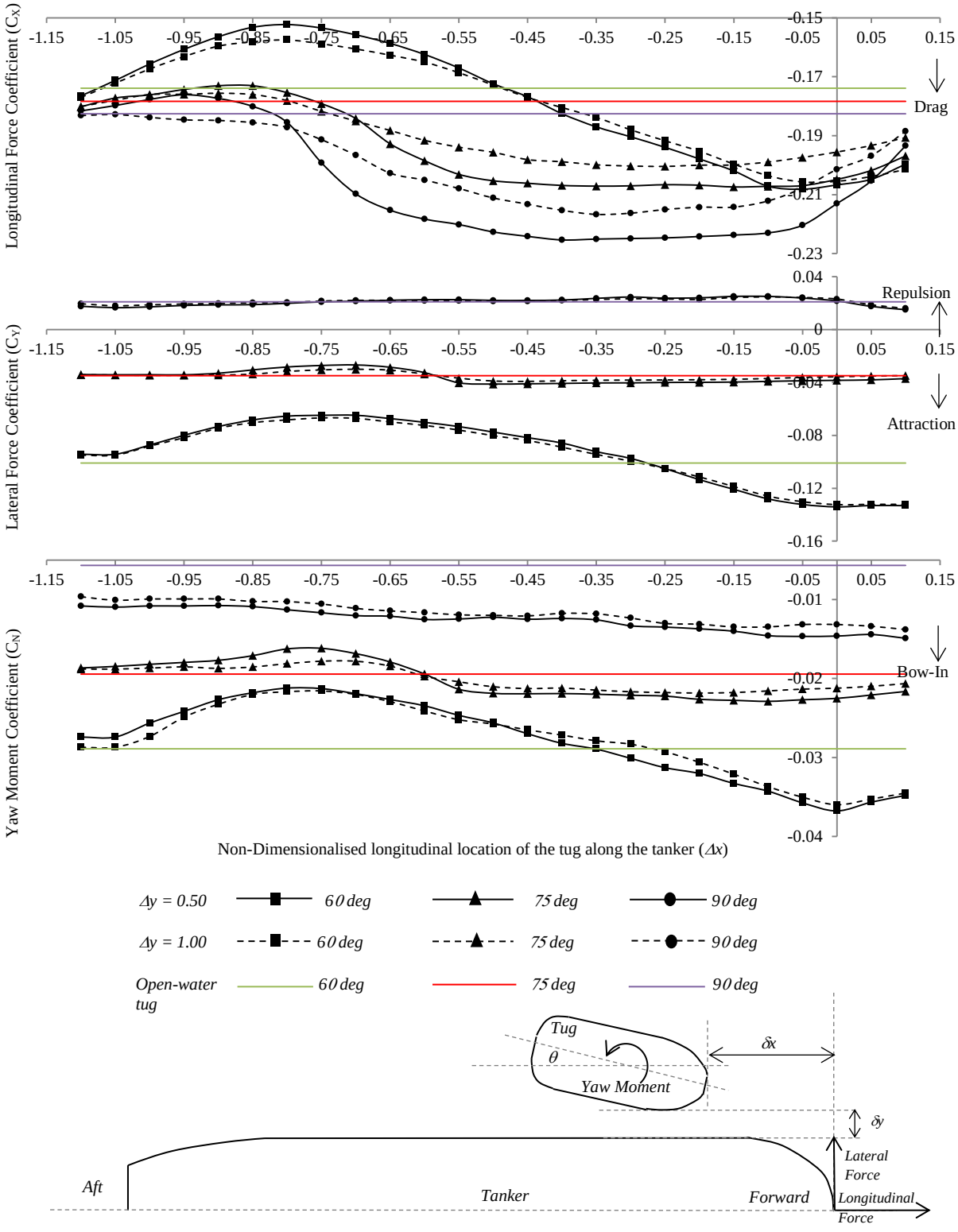

Figure 5.6: CFD predicted forces and moment coefficients for a tug operating at the non-dimensionalised lateral separation (Δy) of 0.50 and 1.00 from a tanker, at tug drift angles (θ) of 60, 75, and 90 degrees in comparison to an open-water tug. Δx is the non-dimensionalised longitudinal separation.

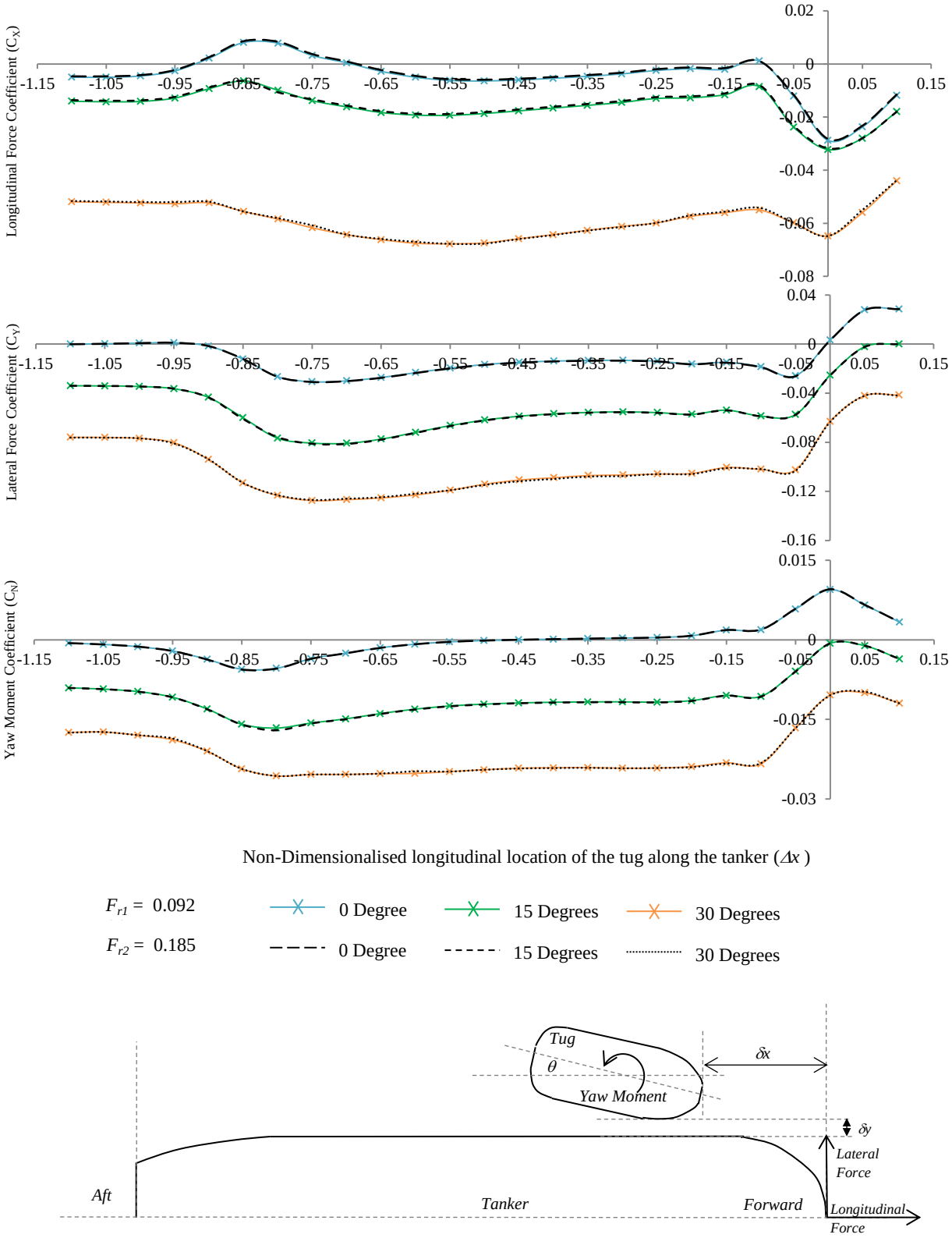

Figure 5.7: CFD predicted forces and moment coefficients for the interacting tug operating at Froude numbers (F_r) 0.092 and 0.185 at tug drift angles (θ) of 0, 15, and, 30 degrees. Non-dimensionalised lateral separation from the tanker is Δy = 0.03. Δx is the non-dimensionalised longitudinal separation.

5.6.3 Effect of the Froude number on interaction effects

In order to investigate the Froude number effects on the induced interaction on the tug during ship-assist manoeuvres, two full-scale speeds of 3 knots and 6 knots (tug length based Froude numbers of 0.092 and 0.185 respectively) were investigated. The speeds represented the usual tug speed range during such manoeuvres (Hensen, 2003). Figure 5.7 shows the predicted forces and moment coefficients on the tug operating at these two Froude numbers, at drift angles of 0, 15 and 30 degrees, and at a non-dimensionalised lateral separation (Δy) of 0.03. The overall results indicate that the respective force and moment coefficients predicted for the two Froude numbers are within 2.7% of each other, thus establishing reasonable Froude number independence within the operational speed range. Although the results at Δy = 0.50 and 1.00 are not presented here, they too show a similar trend thus confirming the Froude number independence.

5.6.4 Effect of the lateral separation on interaction effects

In this section, the interaction effects on the tug operating within the forward, midship and aft regions are investigated in detail by changing the lateral separation from 0.03 to 2.00 times the tanker's breadth. The interaction effects are calculated using Equation 5.6 by subtracting the forces and moments acting on the same tug operating in open-waters (i.e. X_o, Y_o and N_o) from the forces and moment acting on the interacting tug (i.e. X_I, Y_I and N_I) at each speed and drift angle.

$$A = A_I - A_0 \tag{5.6}$$

where the variable A represents the forces X and Y, and the moment N in turn.

Figures 5.8, 5.9, and 5.10 show the interaction forces and moment coefficients for the tug located at Δx = -0.10, Δx = -0.50, and Δx = -0.75 longitudinal locations along the tanker respectively. As seen in the figures, irrespective of the tug's longitudinal location, the interaction coefficients decline as the lateral separation is increased for all drift angles. It is further noted that when the non-dimensionalised lateral separation is greater than Δy =

1.00, the decline in the interaction coefficients is clearly apparent at all of the drift angles and locations. From Figures 5.8 and 5.9 it is seen that when the tug is at Δx = -0.10 and -0.50 locations, the interaction longitudinal force and yaw moment coefficients have their maximum magnitudes when the drift angle is 90 degrees.

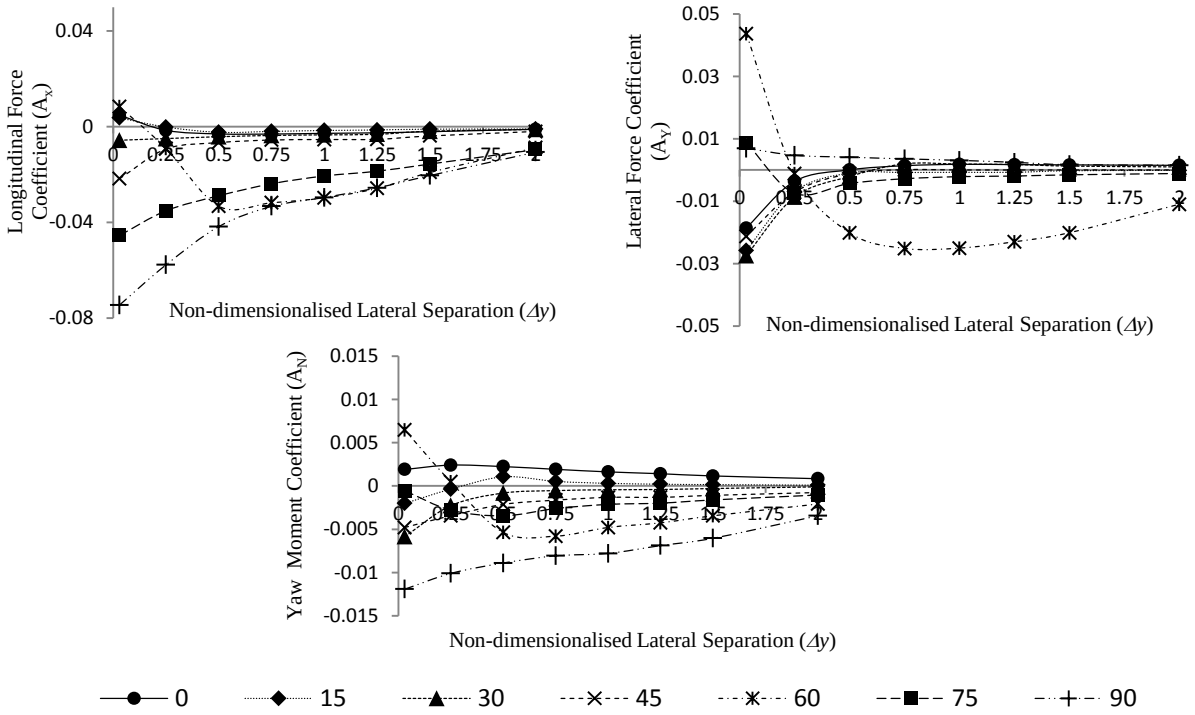

Figure 5.8: Interaction effect coefficients for a tug operating at Δy = 0.03 to 2.00 non-dimensionalised lateral separations with a tanker at zero to 90 degrees drift angles (θ) at Δx = -0.10 non-dimensionalised longitudinal location along the tanker.

The interaction lateral force coefficient is a maximum for the 60 degree drift angle at Δx = -0.10, and for the 45 degree angle at Δx = -0.50. When the tug is at the Δx = -0.75 location, the 60 degree drift angle shows the maximum interaction longitudinal force and yaw moment coefficients. The magnitudes of the interaction lateral force coefficient are at a maximum at the 45 degree drift angle for most of the lateral separations. For the majority of tug drift angles, it is seen from Figures 5.8, 5.9, and 5.10 that the interaction force and moment coefficients have the smallest magnitudes at a drift angle of 15 degrees among the drift angle range investigated. However, when the tug is at Δx = -0.10 location and at 75 and 90 degree drift angles, the lateral force and yaw moment coefficients experience their lowest magnitudes for a lateral separation Δy = 0.03. At a few tug drift angles and locations, e.g. 60 degrees when the tug is at Δx = -0.10 and 90 degrees when the tug is at Δx = -0.50

and -0.75, the interaction force and moment coefficients vary in a different manner in comparison to the majority of the conditions investigated. In order to understand the reason the variation, additional simulations at small increments of drift angles and lateral separations are required. However, such a detailed analysis was not the aim of the current study and it is therefore left to be addressed in future work.

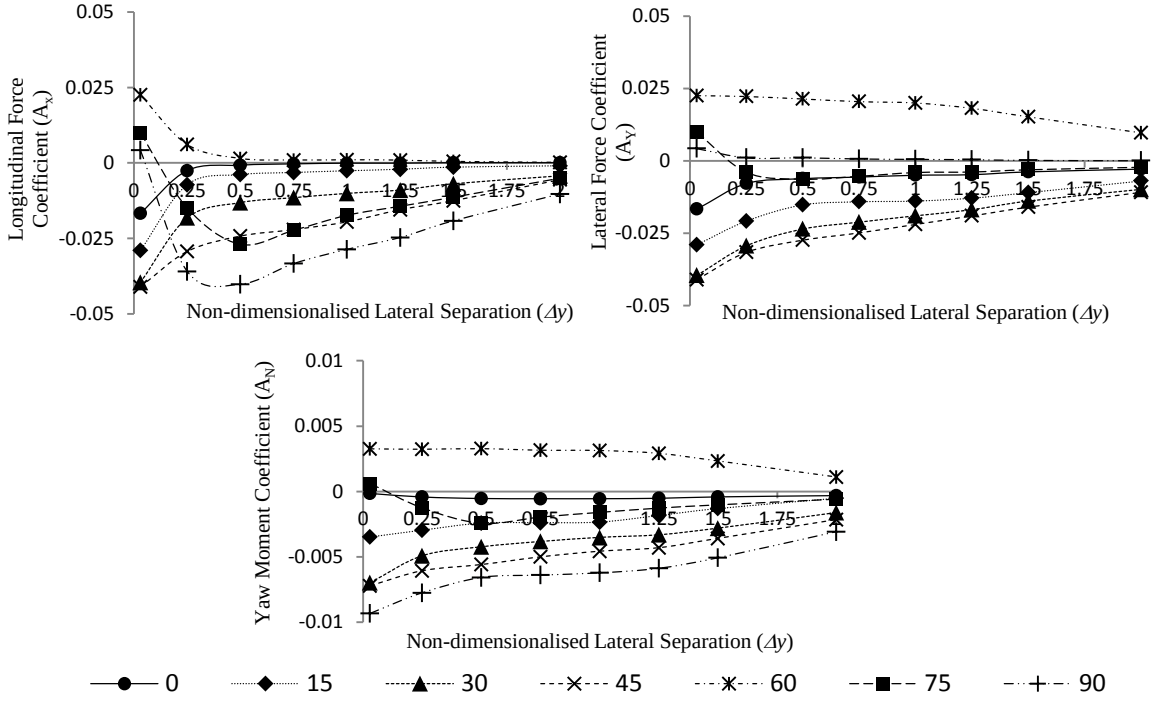

Figure 5.9: Interaction effect coefficients for a tug operating at Δy = 0.03 to 2.00 non-dimensionalised lateral separations with a tanker at zero to 90 degrees drift angles (θ) at Δx = -0.50 non-dimensionalised longitudinal location along the tanker.

Figure 5.11 illustrates the CFD pressure plots for the tug at the tanker's forward and midship regions at drift angles of zero and 90 degree. The figure shows that with the increasing lateral separation, the tug moves away from the tanker's pressure field, thus reducing the interaction effects as expected. Furthermore, between Δy = 0.03 and 1.00 lateral separations, it is seen that the pressure field around the interacting tug is significantly affected by the tanker's presence compared to the open-water tug. This creates a large deviation of the pressure around the interacting tug, thus making it difficult to safely manoeuvre the tug within that region of the tanker. At Δy = 2.00, the pressure around the tug settles to a magnitude and distribution similar to the pressure field of the open-water tug. Thus, as seen in Figures 5.8, 5.9, and 5.10, at Δy = 2.00, the effects of the interaction are negligible, providing a safe region for the tug to operate within.

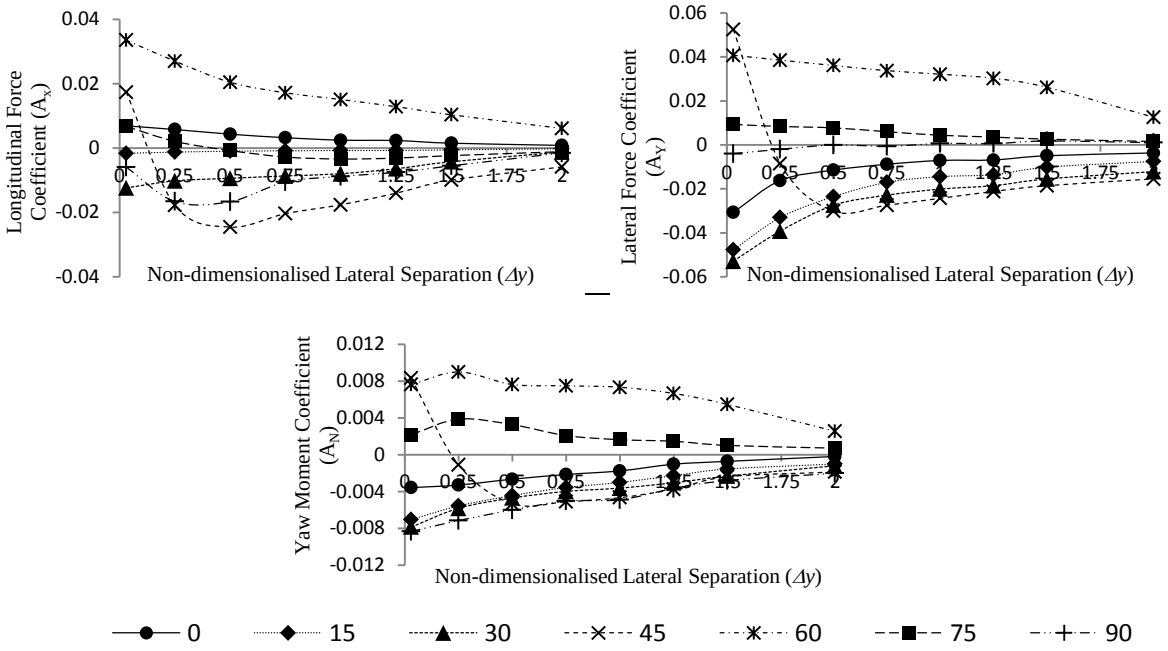

Figure 5.10: Interaction effect coefficients for a tug operating at Δy = 0.03 to 2.00 non-dimensionalised lateral separations with a tanker at zero to 90 degrees drift angles (θ) at Δx = -0.75 non-dimensionalised longitudinal location along the tanker.

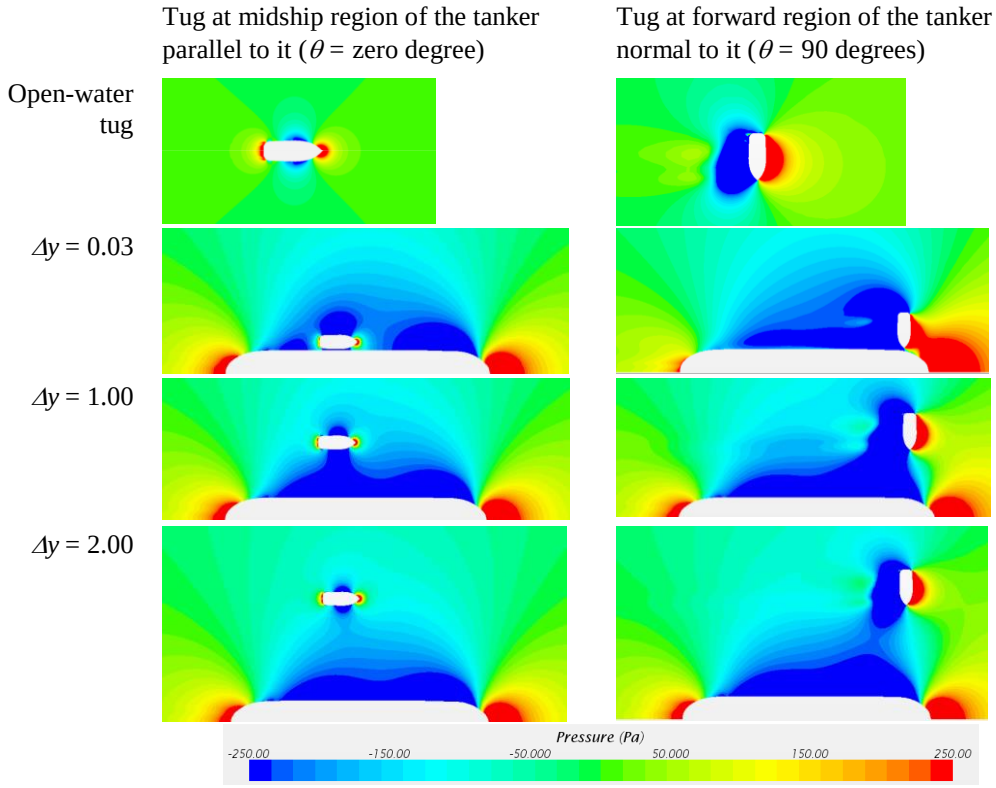

Figure 5.11: CFD Pressure Plots for the tug operating at Δy = 0.03, 1.00, and 2.00 non-dimensionalised lateral separations with drift angles of zero and 90 degrees at the midship and forward regions of the tanker respectively.

5.7 Safe Tug Operations

5.7.1 Safe tug operational envelope

Figure 5.12 shows critical lateral regions that tug operators should be aware of during ship-assist manoeuvres, which is developed based on the results discussed in Section 5.6. As seen in the figure, when the lateral separation between the vessels is less than 0.5 times the ship's breadth (i.e. Δy < 0.50), the interaction effects induced on the tug become critical with significant influence on the tug's behaviour. As most ship-assist manoeuvres require tugs to operate within this region, it is essential that tug operators are aware of the interaction effects and the resulting behaviour at the various longitudinal locations (Δx) in order to ensure safe operations. The region between Δy = 0.50 and 1.00 shows a reduction in the interaction effects, while beyond Δy = 1.00 the interaction effects reduce significantly as discussed in Section 5.6.4. Beyond Δy = 2.00, the interaction effects become almost negligible, and is thus relatively safe for the tugs to operate in during ship escort manoeuvres. Although the length of the tow lines used between the two vessels during tug escort operations is generally around 100 m to 150 m, i.e. Δy = 2.70 and 4.10, some tug operators use smaller tow-line of around 60 m to 80 m, i.e. Δy = 1.60 and 2.10, (Hensen, 2003). Based on the findings of this study, it is prudent to maintain a gap of at least 2.00 times the larger ship's breadth between the vessels, thus requiring a sufficiently long tow line.

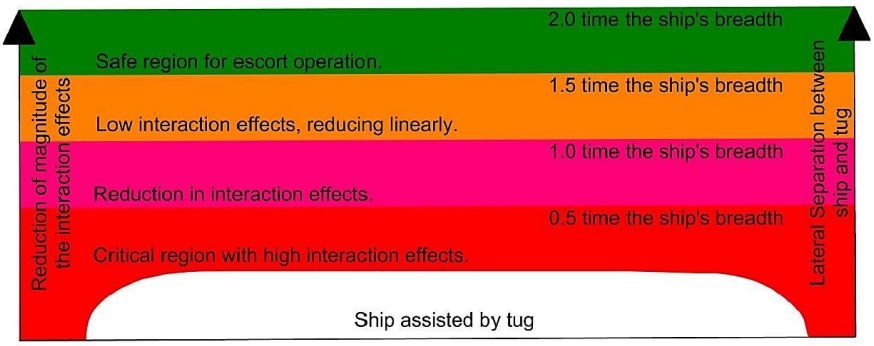

Figure 5.12: Regions around a ship showing the interaction effects induced on a tug operating in close proximity during ship-assist manoeuvres.

5.7.2 The safest paths for tugs to approach large ships

Based on the finding presented in this study, it is possible to identify safe paths for a tug to take in order to approach the forward, midship, and aft regions of a larger ship. For each location, the interaction forces and moment coefficients (see Equation 5.6) acting on the tug will be presented using the sign convention shown in Figure 5.13, which is based on that used in this study. The magnitudes of the coefficients are highlighted in red within the corresponding axis bars (see Figures 5.13 and 5.14).

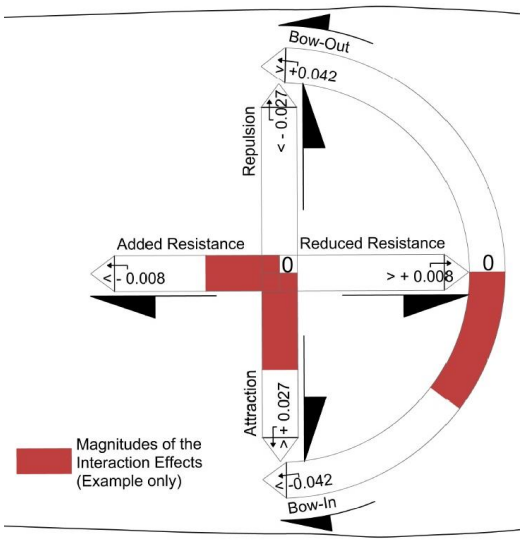

Figure 5.13: Interaction scale used to represent the interaction forces and moment coefficients and their magnitudes (see Figure 5.14).

In Section 5.6.1, it was shown that the interaction effects induced on the tug during ship-assist manoeuvres are at their lowest when the drift angle is less than 15 degrees. Thus, it is advisable for tugs approaching larger ships to maintain their drift angles at less than 15 degrees to reduce the adverse effects due to interaction. Taking this into consideration, Figure 5.14 shows possible safe paths for a tug to approach a larger ship at the forward, midship, and aft regions. The figure includes the interaction effect coefficients acting on the tug at each location using the scale introduced in Figure 5.13. This will provide tug operators with information to better understand the adverse effects on their tug due to the interaction experienced during ship-assist manoeuvres.

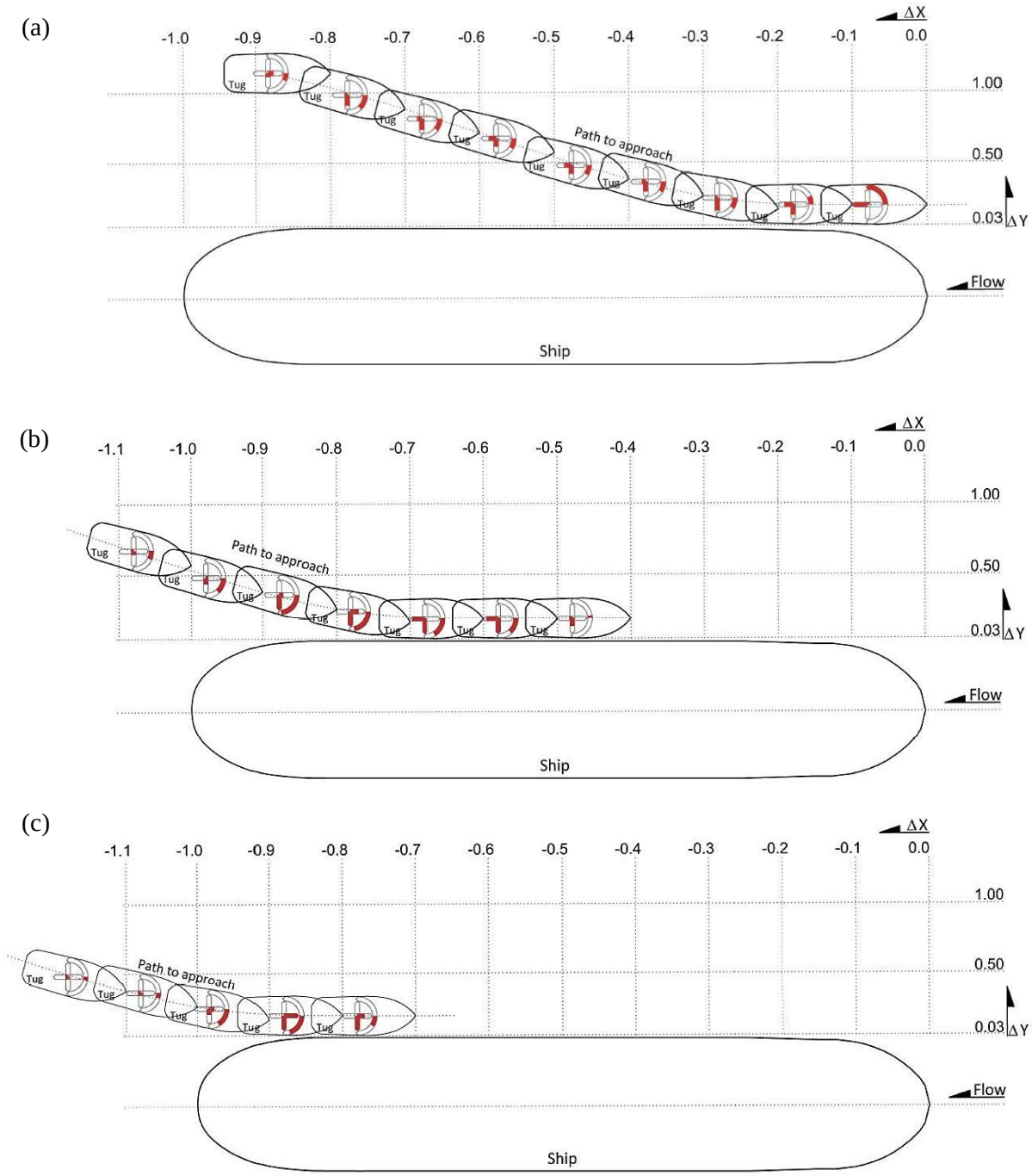

Figure 5.14: Safest path for tugs to approach larger ships, including the magnitudes of the interaction effects at each location. Tug approaching the larger ship's: (a) forward region; (b) midship region; and (c) aft region. The figure is to scale.

As seen in Figure 5.14 (a), the safest path for a tug to enter the forward region of a large ship is to approach the latter just aft of its shoulder (~Δx = -0.2) with a low drift angle (<15 degrees). When sufficiently close to the larger vessel, the tug can straighten to zero degrees

drift, i.e. parallel to the ship, and move forward into the required position. Throughout this path in the figure, the longitudinal force experienced by the tug due to the interaction increases, progressively becoming a maximum when the tug reaches the Δx = 0.00 location. Therefore, tug operators should be prepared to encounter higher longitudinal force due to the interaction as they approach the bow of the vessel. From Figure 5.14 (a) it is also seen that the interaction lateral (attraction) force on the tug significantly increases as the tug moves forward and inwards, until it reaches the Δx = -0.10 location. This lateral force 'sucks' the tug towards the larger ship requiring corrective action from the operator, until it reduces to a negligible value at Δx = 0.00. The interaction yaw moment on the tug shows a steady bow-in pattern until the Δx = -0.20 location, where it begins to reverse and yaw the bow-out and away from the larger ship. This change in interaction effect will require the tug operator to change the tug's yaw control to counter the two different conditions as the tug moves along the length of the ship.

Considering the entry to the midship region (Figure 5.14 (b)), a similar approach is required where the operator should maintain a low drift angle (<15 degrees). As the tug moves forward past the stern region of the larger ship and towards it, the tug will experience an increased suction force and an excessive bow-in yawing moment due to the interaction. Thus, the tug operator will have to counter these effects as the tug moves towards the midship region. However, once the tug reaches the midship region, the interaction effects will diminish enabling the tug to maintain position as required.

A tug approaching the aft region of the larger ship (Figure 5.14 (c)) will also encounter similar interaction forces as described for the previous two cases. It is thus recommended that the tug should follow the path shown in the figure to minimise the interaction forces and moment. As the tug approaches the ship, the low pressure region between the two vessels will result in a suction force and a yaw moment towards the ship. Therefore, as the tug nears the ship the tug operator should expect the suction effect and take appropriate action to maintain separation and heading. It is also not advisable to increase the thrust of the tug as it would accelerate the flow between the vessels, reducing the pressure and further increasing the suction force. Due to the strong suction force and bow-in yaw

moment, it is harder to maintain position around the stern region of the ship for tasks such as rope handling. This is exacerbated due to the presence of the ship's propellers in that region. Therefore, it is essential that tug operators are aware of these interaction forces and their locations, and be trained on the action required to avoid putting the tug in a dangerous situation.

5.8 Conclusion

The aim of this study was to investigate the interaction effects induced on a tug during a ship-assist operation at different lateral and longitudinal distances from a larger ship and at different tug drift angles. A CFD simulation model validated through model-scale experimental measurements was used to determine the interaction effects at full-scale for a range of relative locations between a tug and a larger ship (tanker), at a number of tug drift angles. The results presented in this chapter and the preceding discussion provides the following conclusions with respect to the interaction effects between the two vessels and the safe operating envelop for the tug.

- During ship escort manoeuvres, it is important that the tug maintains a lateral separation of at least 2.0 times the larger ship's breadth to minimise the dynamic (fluctuating) interaction forces and moments. The best location to operate is within the midship region of the larger ship, where the magnitudes of the interaction effects are relatively constant.

- Lateral separations of less than 0.5 times the larger ship's breadth will result in hard to counter fluctuations in the interaction effects at all drift angles. Thus, if possible it is advisable to avoid such small separations during ship-assist manoeuvres.

- Tug drift angles between 45 and 60 degrees have the highest magnitudes and fluctuation in the interaction effects, and thus is best avoided if possible.

- In order to minimise interaction effects, it is best to maintain the smallest possible tug drift angle (less than 15 degrees) and approach the larger vessel close to its midship region.

- Regardless of the speed of the two vessels, the qualitative pattern of the interaction effects is similar. Thus tug operators should be aware that the forward and aft regions of larger ships remain critical areas for interaction effects at most vessel speeds.
- Equations used for non-dimensionalising interaction forces and moment can be used along with the interaction effect plots to calculate the magnitudes of forces and moments that tugs experience during ship-assist manoeuvres.

It is important to inform tug operators on the interaction effects at various locations alongside a large ship during ship-assist manoeuvres and provide them with the required training to deal with such effects. This will include the use of appropriate ship handling simulators that can accurately replicate the interaction effects encountered during such manoeuvring. The findings presented in this chapter will provide the required data to develop Hydrodynamic Interaction Region Plots (HIRPs) for use by tug operators to understand safe tug operational envelopes during ship-assist manoeuvres. Furthermore, the findings provide data to develop algorithms using techniques such as non-linear regression analysis to predict interaction effects, which in turn can be programed to better represent interaction effects within ship handling simulators.

Chapter 6

Hydrodynamic Interaction Region Plots (HIRPs)

This chapter consists of two subchapters:

Part A Hydrodynamic Interaction Effects on Tugs Operating within the Midship Region alongside Large Ships.

Part B Safe Operation of Tugs within Close Proximity to the Forward and Aft Regions of Large Ships.

Chapter 6 – Part A

Hydrodynamic Interaction Effects on Tugs Operating within the Midship Region alongside Large Ships

This subchapter has been published in the Proceedings of the 9th International Research Conference of the General Sir John Kotelawala Defence University, Ratmalana, Sri Lanka. The citation for the research article is:

Jayarathne, B. N., Leong, Z. Q. & Ranmuthugala, D. (2016). 'Hydrodynamic Interaction Effects on Tugs Operating within the Midship Region alongside Large Ships'. *The 9th International Research Conference.* Ratmalana, Sri Lanka: General Sir John Kotelawala Defence University.

Chapter 6A has been removed for copyright or proprietary reasons.

Chapter 6 – Part B

Safe Operation of Tugs within Close Proximity to the Forward and Aft Regions of Large Ships.

This subchapter has been published in the Proceedings of the 10th International Research Conference of the General Sir John Kotelawala Defence University, Ratmalana, Sri Lanka. The citation for the research article is:

Jayarathne, B. N., Ranmuthugala, D. & Leong, Z. Q. (2017). 'Safe Operation of Tugs within Close Proximity to the Forward and Aft Regions of Large Ships'. *The 10th International Research Conference.* Ratmalana, Sri Lanka: General Sir John Kotelawala Defence University.

Chapter 6B has been removed for copyright or proprietary reasons.

Chapter 7

Summary, conclusion and recommendations for future work

This chapter summarises the work carried out in this project and brings together the results of the individual chapters of this thesis, concluding on their overall findings. It also discusses the implications, contributions, and limitations of this study, and recommendations for further work.

7.1 Summary

This project investigated the hydrodynamic interaction effects induced on a tug operating in close proximity of a large ship during tug assist manoeuvres. The motivation behind this study was to quantify the hydrodynamic interaction that influences a tug's ability to safely manoeuvre in close proximity to a ship, as well as to identify a safe operating envelope for the tug. Thus, the specific research question for this project was:

"What are the adverse hydrodynamic interaction effects induced on a tug, and what is the safe operating envelope to minimise these effects while manoeuvring in close proximity to a larger ship?"

Although there are a number of findings in the literature that discusses interaction effects acting on vessels operating in close proximity, they are generally limited to vessels operating on parallel courses. However, during ship-assist manoeuvres, tugs need to frequently change their location, distance, and orientation alongside large ships in order to guide the ship along the intended path. The tug will therefore need to operate at various drift angles and at different longitudinal and lateral locations relative to the ship. Therefore, it is important to have a good understanding of the hydrodynamic interaction between the vessels, which will enable tug operators to identify safe operating envelopes during such manoeuvres.

This study was conducted using CFD simulations that were validated using results obtained from captive model tests conducted in the Model Test Basin at the Australian Maritime College. The CFD-RANS simulations were selected after comparison against Potential Flow (PF) solvers and after a comprehensive verification and validation programme. The simulations were carried out at model-scale for validation purposes and at full-scale to identify scaling effects, with the latter enabling the non-dimensionalisation of the interaction effects and relative positions for vessels of different sizes and ratios. A comprehensive full-scale simulation matrix enabled the identification of safe operating envelopes for tugs operating in close proximity to large ships. This enabled the development

of hydrodynamic interaction region plots (HIRPs) for tugs operating in the forward, midship and aft regions of large ships.

7.2 Conclusions

Based on the findings from the preceding chapters, the main conclusions on the hydrodynamic interaction effect for a tug operating in close proximity to a large ship during ship-assist manoeuvres are presented below.

7.2.1 Hydrodynamic interaction effects induced on tugs

Relative longitudinal and lateral positions

The midship area of a large ship was identified as the safest place for a tug to operate within, as it experiences the least amount of fluctuations in the hydrodynamic interaction forces and moments. Thus, if a tug is escorting a larger ship, it is advisable that it operates within its midship region. The bow region of the ship is difficult for a tug to approach, as the strong interaction effects due to the high pressure region act to repel the tug away from the ship. Conversely in the stern region of the larger ship, the interaction effects tend to attract the tug towards the ship, which increases the risk of collision. The bow and stern regions of the ship also present a challenge to the tug's manoeuvrability, due to the rapid changes in the magnitude of the interaction forces and moments in response to small changes in the relative longitudinal position. Thus, wherever possible tugs should attempt to operate closer to the midship region of large ships during tug assist operations.

Although the effects on the tug's longitudinal force coefficient as a function of the lateral distance to the ship was relatively small, the changes to the lateral force and yaw moment coefficients were sufficiently high to significantly affect the tug's manoeuvrability. A general trend in the tug's interaction effect coefficients at different lateral separations as a function of the longitudinal position of the tug was less observable. Nevertheless, the maximum and minimum values, and the qualitative trends in the interaction behaviour as a function of longitudinal position were found to be similar at different lateral positions.

Tug drift angle

Tug drift angles ranging from zero to 15 degrees and 75 to 90 degrees resulted in the lowest magnitudes and variations in the interaction effects. The parallel operation (zero degrees drift angle) had the least variation in the interaction behaviour of all the drift angles examined. For the drift angle range between 15 to 75 degrees, small changes in the drift angle resulted in complex variations in the magnitudes and directions of the induced interaction forces and moments at most tug locations relative to the ship. Thus, tug operators should attempt to avoid or minimise operating within this drift angle range in any relative location, if possible.

Non-dimensionalisation method for lateral distance

A number of methods were investigated to identify a method to non-dimensionalise the lateral distances between the vessels of different sizes. To compare the interaction effects between model-scale and full-scale vessels of different sizes, the lateral distance between the vessel centrelines is best non-dimensionalised as a ratio of the larger ship's breadth. The results obtained using this approach revealed good agreement for interaction effects between vessels of the different sizes and scales. By using the larger ship's breadth as the reference dimension for the non-dimensionalisation, the interaction behaviour results obtained for one relative size ratio between the vessels to predict the safe operating distances for other size ratios.

Froude number

The induced force and moment interaction effects on the tug were found to be independent of the tug length Froude number within the usual speed range for ship-assist operations. Thus, tug operators could utilise the results of this study to predict the critical regions around a large ship during ship-assist manoeuvres at typical vessel speeds for such operations. The predicted coefficients can be used to calculate the magnitudes of the interaction effects on the tug at different speeds during ship-assist manoeuvres.

Tug manoeuvring limits due to hydrodynamic interaction

When a tug approaches a large ship underway, it is best to do so at a drift angle of less than 15 degrees. Although a tug at a drift angle between 75 and 90 degrees will experience a low

lateral force, the longitudinal force is significant, requiring the tug to possess strong lateral manoeuvring capability. When a tug operates on a parallel course to the ship during tug assist manoeuvres, such as rope handling and course guidance, it is best to follow a path which results in a tug angle of less than 15 degrees to the ship all the time, as it results in the least interaction effects. Thus, the tug should commence its approach to the ship at a considerable distance from the vessel, enabling the tug to gradually approach the ship at a small drift angle. The HIRPs presented in the thesis provide tug operators with safe paths to approach large ships and safe operating envelopes around such ships during ship-assist and escort manoeuvres.

7.2.2 Simulation and experimental programmes

Use of PF solvers

A commercially available PF solver, i.e. Futureship®, was unable to accurately predict the forces and moments induced on a tug when operating with a wet transom or at drift angles. Thus, PF solvers were deemed inadequate to predict the hydrodynamic interaction effects on tugs during ship-assist manoeuvrers. This was supported by poor agreement against experimental data and analysis of the flow structures, showing that PF solvers could not adequately resolve the wake region in the leeward region of the tug. Similar issues of PF solvers were previously found by Maki (2006), Saha and Tarafder (2013), Tarafder et al. (2009), Doctors (2006), Doctors and Beck (2005) also in their studies. However, it is noted that other PF solvers with relevant modifications may be able to better capture the forces and moments under these conditions.

RANS-based CFD simulations, including turbulence models and near wall mesh

CFD-RANS simulation models were able to adequately capture the interaction effects and behaviour of a tug operating in close proximity to a large ship. However, the quality and accuracy of the CFD predictions were highly dependent on the selection of the turbulence model and mesh refinement around the vessels.

It was shown that a $y^+ \leq 1$ for the near wall mesh with the SST turbulence model offered good agreement against the experimental measurements, for both the parallel and drifted

tug manoeuvres at the speed range tested. The RKE turbulence model results closely followed the SST results, while the SA turbulence model showed significantly larger discrepancy. A dimensionless wall distance between $5< y^+ <20$ did not provide good results with any of the three turbulence models used in this study. If the available computational resources are limited, then a y^+ of between 20 and 30 with the wall function model can provide a reasonable representation of the interaction trend, but not an accurate measure of the actual forces and moments. A $y^+ >30$ was found to be inadequate to predict the interaction effects due to the large deviations in the results. The use of CFD simulations to predict the interaction behaviour was deemed essential in this thesis due to the large range of conditions and vessel shapes investigated.

Experiments

The experimental data used to validate the CFD predictions has provided a valuable insight into the characteristics of the hydrodynamic interaction between a tug and a larger vessel. Despite the advantages of CFD over the spatial limitations of experiments, the results of this study clearly show that CFD still requires experimental data for validation in order to optimise the computational mesh domain and the numerical settings. The good agreement between the CFD and experimental results provided the necessary confidence in the techniques and settings used to develop the simulation models, which can be used to develop future simulation models. Furthermore, the experimental measurements provide data for validation of future simulation models and comparison with other experimental programmes. In addition, the detailed experimental uncertainty analysis carried out can be used as a guide to perform similar analysis.

7.3 Implications and Contribution to the Research Area

In this project, the numerical and experimental studies were conducted to investigate the hydrodynamic interaction between a tug operating in close proximity to a ship during ship-assist manoeuvres. The work focuses only on the bare hull forms of the vessels (i.e. without appendages such as propellers, rudders, stabilisers, etc.), thus enabling the investigation of the effects of tug's relative position to the ship, its drift angle, and its size in comparison to

the larger ship on the interaction behaviour to be unadulterated by the influence of the appendages. The proven numerical and experimental methodologies developed and presented will be valuable to other researchers to conduct similar studies and extend upon the conditions covered within this project. The novel aspect and contributions by this work to the area of hydrodynamic interaction during tug-ship operations are outlined in Section 1.6 in Chapter 1, as is the limitation of the study in Section 1.5.

The experimental data generated during the project for dissimilar size vessels operating in different relative locations and configurations provides researches with validation data currently lacking in the public domain. They also provide information on interaction effects during such operations, albeit at model-scale. Similarly, the numerical results provide data for comparison and analysis to understand and quantify the hydrodynamic interaction effects on tugs during tug assist operations, both at model-scale and full-scale.

The range of manoeuvres discussed in this chapter provides a comprehensive overview of the hydrodynamic interaction effects on a tug during ship-assist manoeuvres. The results of this study were used to prepare a number of interaction effect plots showing critical locations around the ship and drift angles that tug operators should be aware of during ship-assist manoeuvres. The HIRPs presented in the thesis enables tug operators to identify safe operating envelopes for a tug to approach a larger vessel during ship-assist manoeuvres. Furthermore, the validated non-dimensionalisation methods together with the HIRPs developed in this project can be used to estimate the forces and moments during such operations, and thus identify safe operating distances for a range of ship-to-tug size ratios. This could be of significant practical value to tug operators in preparation to and during such operations.

The hydrodynamic interaction data presented in this thesis is relatively comprehensive, and can be used by ship handling simulator developers in order to upgrade the mathematical algorithms and models used to predict the interaction effects on tugs. This is an area that has constantly been earmarked for improvement in modern ship handling simulators (Hensen, 2012, Hensen et al., 2013, Lindberg et al., 2012, Pinkster and Bhawsinka, 2013, Jong, 2007). This study provides the required tools and data to commence this process.

7.4 Further Work

The work presented in this thesis can be extended to address additional operating configurations and manoeuvres, as well as developing operational guidance material for tug operators. The findings of this study can lead to the following direct extensions.

1. Develop guidance materials, e.g. guidelines, pamphlets, polar plots, posters and animations, for tug and ship operators and ship pilots on the potential risks and hazards, and generate recommended operational guidelines for ship-assist manoeuvres.

2. Develop mathematical algorithms and models to predict interaction effects on tugs during ship-assist manoeuvres. This would enable simulators to use results obtained for a large number of tug-ship combinations and improve current models and interaction behaviour within ship handling simulators.

3. Investigate the interaction effects acting on tugs with relative motion between the tug and the larger ship. This will enable a more extensive and transient representation of the interaction effects on tugs approaching, leaving, and manoeuvring in close proximity to larger ships at different speeds.

4. Utilise fully-appended models of the vessels in the simulation, enabling comparison against the unappended data in this study, in order to identify the influence of these appendages on the interaction effects.

5. Include both shallow water effects and restricted waters/bank interaction effects on tugs during ship-assist manoeuvres. This will enable ship operators to develop a comprehensive knowledge base on the effect of the interaction on a tug during such manoeuvres.

6. Conduct experiments at large tug drift angles (i.e. greater than 60 degrees) to validate the interaction forces and moments predicted by the CFD simulations carried out in this study.

References

Artyszuk, J. (2013), 'Types and Power of Harbour Tugs - The Latest Trends', *Prace Naukowe Politechniki Warszawskiej - Transport*, vol. z.98.

Brandner, P. (1995), 'Performance and effectiveness of omni-directional stern drive tugs', PhD thesis, University of Tasmania.

Brendan, S. (2009), 'Escort Tug Performance Prediction: A CFD Method', Master of Applied Science thesis, University of Victoria.

CD-Adapco (2015), *User Manual of StarCCM+ Version 10.02*.

Chen, G.R. & Fang, M.C. (2001), 'Hydrodynamic Interactions Between Two Ships Advancing in Waves', *Ocean Engineering*, vol. 28, no. 8, pp. 1053-1078.

Dand, I.W. (1975), 'Some Aspects of Tug-Ship Interaction', in KD Troup (ed.), *The 4th International Tug Convention*, New Orleans, Louisiana, USA.

Dand, I.W. (1978), 'The Physical Causes of Interaction and its Effects', paper presented to The Nautical Institute Conference on Shiphandling, Plymouth Polytechnic, 24-25 Nov. 1977.

Dand, I.W. (1995), 'Interaction', in *The Nautical Institute, Humberside Branch Seminar*, Humberside, UK, pp. 1-20.

DNV GL Maritime (2014), *User Manual of FS-Flow Version 14.0228*.

Doctors, L.J. (2006), 'A Numerical Study of the Resistance of Transom Stern Monohulls', in *The 5th International Conference on High Performance Marine Vehicles*, Australia.

Doctors, L.J. & Beck, R.F. (2005), 'The Separation of the Flow Past a Transom Stern', in *The 1st International Conference on Marine Research and Transportation (ICMRT '05)*, Ischia, Italy, pp. 1-14.

Eliasson, S. & Olsson, D. (2011), 'Barge Stern Optimization: Analysis on a Straight Shaped Stern using CFD', MSc thesis, Chalmers University of Technology.

Falter, J. (2010), 'Validation of a Potential Flow Code for Computation of Ship-Ship Interaction Forces with Captive Model Test Results', Ghent University, Belgium.

Fonfach, J.M.A. (2010), 'Numerical Study of the Hydrodynamic Interaction Between Ships in Viscous and Inviscid Flow', Instituto Superior Tecnico, Portugal.

Fonfach, J.M.A., Sutulo, S. & Soares, C.G. (2011), 'Numerical Study of Ship to Ship Interaction Forces on the Basis of Various Flow Models', in B Pettersen, TE Berg, K Eloot & M Vantorre (eds), *The 2nd International Conference on Ship Manoeuvring in Shallow and Confined Water: Ship to Ship Interaction*, Trondheim, Norway, pp. 137-146.

Fortson, R.M. (1974), 'Interaction Force Between Ships', Massachusetts Institute of Technology, USA.

Geerts, S., Vantorre, M., Eloot, K., Huijsmans, R. & Fierens, N. (2011), 'Interaction Forces in Tug Operation', in B Pettersen, TE Berg, K Eloot & M Vantorre (eds), *The 2nd International Conference on Ship Manoeuvring in Shallow and Confined Water: Ship to Ship Interaction*, Trondheim, Norway.

Gui L., Longo J., Metcalf B., Shao J. & Stern F. (2000), 'Forces, Moment and Wave Pattern for Naval Combatant in Regular Head Waves', in *The 23rd Symposium on Naval Hydrodynamics*, Val de Reuil, France.

Hensen, H. (2003), *Tug Use in Port: A Practical Guide*, Nautical Institute.

Hensen, H. (2012), 'Safe Tug Operation: Who Takes the Lead?', *International Tug & OSV*, vol. 2012 July/August, pp. 70-76.

Hensen, H., Merkelbach, D. & Wijnen, F.V. (2013), *Report on Safe Tug Procedures*, Dutch Safety Board, Netherlands.

Hess, J.L. & Smith, A.M.O. (1964), 'Calculation of Nonlifting Potential Flow about Arbitrary Three-dimensional Bodies', *Journal of Ship Research*, vol. 8, pp. 22-44.

Hess, J.L. & Smith, A.M.O. (1967), 'Calculation of Potential Flow about Arbitrary Bodies', *Progress in Aeronautical Sciences*, vol. 8, pp. 1-137.

ITTC (2002a), *CFD General Uncertainty Analysis in CFD Verification and Validation Methodology and Procedures*, 7.5-03-01-01, International Towing Tank Conference,.

ITTC (2002b), *Testing and Extrapolation Methods - Resistance Uncertainty Analysis*, 7.5-02-02-02, International Towing Tank Conference.

ITTC (2011a), *Resistance Test*, 7.5-02-02-01, International Towing Tank Conference.

ITTC (2011b), *Ship Models*, 7.5-01-01-01, Revision 03, International Towing Tank Conference.

Jayarathne, B.N., Leong, Z.Q. & Ranmuthugala, D. (2016), 'Hydrodynamic Interaction Effects on Tugs Operating within the Midship Region alongside Large Ships', paper presented to 9th International Research Conference, Ratmalana, Sri Lanka, 8th & 9th September.

Jayarathne, B.N., Ranmuthugala, D., Chai, S. & Fei, G. (2014), 'Accuracy of Potential Flow Methods to Solve Real-time Ship-Tug Interaction Effects within Ship Handling Simulators', *International Journal on Marine Navigation and Safety of Sea Transportation*, vol. 8, no. 4, pp. 497-504.

Jayarathne, B.N., Ranmuthugala, D., Leong, Z.Q. & Fei, G. (2017), 'Non-Dimensionalisation of Lateral Distances Between Vessels of Dissimilar Sizes for Interaction Effect Studies ', *Transactions RINA: Part A1- International Journal of Maritime Engineering (Accepted for publication)*.

Jayarathne, B.N., Ranmuthugala, D., Leong, Z.Q., Fei, G. & Chai, S. (2017), 'Numerical and Experimental Prediction of Hydrodynamic Interaction Effects Acting on Tugs during Ship Manoeuvres', *Journal of Marine Science and Technology (Accepted for publication)*.

Jong, J.H. (2007), 'Ship-Assist in Fully Exposed Conditions - Joint Industry Project SAFETUG', paper presented to Tugnology '07, Southampton, UK.

Kongsberg Maritime (2012), *Hydrodynamic Modelling Tool: Mathematical Model of Ship Dynamics*, SU-0689-A18.

Kuniji, K., Hiroshi, H., Yoshihisa, H. & Eijiro, F. (1984), 'On a New Mathematical Model for Manoeuvring Motions of Ships in Low Speed', *Japan Society of Naval Architects*, vol. 155, pp. 15-24.

Lataire, E., Vantorre, M. & Delefortrie, G. (2009), 'Captive Model Testing for Ship-to-Ship Operations', in *MARSIM '09*, Panama.

Lataire, E., Vantorre, M., Delefortrie, G. & Candries, M. (2012), 'Mathematical Modelling of Forces Acting on Ships During Lightering Operations', *Ocean Engineering*, vol. 55, no. November 2013, pp. 101-115.

Lau, Y.-y. & Ng, A.K.Y. (2015), 'The Motivations and Expectations of Students Pursuing Maritime Education', *Journal of Maritime Affairs*, vol. 14, pp. 313-331.

Leong, Z.Q. (2014), 'Effects of Hydrodynamic Interaction on an AUV Operating Close to a Moving Submarine', PhD thesis, University of Tasmania.

Leong, Z.Q., Ranmuthugala, D., Penesis, I. & Nguyen, H. (2014), 'RANS-Based CFD Prediction of the Hydrodynamic Coefficients of DARPA SUBOFF Geometry in Straight-Line and Rotating Arm Manoeuvres', *Transactions RINA: Part A1- International Journal Maritime Engineering*.

Lindberg, O., Bingham, H.B., Engsig-Karup, A.P. & Madsen, P.A. (2012), 'Towards Real Time Simulation of Ship-Ship Interaction', paper presented to The 27th International Workshop on Water Waves and Floating Bodies IWWWFB 2012, Copenhagen, Denmark, April 22-25, 2012.

Lu, H., Yang, C. & Lohner, R. (2009), 'Numerical Studies of Ship-Ship Interactions in Extreme Waves', paper presented to Grand Challenges in Modeling & Simulation USA.

MAIB (2011), *Lessons from Marine Accidents*, Marine Accident Investigation Branch, United Kingdom.

Maki, K.J. (2006), 'Transom Stern Hydrodynamics', PhD thesis, The University of Michigan.

Mantzaris, D.A. (1998), 'A Rankine Panel Method as a Tool for the Hydrodynamic Design of Complex Marine Vehicles', PhD thesis, Massachusetts Institute of Technology.

MCA (2001), *Dangers of interaction*, Maritime & Coastguard Agency, United Kingdom.

Menter, F.R. (1994), 'Two-equation eddy-viscosity turbulence models for engineering applications', *AIAA Journal*, vol. 32, no. 8, pp. 1598-1605.

Mierlo, K.V. (2006), 'Trend Validation of SHIPFLOW based on the Bare Hull Upright Resistance of the Delft Series', MSc thesis, Delft University of Technology.

Newton, R.N. (1960), 'Some Notes on Interaction Effects Between Ships Close Aboard in Deep Water', in *First Symposium on Ship Maneuverability*, Washington D. C.

Olivieri A., Pistani F., Avanzini A. & Stern F. (2001), *Towing Tank Experiments of Resistance, Sinkage and Trim, Boundary Layer, Wake and Free Surface Flow Around a Naval Combatant INSEAN 2340 Model*, The University of Iowa, Iowa City, Iowa.

PIANC (1992), *Capability of Ship Manoeuvring Simulation Models for Approach Channels and Fairways in Harbours*, Report of Working Group no. 20 of Permanent Technical Committee II, Suppliment to PIANC Bulletin No. 77, 49 pp.

Pinkster, J.A. & Bhawsinka, K. (2013), 'A Real-time Simulation Technique for Ship-Ship and Ship-Port Interactions', in *The 28th International Workshop on Water Waves and Floating Bodies (IWWWFB 2013)*, L'Isle sur la Sorgue, France.

Pranzitelli, A., Nicola, C. & Miranda, S. (2011), 'Steady-State Calculations of Free Surface Flow around Ship Hulls and Resistance Predictions', in *High Speed Marine Vehicles (IX HSMV)*, Naples, Italy, pp. 1-14.

Reoseman, D.P. (1987), *The MARAD Systematic Series of Full-Form Ship Models*, The Society of Naval Architects and Marine Engineers, Jersey City, USA.

Roache, P.J. (1998), *Verification and Validation in Computational Science and Engineering*, 1 edn, Hermosa Publishers, New Mexico, USA.

Saha, G.K. & Tarafder, M.S. (2013), 'Computation of Flows Around the Transom Stern Hull by the Modified Rankine Source Panel Method', *Journal of Mechanical Engineering*, no. 43, 1.

Salim, S.M. & Cheah, S.C. (2009), 'Wall y+ Strategy for Dealing with Wall-Bounded Turbulent Flows', paper presented to International Multi-Conference of Engineers and Computer Scientists, Hong Kong, March 18-20.

Shi Xun, Chen Xin-quan & Jia-hua, T. (2010), 'Study of Resistance Performance of Vessels with Notches by Experimental and Computational Fluid Dynamics Calculation Methods', *Journal of Shanghai Jiaotong University (Science)*, vol. 15 (3), pp. 340-345.

Shih, T.-H., Liou, W., Shabbir, A., Yang, Z. & Zhu, J. (1994), 'A new k-epsilon eddy viscosity model for high Reynolds number turbulent flows: Model development and validation'.

Shin, K.W., Bingham, H.B. & Andersen, P. (2008), 'Numerical analysis of ship-ship interaction by a high-order potential flow code with ship motion', in *11th Numerical Towing Tank Symposium*, Brest, FranCe, pp. 47-52.

Simonsen, C.D., Nielsen, C.K., Otzen, J.F. & Agdrup, K. (2011), 'CFD Based Prediction of Ship-Ship Interaction Forces on a Tug Beside a Tanker', in B Pettersen, TE Berg, K Eloot & M Vantorre (eds), *The 2nd International Conference on Ship Manoeuvring in Shallow and Confined Water: Ship to Ship Interaction*, Trondheim, Norway.

Sorensen, P.K., Jensen, P.S., Caspersen, B. & Nielsen, J.H. (2009), 'Latest Developments in the Use of Tug Simulation and Tug Simulation Technology', in *Tugnology '09*, Amsterdam, Netherlands.

Spalart, P.R. & Allmaras, S.R. (1992), 'A one-equation turbulence model for aerodynamic flows', paper presented to 30th Aerospace Sciences Meeting and Exhibition, Reno, NV.

Stern, F., Wilson, R.V., Coleman, H.W. & Peterson, E.G. (2001), 'Comprehensive Approach to Verification and Validation of CFD Simulations - Part 1: Methodology and Procedures', *Journal of Fluids Engineering*, vol. 123, pp. 793-802.

Sutulo, S. & Soares, C.G. (2009), 'Simulation of Close-Proximity Maneuvers using an Online 3D Potential Flow Method', in *International Conference on Marine Simulation and Ship Maneuverability*, Panama City, Panama, pp. 558-567.

Sutulo, S., Soares, C.G. & Otzen, J. (2012), 'Validation of Potential-Flow Estimation of Interaction Forces Acting upon Ship Hulls in Parallel Motion', *Journal of Ship Research*, vol. 56, no. 3, pp. 129-145.

Takashina, J. (1986), 'Ship Maneuvering Motion due to Tugboats and its Mathematical Model', *Japan Society of Naval Architects*, vol. 160, pp. 93-104.

Tarafder, M.S., Khalil, G.M. & Saha, G.K. (2009), 'Analysis of Transom Stern Flows by Modified Rankine Source Panel Method', paper presented to International Conference on Mechanical Engineering 2009, Dhaka, Bangladesh.

Taylor, D.W. (1909), 'Some Model Experiments on Suction of Vessels', paper presented to First Summer Meering, Detroit, USA, June 24, 25, 26.

Tezdogan, T., Demirel, Y.K., Kellett, P., Khorasanchi, M., Incecik, A. & Turan, O. (2015), 'Full-scale unsteady RANS CFD simulations of ship behaviour and performance in head seas due to slow steaming', *Ocean Engineering*, vol. 97, pp. 186-206.

Tu, J., Yeoh, G.H. & Liu, C. (2008), *Computational Fluid Dynamics - A Practical Approach*, Butterworth-Heinemann, Burlington.

Tuck, E.O. & Newman, J.N. (1974), 'Hydrodynamic Interactions Between Ships', in *The 10th Symposium on Naval Hydrodynamics*, USA, pp. 35-69.

Vantorre, M., Verzhbitskaya, E. & Laforce, E. (2002), 'Model Test Based Formulations of Ship-Ship Interaction Forces', *Ship Technology Research*, vol. 49, pp. 124-141.

White, F.M. (2003), *Fluid Mechanics*, 5 edn, McGraw-Hill, New York.

Wilson, R.V., Stern, F., Coleman, H.W. & Peterson, E.G. (2001), 'Comprehensive Approach to Verification and Validation of CFD Simulations - Part 2: Application for RANS Simulation of a Cargo/Container Ship', *Journal of Fluids Engineering*, vol. 123, pp. 803-810.

Yeung, R.W. (1978), 'On the Interactions of Slender Ships in Shallow Sater', *Journal of Fluid Mechanics*, vol. 85, no. Part 1, pp. 143-159.

Yoon H., Longo J., Toda Y. & Stern F. (2015), 'Benchmark CFD Validation Data for Surface Combatant 5415 in PMM Maneuvers – Part II: Phase-Averaged Stereoscopic PIV Flow Field Measurements', *Ocean Engineering*, vol. 109 (2015), pp. 735-750.

Yoon H., Simonsen C.D., Benedetti L., Longo J., Toda Y. & Stern F. (2015), 'Benchmark CFD Validation Data for Surface Combatant 5415 in PMM Maneuvers – Part I: Force/Moment/Motion Measurements', *Ocean Engineering*, vol. 109 (2015), pp. 705–734.

Zhou, X., Sutulo, S. & Soares, C.G. (2012), 'Computation of Ship Hydrodynamic Interaction Forces in Restricted Waters using Potential Theory', *Journal of Marine Science and Application*, no. 2012-03, pp. 265-275.

Zou, L. & Larsson, L. (2013), 'Numerical Predictions of Ship-to-Ship Interaction in Shallow Water', *Ocean Engineering*, vol. 72, no. November 2013, pp. 386–402.

Appendices

Appendix I **The experimental and numerical uncertainty analysis**

Appendix II **Information and transport equations for the RANS modelling and turbulence models used in this study**

Appendix III **The details of hull models used in this study**

Appendix IV **The experimental setup used in the validation programme**

Appendix I The Experimental and Numerical Uncertainty Analysis

AI.1 Experimental Uncertainty Analysis

This appendix provides detailed calculations of the uncertainty analysis for the captive model scale experimental work carried out in AMC's model test basin. The uncertainty analysis procedure given in ITTC (2002b) was followed within this study. In accordance with ITTC (2002b), the total uncertainty limit of a model experiment is divided into bias and precision limits. This section discusses the estimation of the total uncertainties for single and multiple ship model experiments for ship interaction studies. Based on the total uncertainty limit, the percentage of uncertainty was calculated.

The calculations given here are an example, dealing with the longitudinal force calculation for one of the cases investigated, where both vessels are parallel to each other (i.e. θ = 0 degrees) and travelling at a forward speed of 0.41 m/s with the tug located at Δx = 1.0 and Δy = 1.09. The longitudinal, lateral and yaw coefficients were calculated based on the following formulae (Sutulo and Soares, 2009, Fonfach et al., 2011, Simonsen et al., 2011):

$$C_X = \frac{2X}{u^2 \nabla_t^{1/3} \nabla_s^{1/3} \rho} \quad \text{(AI.1)}$$

$$C_Y = \frac{2Y}{u^2 \nabla_t^{1/3} \nabla_s^{1/3} \rho} \quad \text{(AI.2)}$$

$$C_N = \frac{2N}{u^2 \nabla_t^{1/3} \nabla_s^{1/3} L_t \rho} \quad \text{(AI.3)}$$

For the longitudinal and lateral force coefficients, the following bias limits were considered:

- longitudinal force and lateral force (B_X, B_Y);
- speed (B_U);
- volume of displacement (B_{∇_t}); and
- density measurement (B_ρ).

For the yaw moment coefficient, the bias limits were as follows:

- lateral force forward and aft (B_Y);
- speed (B_U);
- volume of displacement (B_{∇_t});
- density measurement (B_ρ); and
- tug length (B_{L_t}).

Error sources creating the bias limits are shown in the Figure AI.1. Uncertainty sources that were smaller than 25% of the largest sources were neglected. Hence, acceleration due to gravity was not included in the calculation.

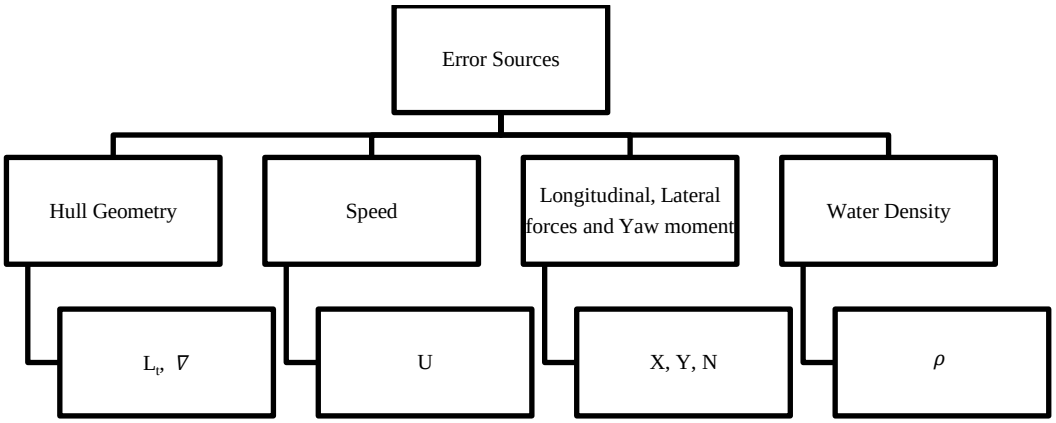

Figure AI.1: Error sources used for the uncertainty analysis.

The total experimental uncertainty is given by the root sum square of the uncertainties of the total bias and precision limits,

$$\sigma_T{}^2 = B_T{}^2 + P_T{}^2 \qquad \text{(AI.4)}$$

where,

$\sigma_T =$ total experimental uncertainty

$B_T =$ total bias limit

$P_T =$ total precision limit.

AI.1.1 Longitudinal Force (Example calculation)

For the longitudinal force coefficient, Equation AI.4 is modified as follows,

$$\sigma_{T_{C_x}}{}^2 = B_{T_{C_x}}{}^2 + P_{T_{C_x}}{}^2 \quad \text{(AI.5)}$$

where,

$\sigma_{T_{C_x}}$ = total experimental uncertainty for surge force coefficient

$B_{T_{C_x}}$ = total bias limit for surge force coefficient

$P_{T_{C_x}}$ = total precision limit for surge force coefficient

$$B_{T_{C_x}}{}^2 = \left(\frac{\partial C_x}{\partial X} B_X\right)^2 + \left(\frac{\partial C_x}{\partial U} B_U\right)^2 + \left(\frac{\partial C_x}{\partial \rho} B_\rho\right)^2 + \left(\frac{\partial C_x}{\partial \nabla_t} B_{\nabla_t}\right)^2 \quad \text{(AI.6)}$$

where;

$$\frac{\partial C_x}{\partial X} = \frac{2}{U^2 \nabla_t^{\frac{1}{3}} \nabla_s^{\frac{1}{3}} \rho} \quad \text{(AI.7)}$$

$$\frac{\partial C_x}{\partial U} = \frac{-4X}{U^3 \nabla_t^{\frac{1}{3}} \nabla_s^{\frac{1}{3}} \rho} \quad \text{(AI.8)}$$

$$\frac{\partial C_x}{\partial \rho} = \frac{-2X}{U^2 \nabla_t^{\frac{1}{3}} \nabla_s^{\frac{1}{3}} \rho^2} \quad \text{(AI.9)}$$

$$\frac{\partial C_x}{\partial \nabla_t} = \frac{-2X}{3U^2 \nabla_t^{\frac{4}{3}} \nabla_s^{\frac{1}{3}} \rho^2} \quad \text{(AI.10)}$$

AI.1.1.1 Calculation for B_X

Three major bias sources considered for B_X; i.e.as the bias due to the calibration weight (B_{X1}), bias from the calibration factor (B_{X2}) and bias due to the load cell misalignment (B_{X3}).

Bias due to the calibration weight (B_{X1})

The tolerance of the standard calibration weights used for the experiments was $\pm 0.005\%$. The measured longitudinal force at the selected case was 0.8370 N.

$B_{X1} = 0.005 \times 0.8370 \text{ N} = 0.004185 \text{ N}.$

Bias from the calibration factor (B_{X2})

Maximum error found in a series of calibrations done during the experiments was 2.44 g. Load cell error including hysteresis and non-linearity was 0.4%. Therefore, the maximum expected bias is,

$B_{X2} = (2.44 \times 9.81 \div 1000)(1 + 0.004)\text{N}$

$B_{X2} = 0.02403 \text{ N}.$

Bias due to the load cell misalignment (B_{X3})

This error was manifested due to the load cell misalignment during calibration and testing. The maximum bias limit expected was ± 0.5 degrees and it will affect the resistance measurement as follows,

$B_{X3} = X - (\cos 0.5\, X)$

$B_{X3} = 0.8370 - (\cos 0.5\, 0.8370)$

$B_{X3} = 0.000032 \text{ N}.$

Total bias limit on force measurement (B_X)

The total bias limit on the longitudinal force is obtained by the root sum square of the components considered above, i.e.,

$$B_X{}^2 = B_{X1}{}^2 + B_{X2}{}^2 + B_{X3}{}^2 \quad \text{(AI.11)}$$

B_X = 0.02439 N.

AI.1.1.2 Calculation for B_U

Bias limit for the speed was calculated using the speed displayed on the carriage display and the real speed expected without error. The speed voltage calibration factor was 0.5 m/s/V and the voltage reading at the average speed was 0.825535 V. Therefore, the expected speed was 0.4127 m/s. However the speed displayed on the model test basin display was 0.4102 m/s. Therefore, the expected bias limit is obtained as the difference of these speeds.

B_U = 0.0025 m/s.

AI.1.1.3 Calculation for B_ρ

In order to calculate bias limit for the density; three factors are considered, i.e. the bias limit of the temperature measurements (B_t), bias limit for the density calibration ($B_{\rho 1}$), and bias limit for the data reduction ($B_{\rho 2}$).

Bias limit of the temperature measurements (B_t)

Since the temperature is involved in density calculation, the bias limit of the temperature measurements is required. Accuracy of the thermometer used for temperature measurements was $\pm$ 0.3 degrees Celsiuswithin -5 to 50 degrees Celsius. The temperature reading for the selected case was 17 degrees Celsius. Therefore, the bias limit for the temperature was obtained as,

$B_t = 0.3$.

Bias limit for the density calibration ($B_{\rho 1}$)

In order to calculate the bias limit for the density measurement (B_ρ), the following formulae (ITTC, 2002b) was used,

$$\rho = 1000.1 + 0.0552\,t - 0.0077\,t^2 + 0.0004\,t^3 \quad \text{(AI.12)}$$

$$\left|\frac{\partial \rho}{\partial t}\right| = |0.0552 - 0.0154\,t + 0.00012\,t^2| \quad \text{(AI.13)}$$

For t = 17^0 and $B_t = 0.3$

$B_{\rho 1} = 0.052\ \mathrm{kg/m^3}$.

Bias limit for the data reduction ($B_{\rho 2}$)

When the nominal temperature was substituted in to Equation AI.12, the density ρ was obtained as 1000.7783 kg/m^3.

However, from the density tables, the density was found as 998.7780 kg/m^3 for a temperature of 17 degrees Celsius.

Therefore the difference in density is 0.232kg/m^3.

Hence,

$B_{\rho 2} = 2.0003\ \mathrm{kg/m^3}$.

Total bias limit for the density (B_ρ)

$${B_\rho}^2 = {B_{\rho 1}}^2 + {B_{\rho 2}}^2 \quad \text{(AI.14)}$$

$B_\rho = 2.001\ \mathrm{kg/m^3}$.

AI.1.1.4 Calculation for B_{∇_t}

The tug's volume of displacement (∇_t) was calculated by dividing the mass (m) of the model (measured using a floor scale) by the density (ρ) of the water in the model test basin. Hence the bias limit of the density and mass should be included in the bias limit for the volume of displacement.

$$\nabla_t = \frac{m}{\rho} \quad \text{(AI.15)}$$

$$B_{\nabla_t}{}^2 = \left(\frac{\partial \nabla_t}{\partial m} B_m\right)^2 + \left(\frac{\partial \nabla_t}{\partial \rho} B_\rho\right)^2 \quad \text{(AI.16)}$$

where,

$$\frac{\partial \nabla_t}{\partial m} = \frac{-m}{\rho} \quad \text{(AI.17)}$$

$$\frac{\partial \nabla_t}{\partial \rho} = \frac{-m}{\rho^2} \quad \text{(AI.18)}$$

$B_m = 0.05$ kg for the floor scale used

B_ρ = 2.001 kg/m^3 as calculated before

nominal $'\mathrm{m}' = 79.55$ kg

nominal $'\rho' = 998.778$ kg/m^3

Therefore,

$B_{\nabla_t} = 0.00398$ m^3.

AI.1.1.5 Calculation for $B_{T_{C_x}}$

Using the nominal values calculate above, the partial derivatives for each bias limit is obtained from Equations AI.7 to AI.10 and the following values,

$X = 0.837$ N

$U = 0.4102675$ m/s

$\nabla_t = 0.07964$ m^3

$\nabla_s = 0.531$ m^3

$\rho = 998.778$ kg/m^3

The partial derivatives become,

$\frac{\partial C_x}{\partial X} = 0.0341.$

$$\frac{\partial \, \mathrm{C_x}}{\partial \, \mathrm{U}} = \ 0.1393.$$

$$\frac{\partial \, C_x}{\partial \, \rho} = \ 2.8615 \times 10^{-5}.$$

$$\frac{\partial \, C_x}{\partial \, \nabla_t} = 0.1196.$$

Thus, from the Equation AI.6 we get the total bias limit for the longitudinal force coefficient as,

$$B_{T_{C_x}} = 0.001022.$$

AI.1.1.6 Calculation for $P_{T_{C_x}}$

In order to establish the precision limit, the standard deviation of the number of tests with the model removed and reinstalled between two runs must be determined. Hence six different runs with the same speed and location settings were conducted to measure the forces acting on the tug.

The precision limit for multiple tests $P(M)$ and precision limit for a single run $P(S)$ are calculated according to (ITTC, 2002b) as,

$$P(M) = \frac{K.SDev}{\sqrt{M}} \quad \text{(AI.19)}$$

$$P(S) = k.SDev \quad \text{(AI.20)}$$

where;

K = 2 according to the methodology

SDev = standard deviation established by multiple runs

M = number of runs

Using Equations AI.19 and AI.20 we get,

$P(M) = 0.00069.$

$P(S) = 0.00169.$

Therefore, the total longitudinal force uncertainty using Equation AI.5 is established as,

$\sigma_{T_{C_x}} = 7\%.$

AI.1.2 Lateral Force and Yaw Moment

In order to establish the uncertainty limit for the lateral force and yaw moment, similar calculations were conducted giving,

$\sigma_{T_{C_y}} = 9.4\%.$

$\sigma_{T_{C_n}} = 7\%.$

All these calculations were repeated for the different drift angles and different speeds of the tug boat, enabling the calculation of error bars for the result plots as shown in Table AI.1.

Table AI.1. Experimental uncertainty percentages calculated for the interaction effects at three drift angles.

Interaction Effect	0 degree Drift Angle	8.4 degrees Drift Angle	16.8 degrees Drift Angle
Longitudinal Force	7.0%	13.3%	13.2%
Lateral Force	9.4%	15.8%	11.4%
Yaw Moment	7.0%	15.1%	14.5%

AI.2: Example Numerical Uncertainty Analysis (used in Chapter 3)

Longitudinal force, lateral force, and yaw moment acting on the tug boat using three selected CFD grids (Table AI.2) were used to investigate the numerical accuracy of the CFD solutions in accordance with ITTC (2002a) procedures. Once the numerical accuracy was investigated, y^+ and turbulence model combinations were varied to observe their effects on the computational results as discussed in Chapter 3.

In order to investigate numerical accuracy of the CFD solutions, iterative convergence (see Table AI.2), grid convergence (see Table AI.3), and time step convergence (see Table AI.4) were selected and overall verification uncertainty was quantified for corrected and uncorrected results. This was then compared with the magnitude of the error to envisage the numerical accuracy of the CFD solutions.

Table AI.2. Calculated iterative uncertainties for the fine (G_1), medium (G_2) and coarse (G_3) grids.

Grid label	No of cells	Iterative Uncertainties		
		Longitudinal Force	Lateral Force	Yaw Moment
G_1	8.94M	0.07%*EFD*	0.15%*EFD*	0.21%*EFD*
G_2	6.31M	0.09%*EFD*	0.15%*EFD*	0.22%*EFD*
G_3	4.50M	0.09%*EFD*	0.18%*EFD*	0.22%*EFD*

Table AI.3. Results obtained from the grid convergence study for the longitudinal force (*X*), lateral force (*Y*), and yaw moment (*N*) as a percentage of the finest grid results ($\%G_1$).

Parameter	δ_G^* $(\%G_1)$	U_G $(\%G_1)$	U_{G_C} $(\%G_1)$
X	0.054071	-5.817	-0.034
Y	0.000002	-0.587	-0.292
N	0.060046	2.731	1.321

Note: δ_G^* is the estimated grid convergence error, U_G is the grid convergence uncertainty and U_{G_C} is the corrected grid convergence uncertainty.

Table AI.4. Results obtained from the time step convergence study for longitudinal force (*X*), lateral force (*Y*), and yaw moment (*N*) as a percentage of finest grid results $(\%G_1)$.

Parameter	δ_T^* $(\%G_1)$	U_T $(\%G_1)$	U_{T_C} $(\%G_1)$
X	0.005580	-1.639	-0.519
Y	0.001667	-4.617	-1.847
N	0.000004	0.176	0.086

Note: δ_T^* is the estimated grid convergence error, U_T is the grid convergence uncertainty and U_{T_C} is the corrected grid convergence uncertainty.

Table AI.5. Verification uncertainty values (U_V) as a percentage of the EFD for CFD generated longitudinal force (*X*), lateral force (*Y*), and yaw moment (*N*) results and corrected longitudinal force (X_c), lateral force (Y_c), and yaw moment (N_c) results.

Parameter	U_{SN} $(\%EFD)$	U_D $(\%EFD)$	U_V $(\%EFD)$	$\%\|E\|$
X	-5.99	7.0	9.21	0.85
Y	-4.94	9.4	10.62	6.17
N	2.94	7.0	7.59	7.27
X_C	-0.52	7.0	7.02	6.00
Y_C	-1.99	9.4	9.61	9.43
N_C	1.42	7.0	7.14	5.67

Note: U_{SN} is the numerical uncertainty, U_D is the experimental uncertainty, and $\%|E|$ is the magnitude of the percentage error given in ITTC (2002a). These uncertainty values (U_V) were greater than the absolute value of the comparison error, $|E|$ as seen in Table AI.5 and thus the finest grid with 8.94 million cells was utilized for the cases investigated in this study.

Appendix II Information and Transport Equations for the RANS Modelling and Turbulence Models used in this Study

AII.1 RANS Modelling

As discussed in the Chapter 1, CFD is a cheaper alternative to experiments to determine the interaction effects acting on tugs. It is a branch of fluid mechanics which involves conversion of the governing equations within fluid dynamics (for example the RANS equations) and auxiliary conditions into a system of discrete algebraic equations, i.e. discretization. The resulting discrete algebraic equations are then solved for variables at grid points within the fluid domain through an iterative process (Tu et al., 2008). The RANS equations are decomposed from the Navier-Stokes equations to facilitate the simulations of real-world engineering flow models. With the intention of dealing with randomly fluctuating fluid flow at the turbulent boundary region, the turbulent Navier-Stokes equations are simplified by averaging the sum of the steady and fluctuating components to create RANS equations. In order to simulate the flow around a tug hull, the effects on the flow patterns due to minor temperature variations can be neglected. Therefore, the thermodynamic components of the RANS equations can be eliminated from the solution algorithm and the basic governing RANS momentum equations can be presented as Equations AII.1 to AII.3.

$$\rho\left(\bar{u}\frac{\partial\bar{u}}{\partial\bar{x}}+\bar{v}\frac{\partial\bar{u}}{\partial\bar{y}}+\bar{w}\frac{\partial\bar{u}}{\partial\bar{z}}\right)=-\frac{\partial\bar{p}}{\partial\bar{x}}+\mu\Delta\bar{u}-\rho\left(\frac{\partial\sigma'_{x}}{\partial\bar{x}}+\frac{\partial\sigma'_{xy}}{\partial\bar{y}}+\frac{\partial\sigma'_{xz}}{\partial z}\right) \quad \text{(AII.1)}$$

$$\rho\left(\bar{u}\frac{\partial\bar{v}}{\partial\bar{x}}+\bar{v}\frac{\partial\bar{v}}{\partial\bar{y}}+\bar{w}\frac{\partial\bar{v}}{\partial\bar{z}}\right)=-\frac{\partial\bar{p}}{\partial\bar{y}}+\mu\Delta\bar{v}-\rho\left(\frac{\partial\sigma'_{xy}}{\partial\bar{x}}+\frac{\partial\sigma'_{y}}{\partial\bar{y}}+\frac{\partial\sigma'_{yz}}{\partial z}\right) \quad \text{(AII.2)}$$

$$\rho\left(\bar{u}\frac{\partial\bar{w}}{\partial\bar{x}}+\bar{v}\frac{\partial\bar{w}}{\partial\bar{y}}+\bar{w}\frac{\partial\bar{w}}{\partial\bar{z}}\right)=-\frac{\partial\bar{p}}{\partial\bar{z}}+\mu\Delta\bar{w}-\rho\left(\frac{\partial\sigma'_{xz}}{\partial\bar{x}}+\frac{\partial\sigma'_{yz}}{\partial\bar{y}}+\frac{\partial\sigma'_{z}}{\partial z}\right) \quad \text{(AII.3)}$$

AII.2 Turbulence Models Used

For most engineering fluid flow problems it is unnecessary to resolve the detailed turbulence fluctuations. Nevertheless the turbulence models integrated in CFD allow the calculation of the effect of turbulence on mean flow without solving the detailed turbulence fluctuations (Tu et al., 2008). These additional turbulence models simplify the turbulent flow using assumptions, providing solutions within acceptable accuracy while significantly reducing computation time (Tu et al., 2008). When using these turbulence models, it is important to select models that are suitable for the task at hand, as they are optimized for different situations. There are a number of RANS-based turbulence models available within StarCCM+®, and three distinct turbulence models: Realizable Two Layer k-Epsilon (RKE), k-Omega Shear Stress Transport (SST), and Standard Spalart-Allmaras (SA); were evaluated to identify the most suitable model to accurately predict the ship-tug interaction behaviour.

AII.2.1 Realizable Two Layer k-ε (RKE)

This is a two-equation turbulence model in which transport equations are solved for the turbulent kinetic energy k and its dissipation rate ε. This model gives accurate and robust solutions for general simulations. Shih et al. (1994) developed an improved version of the standard k-ε model with a new transport equation for the turbulence dissipation rate. (CD-Adapco, 2015). The modifications help to model certain mathematical constraints on the normal stresses consistent with the physics of turbulence (i.e. realizability). The *Realizable* k-ε model is substantially better than the standard k-ε model for many engineering applications involving rotational flow, boundary layers with strong pressure gradients or separation, and recirculation (CD-Adapco, 2015). Furthermore, its two-layer wall treatment approach is an alternative to the low-Reynolds number wall treatment approach that enables the improvement of the boundary layer modelling within the k-ε model to be applied in the viscous sub-layer.

In the two-layer wall treatment approach, the computation of the boundary layer is divided into two layers. In the layer next to the wall, the turbulent dissipation rate ε and the turbulent viscosity μ_t are specified as functions of the wall distance (CD-Adapco, 2015). The values of ε specified in the near-wall layer are blended smoothly with the values computed from solving the transport equation far from the wall. The equation for the turbulent kinetic energy, *k*, is solved in the entire flow (CD-Adapco, 2015). The two-layer formulations work with either low-Reynolds number type meshes, y^+~1 or wall-function type meshes and y^+>30 (CD-Adapco, 2015). Thus, this turbulence model was included in the verification study. Transport equations of the turbulence model are given below.

The transport equations for RKE model (CD-Adapco, 2015) are:

$$\frac{\mathrm{d}}{\mathrm{dt}}\int_{\mathrm{V}}\alpha_{\mathrm{i}}\,\rho_{\mathrm{i}}\mathrm{k}_{\mathrm{i}}\mathrm{dV}+\int_{\mathrm{A}}\alpha_{\mathrm{i}}\,\rho_{\mathrm{i}}\mathrm{k}_{\mathrm{i}}\left(\mathrm{v}_{\mathrm{i}}-\mathrm{v}_{\mathrm{g}}\right)\cdot\mathrm{da}\;=\int_{\mathrm{A}}\alpha_{\mathrm{i}}\left(\mu_{\mathrm{i}}+\frac{\mu_{\mathrm{i}}'}{\sigma_{\mathrm{k}}}\right)\nabla\mathrm{k}_{\mathrm{i}}\cdot\mathrm{da}+\int_{\mathrm{V}}\alpha_{\mathrm{i}}\left[\mathrm{f}_{\mathrm{i}}^{\mathrm{c}}\mathrm{G}_{\mathrm{i}}^{\mathrm{k}}+\mathrm{G}_{\mathrm{i}}^{\mathrm{b}}-\rho_{\mathrm{i}}((\varepsilon_{\mathrm{i}}-\varepsilon_{\mathrm{o}})+\mathrm{Y}_{\mathrm{i}}^{\mathrm{M}})+\mathrm{S}_{\mathrm{i}}^{\mathrm{k}}+\mathrm{S}_{\mathrm{i}}^{\mathrm{kr}}\right]\mathrm{dV}+\sum_{\mathrm{j}\neq\mathrm{i}}\left(\mathrm{m}_{\mathrm{ij}}\mathrm{k}_{\mathrm{j}}^{(\mathrm{ij})}-\mathrm{m}_{\mathrm{ij}}\mathrm{k}_{\mathrm{i}}\right) \tag{AII.4}$$

$$\frac{d}{dt}\int_{V}\alpha_i\,\rho_i\varepsilon_i dV+\int_{A}\alpha_i\,\rho_i\varepsilon_i\left(v_i-v_g\right)\cdot da\;=\int_{A}\alpha_i\left(\mu_i+\frac{\mu_i'}{\sigma_\varepsilon}\right)\nabla\varepsilon_i\cdot da+\int_{V}\alpha_i\left[f_i^{c}C_{\varepsilon_1}S\varepsilon+\frac{\varepsilon_i}{k_i}\left(C_{\varepsilon_1}C_{\varepsilon_3}G_i^{b}\right)-\frac{\varepsilon_i}{k_i+\sqrt{v\varepsilon_i}}C_{\varepsilon_2}\rho_i(\varepsilon_i-\varepsilon_o)+S_i^{\varepsilon}+S_i^{\varepsilon r}\right]dV+\sum_{j\neq i}\left(m_{ij}\varepsilon_j^{(ij)}-m_{ij}\varepsilon_i\right) \tag{AII.5}$$

where,

S_k and S_ε are the user-specified source terms;

ε_o is the ambient turbulence value in the source terms that counteracts turbulence decay;

f_c is the curvature correction factor;

i denotes the different phases;

α_i is the volume fraction of each phase;

S_i^{kr} and $S_i^{\varepsilon r}$ are source terms for the continuous phase when modelling Eulerian particle induced turbulence; and

f_i^{c} is the curvature correction factor for each phase.

The Turbulent production G_K is evaluated as:

$$G_K = \mu_t S^2 - \frac{2}{3}\rho k \nabla \cdot v \frac{2}{3}\mu_t (\nabla \cdot v)^2 \quad \text{(AII.6)}$$

where,

$\nabla \cdot v$ is the velocity divergent; and

S is the modulus of mean strain rate tensor.

The Buoyancy production G_b is evaluated as:

$$G_b = \beta \frac{\mu_t}{\sigma_t} (\Delta T \cdot g) \quad \text{(AII.7)}$$

where,

β is the coefficient of thermal expansion;

ΔT is the temperature gradient vector; and

σ_t is the turbulent Prandtl number.

Compressibility Modification:

$$Y_M = \frac{C_M k \epsilon}{c} \quad \text{(AII.8)}$$

where,

$C_M = 2.$

c is the speed of sound.

AII.2.2 Shear Stress Transport (SST)

This is the second turbulence model employed in the study, which is a hybrid of the standard *k*-ε and standard *k*-ω models and has been developed to overcome the shortcomings of both. It blends the two standard models in free flow and turbulent flow ensuring a smooth transition. The problem of the standard *k*-ω sensitivity to free-stream/inlet conditions was addressed by Menter (1994), who recognized that the ε transport equation from the standard *k*-ε model could be transformed into an ω transport equation by variable substitution.

The transformed equation looks similar to the one in the standard *k*-ω model, but adds an additional non-conservative cross-diffusion term containing the dot-product $\nabla \boldsymbol{k} \cdot \nabla \omega$. Inclusion of this term in the ω transport equation potentially makes the *k*-ω model produce identical results to the *k*-ε model. Menter (1994) suggested using a blending function (which includes functions of the wall distance) that would include the cross-diffusion term far from the walls, but not near the walls. This approach effectively blends a *k*-ε model in the far-field with a *k*-ω model near the wall (CD-Adapco, 2015). Transport equations of the turbulence model are given below.

The transport equations for the SST model (CD-Adapco, 2015) are:

$$\frac{d}{dt}\int_V \rho k dV + \int_A \rho k(v - v_g)\cdot da = \int_A (\mu + \sigma_k \mu_t)\nabla k \cdot da + \int_V (\gamma_{eff} G_k - \gamma' \rho \beta^* f_{\beta^*}(\omega k - \omega_0 k_0) + S_k) dV$$

(AII.9)

$$\frac{d}{dt}\int_V \rho \omega dV + \int_A \rho \omega(v - v_g)\cdot da = \int_A (\mu + \sigma_\omega \mu_t)\nabla \omega \cdot da + \int_V (G_\omega - \rho \beta f_\beta(\omega^2 - \omega_0^2) + D_\omega + S_\omega) dV$$

(AII.10)

where S_k and S_ω are the user-specified source terms, k_0 and ω_0 are the ambient turbulence values in source terms that counteract turbulence decay, γ_{eff} is the effective intermittency provided by the Gamma Re-Theta Transition model (it was kept as unity in this study as the transition model was not activated).

AII.2.3 Spalart-Allmaras Model (SA)

This is the third turbulence model utilized within this study, which solves a single transport equation that determines the turbulent viscosity. This situation is in contrast to many of the early one-equation models that solve an equation for the transport of turbulent kinetic energy, *k*, and require an algebraic prescription of a length scale. The authors of the original

Spalart-Allmaras turbulence model (Spalart and Allmaras, 1992) presented results for attached boundary layers and flows with mild separation (such as flow past a wing), which are considered to be the most suitable cases for the SA model (CD-Adapco, 2015). Transport equation of the turbulence model is given below.

The transport equation for the SA model (CD-Adapco, 2015) is:

$$\frac{d}{dt}\int_V \rho\tilde{v}\ dV + \int_A \rho\,\tilde{v}\left(v - v_g\right)\cdot da = \frac{1}{\sigma_{\tilde{v}}}\int_A(\mu + \rho\tilde{v})\nabla\tilde{v}\cdot da + \int_V[C_{b2}\,\rho(\nabla\tilde{v}\cdot\nabla\tilde{v}) + G_{\tilde{v}} - r_{\tilde{v}} + S_{\tilde{v}}]dv \quad \text{(AII.11)}$$

where $S_{\tilde{v}}$ is the user-specified source term, and the transported variable $\tilde{v}$ is the modified diffusivity. The terms on the right-hand side represent diffusion, production, and dissipation respectively.

Appendix III The Details of Hull Models used in this Study

AIII.1 Drawings of the ASD Tug Model

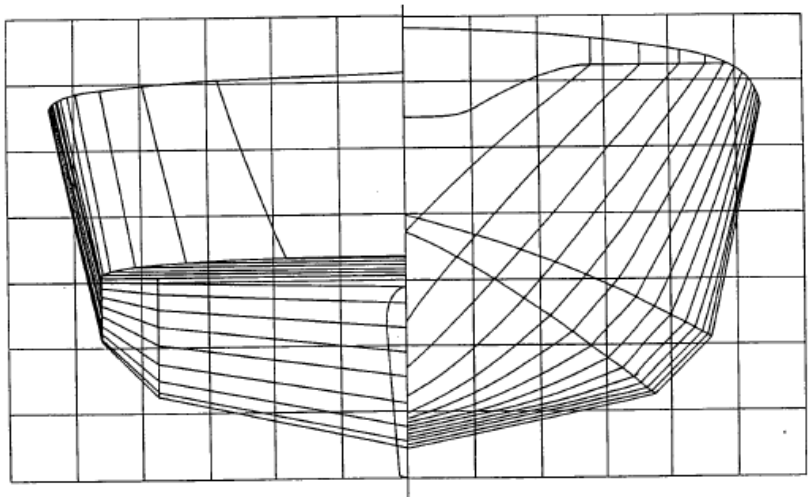

Figure AIII.1: Body Plan of ASD Tug Model used in this study (Brandner, 1995).

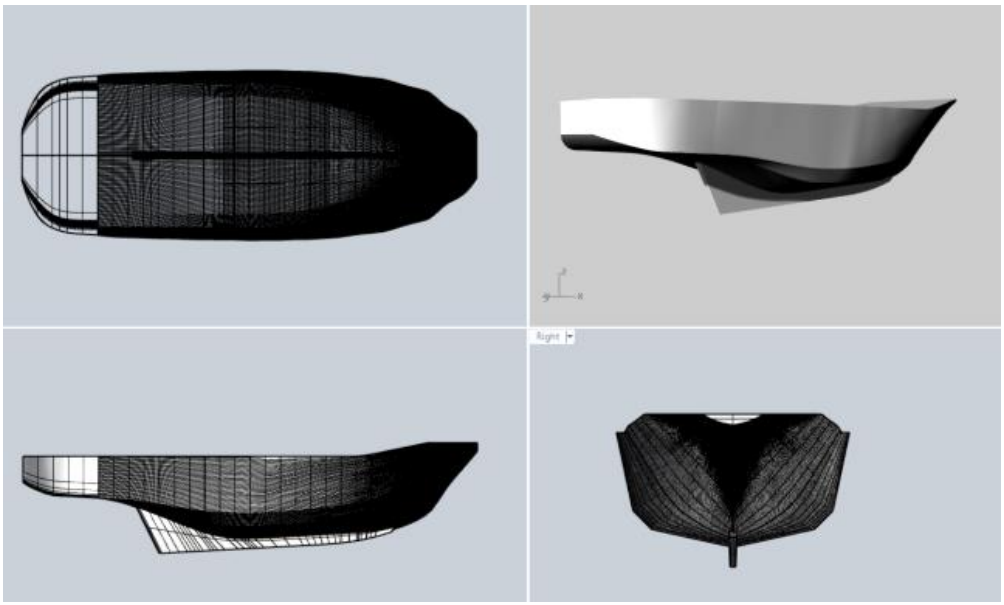

Figure AIII.2: Three Dimensional View of ASD Tug Model used in this study

AIII.2 Drawings of the MARAD-F series hull model

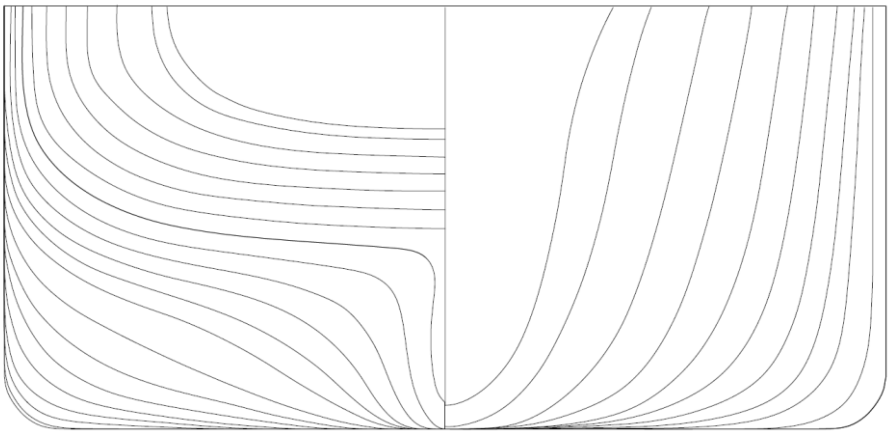

Figure AIII.1: Body Plan of MARAD-F series hull used in this study (Reoseman, 1987).

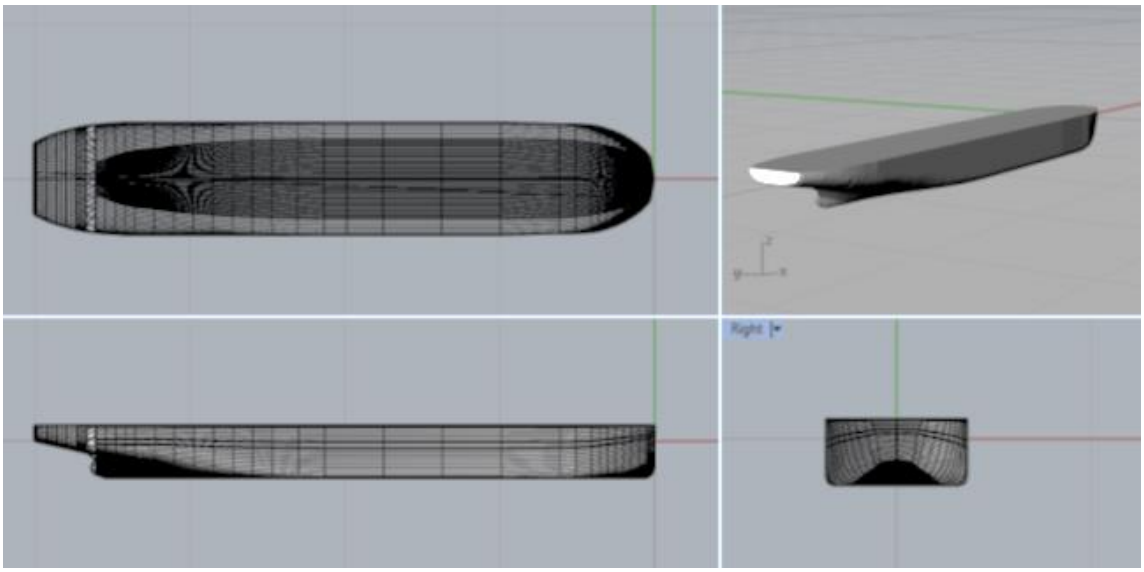

Figure AIII.2: Three Dimensional View of MARAD-F series hull used in this study.

Appendix IV The Experimental Setup used in the Validation Programme

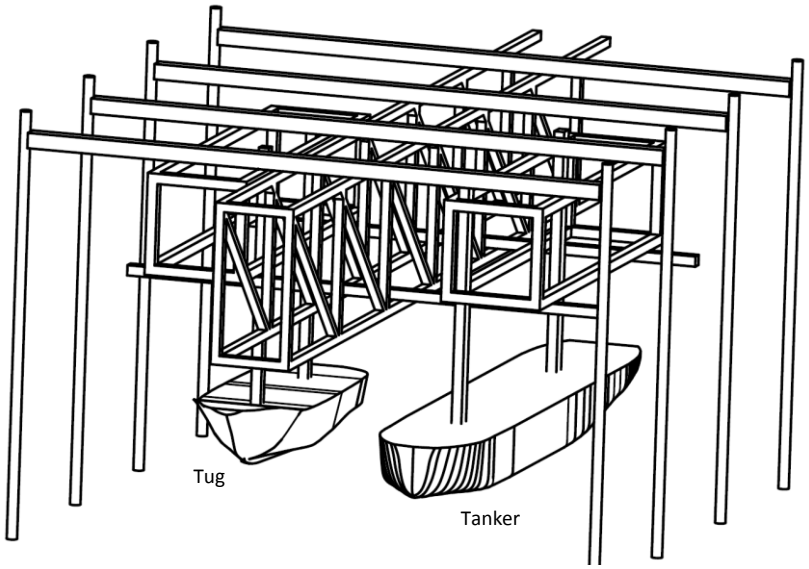

Figure AIV.1: Isometric View of the AMC Model Test Basin's Model Carriage arrangement.

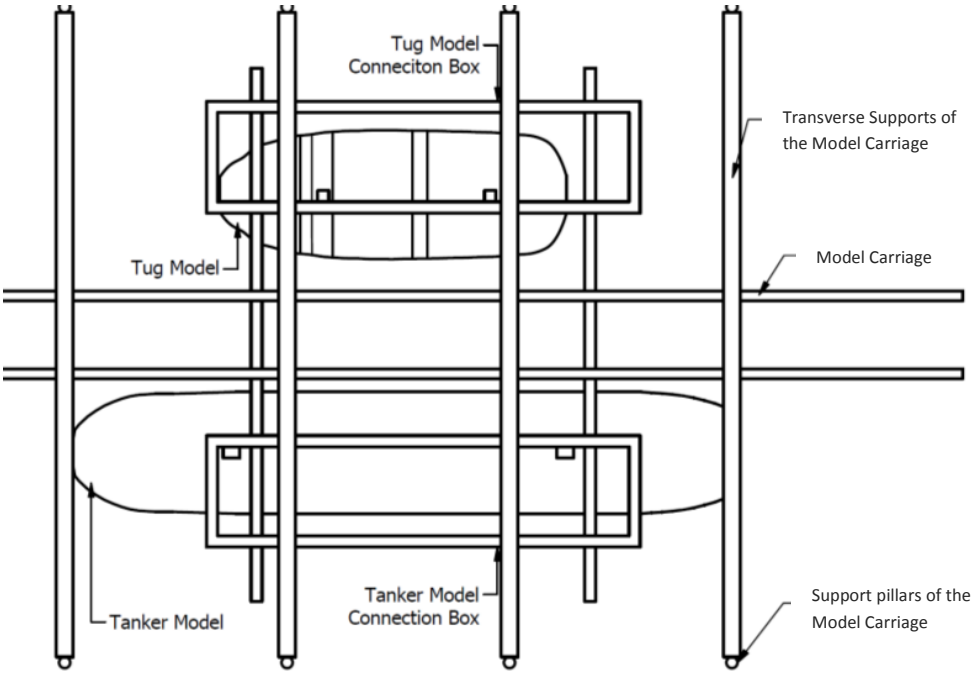

Figure AIV.2: Top View of the AMC Model Test Basin's Model Carriage arrangement.

Figure AIV.3: Model Carriage setup within empty Model Test Basin.

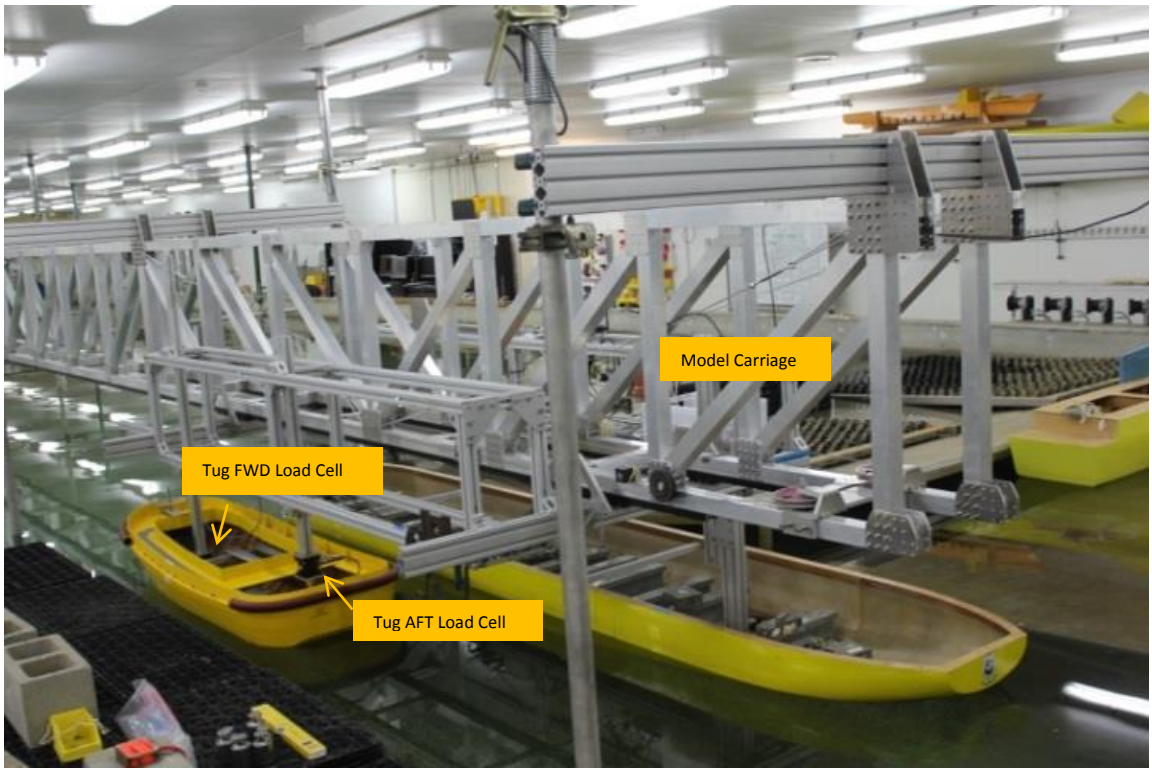

Figure AIV.4: Tug and tanker models with Model Carriage and load cell arrangement.

Figure AIV.5: Parallel tug and tanker models during experiments.

Figure AIV.6: Drifted tug relative to tanker during experiments.